Transient instabilities in turbomachinery

Cvijetić, Gregor

Doctoral thesis / Disertacija

2019

Permanent link / Trajna poveznica: https://urn.nsk.hr/urn:nbn:hr:235:294732

Download date / Datum preuzimanja: **2025-03-31**

Repository / Repozitorij:

Repository of Faculty of Mechanical Engineering and Naval Architecture University of Zagreb

University of Zagreb

Faculty of Mechanical Engineering and Naval Architecture

Gregor Cvijetić

Transient Instabilities in Turbomachinery

DOCTORAL THESIS

Zagreb, 2019

University of Zagreb

Faculty of Mechanical Engineering and Naval Architecture

Gregor Cvijetić

Transient Instabilities in Turbomachinery

DOCTORAL THESIS

Supervisor: prof. Hrvoje Jasak, PhD

Zagreb, 2019

Sveučilište u Zagrebu

Fakultet strojarstva i brodogradnje

Gregor Cvijetić

Prijelazne pojave u rešetkama turbostrojeva

DOKTORSKI RAD

Mentor: prof. dr. sc. Hrvoje Jasak

Zagreb, 2019

Bibliography data

Acknowledgement

I would like to express my gratitude to all those whose comments, insights and advices were of great help to me while working on the thesis.

I am truly thankful to my supervisor, professor Hrvoje Jasak, for his valuable guidance, constructive comments and encouragement over the last few years. Among other, even short discussions and seemingly brief consultations would always point me in the right direction, being the right motivation at the right time.

My friends and colleagues deserve my sincere *thank you*, for helping me with the topic, but also for taking my mind off work.

Words cannot express my thanks to my darling, Tamara for your infinite positive attitude, for your support and for surpassing understanding and patience.

Finally, I would like to express a memorable thank you to the canteen ladies for always filling up the plate more than specified and always being ready to share a smile in a cheerful atmosphere.

<div align="right">

Thank you,

Gregor Cvijetić

</div>

Abstract

Turbomachinery CFD simulations have become a standard in industry, although still presenting quite expensive and time consuming process. In order to alleviate this, a number of tools and methods have been developed, being an approximation or simplification of the ongoing process within turbomachinery. Some of these methods include the steady state Multiple Reference Frame approach (MRF), taking into account the rotation even though a steady state simulation is run. Another more recent method is the Harmonic Balance method, a quasi-steady state method due to a number of time instants being solved via coupled steady state equations. Finally, the approach with least approximations is the transient simulation where a large number of successive time steps are solved, thus obtaining the detailed insight into flow development, wakes propagation, etc. In order for time-accurate simulation to present valid results, a periodic steady state has to be reached: simulating a single period is not enough. It should be made sure that the simulation start instabilities do not affect the solution and that resulting flow features are no longer within the domain, therefore reaching periodic steady state is what makes transient simulation expensive. In certain cases this means simulating 5-10 periods, but if a high level of unsteadiness is present, the number of needed periods can even go up to 50. From the perspective of CPU time consumption, the transient simulation is the most expensive one, followed by Harmonic Balance and then by MRF as the shortest. The focus of this work is on the Harmonic Balance method, which is extensively used for periodic problems, mostly vibrations, acoustics and turbomachinery.

Compared to conventional transient methods, the benefit of the Harmonic Balance method is the ability to capture transient flow features at significantly

lower CPU time cost, while still being sufficiently accurate. This is presented by performing the comparison with transient approach and steady state MRF method, demonstrating the speed-up of at least an order of magnitude. Depending on the number of harmonics used, the size of the system of equations changes, as well as the accuracy. n number of harmonics yield a system of $2n + 1$ coupled equations, where larger number of harmonics will take more time to converge, while offering greater accuracy as higher order effects do not get neglected. As the method is based on the Fourier series expansion, the frequency of the motion should be known in advance, suggesting that problems with imposed periodic motion are the most suitable for Harmonic Balance. In this work, the Harmonic Balance method is implemented in the Finite Volume framework within the open source software OpenFOAM, using a segregated pressure-based algorithm.

Turbomachinery start-up and shut-down present a challenging problem for CFD investigation. Furthermore, change of operating points requires special attention as well. Depending on the type of the machine considered, the change of regime can take from several periods up to several dozen periods, making the simulations of such process highly expensive. The change of regime is a transient process during which the flow can change significantly and mass flow through the machine changes according to the newly reached regime. Rotor angular velocity can change as well in this process, making steady state simulations unusable.

The modified version of the Harmonic Balance method is deployed here as a quasi-steady method in order to reduce the simulation time and capture the behavior during regime change. Non–periodic process such as start-up or shut-down is made periodic by considering both start-up and shut-down as a complete process. The period then consists of two complementary regime changes, with $2n + 1$ coupled simulations throughout the period of start-up and shut-down. Due to two distinctive time-scales of rotor period (inner) and complete start-up/shut-down period (outer), a nested Harmonic Balance structure is deployed. Therefore, the $2n + 1$ Harmonic Balance simulations for $2n + 1$ time instants are interconnected with additional Harmonic Balance source term for the outer coupling.

The validation of the time-spectral Harmonic Balance method is performed

on industrially relevant test case of ERCOFTAC centrifugal pump by performing the comparison with other conventional methods (time-accurate, MRF) and with experimental data. Furthermore, the comparison of computational resources is performed in terms of CPU time, showing the Harmonic Balance method approximately 30 times faster than time-accurate simulation. The nested Harmonic Balance is validated using Francis-99 test case for shut-down and start-up processes. Comparison is performed against experimental data for power variation and pressure probes during complete period with good agreement achieved in a fraction of time otherwise needed by the time-accurate simulation.

Prošireni sažetak

Uvod

Periodični problemi su česta pojava u znanstvenim i industrijskim istraživanjima, a javljaju se kod analize raznih rotirajućih strojeva, problema valne prirode, raznih tokova s induciranim periodičnim rubnim uvjetima ili periodičnim kretanjem tijela (osciliranje krila, ventili, itd.). Iako su već postale standard u industriji, simulacije turbostrojeva i dalje predstavljaju izrazito skup i vremenski zahtjevan zadatak. Kako bi se to izbjeglo razvijene su razne metode i alati koji predstavljaju aproksimaciju ili pojednostavljenje procesa koji se odvija u turbostroju. Neke od tih metoda su *Multiple Reference Frame* (MRF) koja uzima u obzir rotaciju domene iako se radi o stacionarnoj simulaciji. Druga, novija metoda je metoda harmonijske ravnoteže, kvazi-stacionarna metoda budući da rješava više spregnutih vremenskih trenutaka koristeći stacionarne, ali međusobno spregnute jednadžbe. Naposljetku, pristup koji nudi najveću razinu točnosti po pitanju vremenske rezolucije je tranzijentna simulacija, pri čemu se rješava niz uzastopnih vremenskih trenutaka i dobiva detaljan uvid u razvoj toka, propagaciju valova, itd. Međutim, kako bi tranzijentna simulacija bila valjana kod periodičnih problema, potrebno je doći do rezultata koji je periodično-stacionaran. Drugim riječima, nije dovoljno simulirati samo jedan period već je potrebno osigurati da su nestabilnosti uzrokovane rubnim uvjetima s početka simulacije u potpunosti napustile domenu i da početni uvjeti ne utječu na rezultat. Tranzijentna simulacija je stoga iznimno skupa budući da treba doći do periodično-stacionarnog stanja. U pojedinim slučajevima to znači 5-10 perioda, no za kompleksnije probleme može biti potrebno simulirati i do 50 perioda. Iz perspektive utroška proračunskog

vremena potrebnog za simulaciju, tranzijentna simulacija je najskuplja, nakon čega slijedi metoda harmonijske ravnoteže te MRF. Fokus ovog rada je na metodi harmonijske ravnoteže koja se koristi za periodične probleme, ponajviše vibracije, akustiku i turbostrojeve.

Pristup istraživanju

Metoda harmonijske ravnoteže je kvazi-stacionarna metoda, što znači da obuhvaća karakteristike i stacionarnog i tranzijentnog pristupa. U odnosu na konvencionalne stacionarne metode, prednost metode harmonijske ravnoteže je mogućnost dobivanja prijelaznih karakteristika toka, uz dodatni utrošak vremena simulacije. Korištenjem stacionarnih metoda kod simulacija turbostrojeva dobiva se rješenje samo za jedan položaj rotora, zbog čega izostaju prijelazne pojave i vrtlozi te takav pristup nije naročito značajan ako su lokalne nestabilnosti od značaja. S druge strane, u odnosu na tranzijentnu metodu, metoda harmonijske ravnoteže omogućuje značajno smanjenje vremena simulacije uz zadržanu točnost metode. Umjesto rješavanja jedne tranzijentne jednadžbe, primjenom metode harmonijske ravnoteže dobiva se sustav spregnutih stacionarnih jednadžbi čije rješavanje daje polje strujanja unutar cijelog reprezentativnog perioda.

Glavne faze istraživanja su:

a) Razvoj osnovnog modela metode harmonijske ravnoteže.

b) Specijalizacija metode harmonijske ravnoteže za upotrebu kod turbostrojeva. Razvoj modela s više frekvencija.

c) Validacija i verifikacija metode.

d) Proširenje metode za simulacije promjene radne točke.

e) Primjena metode za simulacije rada turbostroja van optimalne radne točke i analiza nestabilnosti.

Metoda harmonijske ravnoteže je metoda razvijena za simulacije periodičnih strujanja, a u ovom istraživanju je specijalizirana za primjenu na turbostrojevima. Metoda rješava niz kvazi-stacionarnih međusobno spregnutih Navier-Stokesovih jednadžbi, te se kao rezultat dobiva polje strujanja unutar cijelog reprezentativnog perioda turbostroja. Za uspješnu implementaciju metode, prije diskretizacije jednadžbi metodom kontrolnih volumena potrebno je pretvoriti tranzijentne Navier-Stokesove jednadžbe u kvazi-stacionarne Navier-Stokesove jednadžbe u formi metode harmonijske ravnoteže. Tom procedurom umjesto jedne tranzijentne jednadžbe dobivamo sustav kvazi-stacionarnih jednadžbi. Veličina sustava ovisi o broju odabranih harmonika n, pri čemu je broj jednadžbi u sustavu 2n+1. Nakon uspješne implementacije metode u okružju metode kontrolnih volumena, idući korak je razvoj dodatnih funkcionalnosti metode kako bi bila potpuno primjenjiva kod turbostrojeva. Budući da metoda harmonijske ravnoteže u svom osnovnom obliku uzima u obzir samo jednu frekvenciju, izveden je model metode koji je u mogućnosti koristiti dvije frekvencije (frekvencija rotora i frekvencija statora), a zatim je u obzir uzeta i dodatna frekvencija nestabilnosti koja se razvija kao posljedica ne-optimalnog toka. Metoda harmonijske ravnoteže i svi pripadajući alati implementirani su u programskom paketu OpenFOAM, napisanom u C++ programskom jeziku.

Dvojna metoda harmonijske ravnoteže

Višefrekvencijskim pristupom dolazi se do različitih frekvencijskih domena za rotor i stator, što također zahtjeva poseban tretman. Kako bi se omogućilo korištenje zasebnih frekvencija u različitim domenama, a bez smetnji poduzorkovanja (*aliasing errors*), potrebno je uskladiti vremenske trenutke između domena. Budući da kod turbostrojeva dominantne frekvencije ovise o karakteristikama turbostroja: broju lopatica rotora i statora, brzini vrtnje, broju stupnjeva, itd., moguće je unaprijed odabrati dominantne frekvencije. Točnost metode harmonijske ravnoteže ovisi o broju odabranih harmonika, n, pri čemu je nepoželjno koristiti veliki broj harmonika samo kako bi uzeli u obzir i određenu dominantnu frekvenciju koja je višekratnik osnovne frekvencije.

Pokretanje i zaustavljanje turbostrojeva predstavljaju izazov za CFD zajednicu, kao i procesi promjene radne točke. Ovisno o vrsti stroja, promjena režima rada može trajati od nekoliko perioda rotora do nekoliko desetaka perioda, pri čemu bi simulacije takvih procesa bile iznimno skupe. Nadalje, promjena režima rada turbostroja je prijelazan proces tijekom kojeg se tok unutar turbostroja može značajno promijeniti, kao i maseni protok kroz stroj, ovisno o novom režimu rada. Također se može mijenjati i brzina vrtnje rotora kod određenih turbostrojeva, zbog čega stacionarne simulacije postaju gotovo neupotrebljive.

Modificirana verzija metode harmonijske ravnoteže je upotrebljena u ovom radu, kao kvazi-stacionarna metoda kako bi smanjila proračunsko vrijeme, ali i obuhvatila pojave u turbostroju prilikom promjene režima. Aperiodičan proces kao što je pokretanje ili zaustavljanje turbostroja prikaže se kao periodičan proces tako što se razmatraju istovremeno i zaustavljanje i pokretanje turbostroja kao jedan cjeloviti proces. Ukupni period se u tom slučaju sastoji od dvije komplementarne promjene režima, sa $2n + 1$ spregnutih simulacija kroz ukupni period zaustavljanja i pokretanja. Uzmu li se u obzir dvije različite vremenske skale perioda rotora i ukupnog novog perioda, potrebno je primijeniti metodu harmonijske ravnoteže s dvojnom strukturom, čija forma je predstavljena u ovom radu. Dvojna struktura sastoji se od $2n + 1$ simulacije metodom harmonijske ravnoteže za $2n + 1$ vremenskih trenutaka, pri čemu su simulacije međusobno spregnute dodatnim izvornim članom zaslužnim za "vanjsku" spregu, što znači da jednadžbe imaju dva izvorna člana proizašla iz metode harmonijske ravnoteže.

Validacija predložene metode

Validacija i verifikacija provedena je koristeći osnovne testne slučajeve iz područja turbostrojeva. Usporedba optimalne radne točke izvršina je u odnosu na konvencionalni tranzijentni rješavač i stacionarnu MRF metodu, no provedena je i usporedba s eksperimentalnim podacima. Analiza jedne radne točke izvršena je koristeći centrifugalnu pumpu ERCOFTAC, pri čemu su uspoređene fluktuacije tlaka kroz turbostroj te parametri rada turbostroja (snaga, efikasnost) s eksperimentalnim mjerenjima. Nadalje, usporedba metode

harmonijske ravnoteže s konvencionalnim tranzijentnim i stacionarnim metodama pokazala je da se metodom harmonijske ravnoteže može doći do značajnog rezultata po pitanju točnosti u samo dio proračunskog vremena potrebnog tranzijentnoj simulaciji. Usporedbom proračunskog vremena na istom računalu u jednakim uvjetima pokazano je da simulacija metodom harmonijske ravnoteže traje 30 puta kraće od tranzijentne simulacije.

Validacija metode harmonijske ravnoteže za primjenu kod pokretanja i zaustavljanja turbostrojeva provedena je na industrijski značajnom primjeru vodne turbine tipa Francis. Izvedena je simulacija cjelovitog perioda koji se sastoji od zaustavljanja turbine s optimalne radne točke te ponovnog pokretanja na optimalnu radnu točku, a dobiveni rezultati uspoređeni su s dostupnim eksperimentalnim mjerenjima. Usporedba je izvedena prateći snagu turbine kroz cijeli period, te fluktuacije tlaka u dvije mjerne točke neposredno nakon izlaza iz rotora. Primjenom metode harmonijske ravnoteže postignuta je visoka razina točnosti uz značajnu uštedu proračunskog vremena u odnosu na konvencionalne metode simulacije.

Zaključak

Temeljem provedenog istraživanja i predstavljenih rezultata, može se zaključiti da su postavljeni ciljevi istraživanja uspješno zadovoljeni i hipoteze istraživanja potvrđene. Iako je jasno da su učestale promjene radnih točaka kod turbostrojeva neizbježne, pojave koje se pritom javljaju skraćuju radni vijek stroja i ne mogu biti zanemarene. U svrhu istraživanja i razvoja turbostrojeva, računalna dinamika fluida predstavlja bitan alat u konstrukcijskom procesu, iako je kao alat za redovitu upotrebu još uvijek previše skup i spor, uz duge vremenske zahtjeve za dolazak do rezultata. U ovom radu je stoga predstavljena i validirana pojednostavljena metoda za analizu toka kod promjene radnog režima, koja bi mogla biti značajan korak prema praktičnom alatu u konstrukcijskoj fazi.

U sklopu budućih istraživanja trebalo bi proširiti metodu na preostale tipove problema i turbostrojeva, budući da niz procesa i pojava nisu uzeti u razmatranje u okviru ovog rada: efekt stlačivosti, razne ne-osnosimetrične

pojave poput izlaznog vrtloga kod Francis turbine, zatim turbostrojevi s mnogo stupnjeva, itd. Sve navedene pojave predstavljaju značajan utjecaj na tok u turbostroju, radni vijek i unutarnje pojave, te bi trebale biti razmotrene u okviru zasebnog istraživanja.

Ključne riječi:
metoda harmonijske ravnoteže, turbostroj, Fourierov razvoj, spektralna metoda, Francis, turbina

Contents

List of Figures

List of Tables

Chapter 1

Introduction

Summary

As CFD became a common tool in many design procedures, its further development in terms of accuracy and efficiency became the main target for researchers. In turbomachinery, CFD can provide good prediction of the flow quantities and features, but the high calculation time is the main drawback in using it as an everyday tool. Although the only alternative to CFD is the experiment, it accumulates additional production costs as well as production and labor time. Therefore, the intention to start using CFD regularly as a reliable design and optimisation tool should be the final goal.

Although majority of turbomachines have the same working principle and similar parts, distinctive groups can be formed by categorizing based on two key aspects: working medium and type of turbomachine. Working medium (fluid) behavior should be taken into account while performing calculation, thus an appropriate formulation of the physics model needs to be chosen. In case of water being the working medium, the CFD calculation can be performed using the incompressible flow models. Otherwise, if gas is a working medium, the decision to use compressible or incompressible formulation should be made depending on

the use. Common practice states that for problems with Mach numbers lower than 0.3 the incompressible models can be used. Depending on the type of machine, the fluid can be expanded (turbine) or compressed (compressor).

In terms of CFD, one of possible classifications of current methods can be based on temporal discretisation: time-accurate or transient methods, steady-state methods and spectral methods. Time-accurate methods are based on solving the problem in small intervals throughout the considered time with arbitrary temporal resolution. In terms of stability of explicit models, the limitation of the method is usually the maximal Courant-Friedrichs-Levy (CFL) number of 0.5, which for the high-speed machines results in extremely small time steps and long calculation times. Due to high blade tip velocity and small cells in order to capture the boundary layer, the CFL number condition is usually satisfied only for extremely small time steps. However, the major advantage is usually good temporal resolution as there are many time steps through investigated period, with good ability to capture the appearing phenomena and flow patterns, instabilities and wake propagation.

If steady state simulation is performed, the flow is assumed unchanged throughout the time and the result represents the steady flow condition where no instabilities appear. However, due to rotation in turbomachinery the flow is not steady, but it is repeating with the rotational frequency. In order to obtain the steady state, a modified equation set is used: accounting for centrifugal and Coriolis forces rather than rotating the rotor mesh.   Such steady state simulation provides reasonable insight into flow field, without transient flow features, although the effect of rotation is achieved. Furthermore, this kind of simulation is often referred to as a *frozen rotor* approach, resembling the snapshot of a flow field within a turbomachine. This approach offers reasonable accuracy for general flow field and integral quantities (power, efficiency, etc.), with additional benefit of requiring little CPU time. However, rotor-stator interaction and wake propagation in multistage turbomachinery will not give relevant results.   The assumption that there is no contribution from the temporal term is not correct, which is the main reason of unrealistic wake propagation.

Spectral methods can be used for turbomachinery simulations as well, due

to its periodic nature. With time-accurate methods and steady state methods the equations are solved in time domain, whereas spectral methods provide a transformation between frequency and time domain, therefore evaluation can be performed in any of the two domains, depending on the approach. The Harmonic Balance method is a commonly used spectral method for turbomachinery, with different possible solution procedures for evaluation either in time or frequency domain. Variants of Harmonic Balance method will be discussed in detail in Section 2.1. The Harmonic Balance method allows solving a number of coupled steady state equations, where coupling accounts for temporal change as each equation solves for its unique time instant. This means solving a number of equations, which are iterated to convergence in a steady state manner. The result obtained is valid for the whole representative period $T = \frac{1}{f}$, and can be perceived as a situation when the periodic steady state is reached. In terms of accuracy and CPU time, it can be placed between the *frozen rotor* and time-accurate simulations. Depending on the number of harmonics prescribed, both accuracy and CPU time are affected, thus yielding the solution closer to either of the two methods. The Harmonic Balance can offer significant savings in terms of CPU time compared to time-accurate simulations, on account of reduced accuracy. This thesis is dealing mostly with the Harmonic Balance method, while other methods are introduced for comparison purposes only.

1.1   Thesis Statement

Periodic flows are common in scientific and industrial studies such as rotating machinery, wave-like phenomena, various flows induced by periodic boundary conditions and different periodic body motions (wing oscillations, moving valves, etc.). For such problems transient simulations are used, yielding long CPU time with satisfying accuracy. In order to obtain periodic results and neglect initial transients resulting from simulation start and initialization, a number of periods need to be simulated before reaching the scientifically significant result. The need to reduce simulation CPU time, while still preserving periodic flow features motivated the development of new methods. Harmonic Balance [1, 2] is such a method, developed specially for periodic problems with prescribed harmonic

motion.

The Harmonic Balance method is a quasi-steady state method, incorporating characteristics both of steady state and transient approach. As opposed to conventional steady state methods, the benefit of Harmonic Balance is the ability of capturing transient flow features, at a cost of moderate increas of CPU time. Steady state methods yield single rotor position solution, without the ability of resolving the transient instabilities, therefore this approach cannot be used for obtaining local instabilities or wake propagation. On the other hand, compared to conventional transient simulation, Harmonic Balance offers a significant CPU time reduction [3] with comparable accuracy.

The main idea behind the Harmonic Balance method was to make use of periodicity to reduce the computational time required to compute both small disturbances and large amplitude unsteady flows. Both spatial and temporal periodicity were tackled by Hall and Crawley [4], and later by Clark and Hall [5] by using the time-linearised methods. The assumption was that the unsteady disturbance is small compared to the mean flow, therefore led to linearising the Navier-Stokes equations about a non–linear steady or mean operating conditions. However, the main drawback was the inability to model dynamically non–linear effects. During that time He developed the method initially as a periodic boundary condition [6], which was later extended by He and Ning [7] for application to solving the two-dimensional Navier-Stokes equations. Instead of solving a single transient equation, using the Harmonic Balance treatment a set of coupled steady state equations is obtained by replacing the temporal derivation term with a coupling source term. By solving this set of equations, the flow field within a representative period is obtained.

Recently, Harmonic Balance method has been extensively developed in numerous application areas. Other than oscillating airfoils and wings presented by Dufour et al. [8] and Thomas et al. [9, 10], also aeroelastic flutter and limit cycle oscillations [11, 12] were the topic of many researchers. Hall et al. [13] used complex geometries such as turbines and other rotor-craft to extend and demonstrate the Harmonic Balance capabilities. Additionally, Hall et al. proposed three forms of Harmonic Balance, of which the time-spectral form of Harmonic Balance is the most convenient one for solving.

As the Harmonic Balance method was developed for use in turbomachinery, Gopinath et al. [14] stress the need for involving additional frequencies within the basic Harmonic Balance method to capture different length and time-scales appearing in the machine. Guédeney et al. [15] develop the multiple frequency approach for simulations of multistage turbines where frequency changes in each stage due to a different number of blades in previous and later stages. Furthermore, Guédeney et al. [16] present the two algorithms for non-uniform time sampling in multiple frequency approach of Harmonic Balance, as different frequencies mean solving non-matching time instants in two regions. Furthermore, Ekici and Hall presented Hall's Harmonic Balance technique extended for modelling unsteady flows in multistage turbomachinery with blade excitations at multiple frequencies [17, 18, 19].

He [20] addressed the stability and convergence issues of the Harmonic Balance method, followed by Huang and Ekici [21] who introduced time spectral viscosity as an additional stabilisation factor. Addition of time spectral viscosity eliminates aliasing errors and ensures the convergence towards the physical solution. In order to avoid stability issues at more complex geometric configurations, as reported by Hall et al. [1], the strategies for implementation of implicit Harmonic Balance algorithm are investigated in [22]. Moreover, Sicot et al. [23], Woodgate and Badcock [24], and Su and Yuan [25] have proposed different implicit techniques for the Harmonic Balance method which involve the development of new implicit algorithms. Thomas et al. [23] presented the more favourable approach not requiring new algorithm development, using the two-step approximate factorization approach. Anatheaume and Corre [26] implemented implicit Harmonic Balance method using numerical implicit strategies and block relaxation.

Researchers interested in simulations of turbomachinery are currently undertaking significant research efforts, but such computations mostly deal with design-point performance of the turbomachines. Performance at off-design points cause local instabilities which may propagate and lead to choking of the machine or other undesirable flow-related problems in off-design conditions. In terms of early computational fluid dynamics (CFD) studies, He [27] simulated the growth of both short and long length-scale disturbances. At about the same

time, Hendricks et al. [28] developed a nonlinear compressible model and successfully simulated the inception and growth of the disturbance up to complete choking of turbomachine.

Further CFD work was carried out by Choi et al. [29], who simulated the stalling and unstalling processes. Their results of stalling behavior of the fan agree with common experimental experience. Most recently, Dodds and Vahdati [30, 31] have used CFD to interpret experimental measurements from an engine compressor. They showed that the compressor was operating with two disturbances rotating independently in the first and second stages of the machine. This was also confirmed recently by Houde et al. [32]. Usually, it takes between 10 and 30 periods from instability inception up to complete choking of the turbomachine, depending on the propagation speed, which is different from the rotor rotation speed [33]. Pullan et al. [34] showed that the spike-type stall inception begins near the blade tip due to high local incidence. The separation gives rise to shed vorticity from the leading edge, which develops into a trumpet-shaped vortex stretching between the casing and the suction side of the blade. By further motion of the vortex from suction side of one blade to pressure side of the next blade, the propagation of instability occurs. After the vortex reached the next blade, new vortices appear, the whole process repeats and eventually the choking occurs. During change of operating point the turbomachine undergoes through a number of operating conditions which are not optimal, i.e. off-design conditions. During this process the aforementioned phenomena may appear, yielding unwanted effects. Furthermore, the oscillating power demand often requires switching between operating points, making the unwanted phenomena appear more often than it was considered in the design phase. This means that turbomachinery requires design procedures with flexibility in mind, such that stable operation can be obtained in a variety of operating points [35].

A field unrelated to turbomachinery was also explored and will be briefly presented here. Although the method presented in this work was initially developed mainly for single-phase periodic problems such as turbomachinery, the author and his colleagues saw the opportunity and ability of the method to be used in the problems of naval hydrodynamics and extended its application

accordingly. In naval hydrodynamics the spectral methods present no novelty as this approach is used for several decades [36], but such methods offer no accurate solution to calculate the viscous drag force of ships reliably so far. Therefore, this has yielded several publications to which the reader is referred for more information related to this topic [37, 38, 39, 40].

1.2   Approach

This thesis describes the development and implementation of a numerical model, as well as on the validation of the implemented model.   The implementation includes the development of the mathematical model adapted to finite volume framework. The main part of the mathematical model consists of the Harmonic Balance method for periodic flows, and its specialisation for use in turbomachinery, as well as the development of additional tools for pre-processing and post-processing of Harmonic Balance simulation results.

The Harmonic Balance method and the additional tools are implemented in the CFD software OpenFOAM [41], specifically in a community driven fork `foam-extend`, written in C++ programming language. Special attention was given to the standard and the organisation of the OpenFOAM library in order for the final Harmonic Balance solver to be fully compatible with the toolkit, but also become a general turbomachinery solver which is simple for maintenance and improvements.

Main phases of research are:

a) Development of the basic Harmonic Balance method.
b) Specialisation of the Harmonic Balance method for use in turbomachinery followed by development of multiple frequency version.
c) Validation and verification of the method.
d) Extension of the method for change of operating point.
e) Application of the method for the off-design points and analysis of flow instabilities.

The Harmonic Balance method is developed for periodic problems, whereas in this research it will be extended for use in turbomachinery and investigation of

the start-up and shut-down conditions. The Harmonic Balance method solves
the Navier-Stokes equations in the pseudo-spectral domain and as a result the
flow field within a representative period is obtained. Prior to discretisation of
the equations, the transient Navier-Stokes equations need to be transformed into
a quasi-steady state equations in form of the Harmonic Balance method. This
yields a set of quasi-steady state equations instead of a single transient equation.
The size of the set depends on the number of harmonics, n, and the number of
solved equations is $2n + 1$.

The Harmonic Balance method has not previously been implemented in the
framework of the open source software OpenFOAM, which has been performed
within the scope of this study. Implementation required development of
mathematical model suitable for C++ coding environment along with
consideration on function optimisation and coding simplicity. Adhering to the
OpenFOAM standard, the accompanying libraries have been developed as well,
handling the $2n + 1$ velocity fields, pressure fields, and other variables that
might be used. These libraries include thermophysical models, turbulence
models, finite volume dynamic mesh library, transport models and additional
post-processing tools for field reconstruction, initialization, etc. The main
Harmonic Balance characteristic is that instead of solving one steady equation
or one transient equation which propagates through time, a number of time
instants are solved simultaneously. For n harmonics (chosen by user at the
run-time), $2n + 1$ equidistant time instants are calculated, thus forming the
complete period. For this reason each of the $2n + 1$ time instants requires its
own set of Navier-Stokes equations, turbulence treatment and therefore its own
variables, yielding $2n + 1$ of each variable.

At the point of successful implementation of the Harmonic Balance method in
the finite volume framework, the additional functionality was developed to allow
its use for multistage turbomachinery. The basic form of Harmonic Balance
method takes only one frequency into account, therefore a variant capable of
taking into account a pair of frequencies (rotor frequency and stator frequency)
was developed.

The Harmonic Balance method in its general form can be used for various
periodic problems where dominant frequency is known in advance. To account

for two different dominant frequencies appearing in rotor and stator, a modified version has been developed.   While running single stage turbomachinery simulations, at least two dominant frequencies are taken into account, with the ability to account for higher harmonics as well. Furthermore, solvers for static single-domain problems and for multiple-domain problems with moving mesh are implemented, allowing solution of problems such as pitching airfoils (single dominant frequency) or compressors (several dominant frequencies).   As opposed to regular boundary conditions, the Harmonic Balance method requires boundary conditions aware of $2n + 1$ time instants in which the boundary values can differ Figure 1.1.

(a) Transient simulation mesh rotation,

(b) Inlet velocities at different time steps in Harmonic Balance.
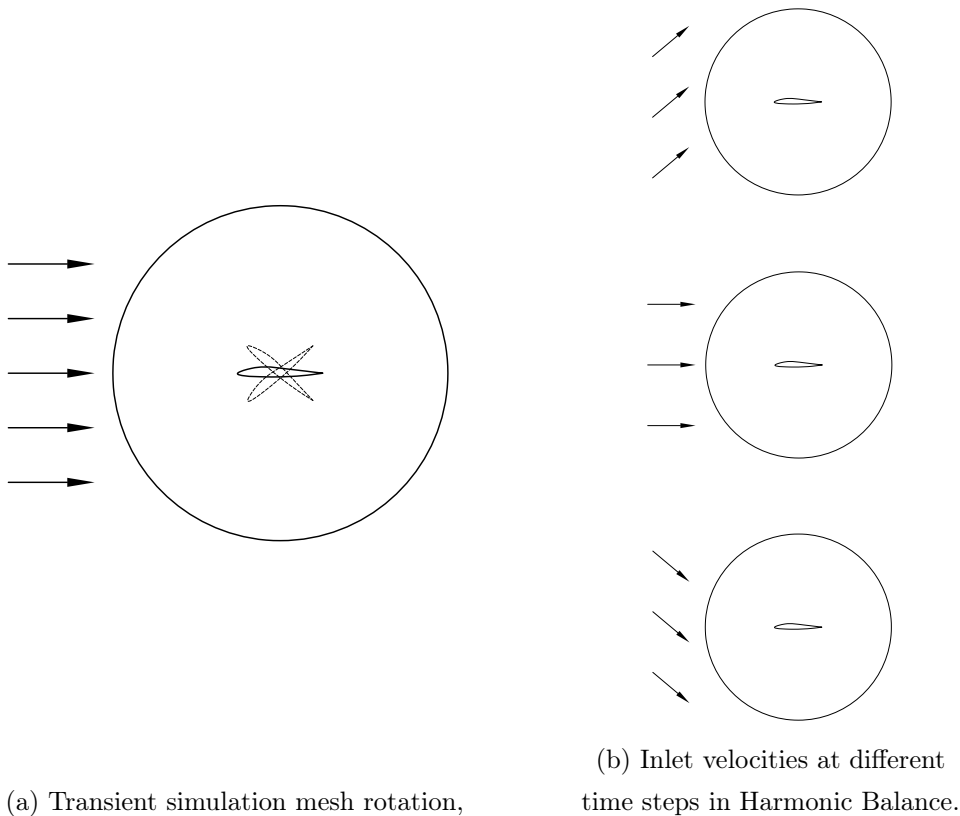
Figure 1.1: Boundary condition treatment
in the transient and the Harmonic Balance simulation.

Some periodic problems can be modelled simply by prescribing fluctuating boundary conditions, such as opening and closing inlet or rotating the inlet velocity direction. Having in mind that the Harmonic Balance method is based

on the Fourier expansion, it is clear that by obtaining the solution at discrete time instances, the whole period can easily be reconstructed. Utilities for period decomposition and reconstruction have been developed within this study, allowing analyses of the whole period, rather than just selected time instants, neglecting the effect of rate-of-change.

The implemented method with accompanying libraries is validated using several canonical turbomachinery test cases. Validation of basic single frequency Harmonic Balance method has been performed and demonstrated in [42]. Simple harmonic wave impulses were imposed at the inlet and successfully recovered through the domain. The increasing level of accuracy with increasing number of harmonics was presented as well. Validation of the multiple frequency approach is performed in this study using the ERCOFTAC centrifugal pump test case. The Harmonic Balance results are compared against the transient approach simulation, steady-state results and available experimental data. Verification is performed by varying the number of used harmonics, where it is expected for the results to converge to a single solution with the increase of harmonics. Good agreement of results allowed proceeding with the development of the Harmonic Balance method for turbomachinery performance at off-design points: start-up and shut-down simulations.

Analysis of the instability inception should give insight into suppression methods and procedures for unstalling. In most cases, it takes between 10 and 30 periods from stall inception to fully choked turbomachine, and such simulations are very CPU time demanding. The Harmonic Balance method should obtain the solution in significantly less time, while still offering satisfactory accuracy.

Having in mind that dominant frequencies in turbomachinery depend on number of blades in rotor and stator, rotational speed, number of stages, etc. it is possible to choose the dominant frequencies in advance. The accuracy of the Harmonic Balance method depends on the number of harmonics, n, where it is inconvenient to use a large number of harmonics in order to take into account higher frequency which is a multiple of the base frequency. Number of solved equations scales with $2n + 1$, therefore including each additional harmonic involves solving the two additional sets of equations. For one harmonic this

means solving 3 sets of governing equations; if increased accuracy is required, for instance with $n = 5$ harmonics, 11 sets of equations are solved. The user should be sufficiently familiar with the method and problem at hand to choose the appropriate number of harmonics, so that satisfying level of accuracy is obtained without the unnecessary CPU time overhead.

The hypotheses that present the motivation behind this work are the following:

- Implementation of the Harmonic Balance method based on the finite volume framework, which casts periodic problems into spectral space, thus making it quasi-steady state would provide a general method for assessing turbomachinery integral parameters and their oscillations through time.

- The developed numerical model will contribute to significant reduction of computational time of turbomachinery simulations compared to available conventional methods.

- The nested approach of the Harmonic Balance method provides a framework for turbomachinery start-up and shut-down simulations, giving insight into integral values and flow patterns through regime change, while being significantly CPU less demanding compared to available conventional methods.

1.3   Present Contributions

The objective of this study is to introduce a new numerical model for turbomachinery simulations, dealing mainly with investigation of regime change and focus on start-stop procedures. The model is implemented in the open source software with the complete framework offering support for multistage turbomachinery. Previous work related to the Harmonic Balance method implementation has been extensively broadened with number of tools and accompanying utilities along with the main method. The work behind this thesis makes the following specific contributions to the field of CFD related to turbomachinery applications:

1. The time–spectral form of the Harmonic Balance is derived in terms of mathematical model and finite volume discretisation. Segregated pressure–velocity equation set for incompressible, turbulent, viscous, single phase flows is used, as well as segregated approach to coupling of the Harmonic Balance equations.

2. Implementation of the Harmonic Balance method within the community driven fork `foam-extend` of the open source library OpenFOAM. Implementation included development of a complete Harmonic Balance library for both single and multistage turbomachinery at specified operating condition. The implementation is made completely general, so that number of resolved harmonics, n, is user-chosen at the run-time and can be adapted to the problem at hand.

3. Extension of existing models to provide support for the Harmonic Balance method has been performed. Dynamic mesh motion models have been adapted for mesh rotation between time instants depending on the number of harmonics, while taking into account the actual mesh flux and wall velocity. Furthermore, the turbulence and transport models have been extended to account for a set of variables, each for one time instant, in order to comply with the Harmonic Balance structure. A number of pre-processing and post-processing tools have been developed as well, of which some include reconstruction utility, so that the solution at any point in time can be obtained instantly, utility for initial boundary condition setup so that it provides a harmonic function through a complete period, etc.

4. Major part of the presented work includes support for regime change simulations, particularly shut-down and start-up simulations. The Harmonic Balance method has not been used for such simulations so far, while promising results are presented in this work. In general, any change

from operating point 1 to operating point 2 can be performed, although the focus of this study was on validation of the proposed procedure for shut-down and start-up of turbomachinery. Although it can be tackled with a variety of tools and methods, this area presents a number of challenges in numerical sense and for specific applications the proposed method offers a notable solution.

1.4   Outline

In the following parts of this thesis, the Harmonic Balance method is introduced and presented with accompanying mathematical derivation. This is followed by validation and comparison with the experiment for a single operating point using the ERCOFTAC centrifugal pump test case. Finally, the turbomachinery start-stop behavior is explored, as well as the Harmonic Balance methods for start-stop simulation which is followed by a validation using a simple 2D test case and a Francis-99 turbine for which experimental data exist.

Chapter 2 presents the mathematical model of the work, including the governing equation sets, Harmonic Balance derivation and treatment of the governing equations, with discussion on types of available Harmonic Balance forms. Numerical model is outlined in Chapter 3, dealing with the discretisation of the governing equations in the Harmonic Balance form and algorithm for segregated pressure-velocity coupling. Sections 3.3 and 3.4 introduce the numerical tools developed for turbomachinery simulations, namely tools for rotating domain treatment and interface treatment in order to couple the two neighbouring regions or make use of spatial periodicity with the aid of periodic boundary conditions.

Start-up and shut-down concerns are explained in Chapter 4, dealing with start-stop procedures in general and covering some of the effects appearing during regime change. Furthermore, challenges for the CFD are presented and the Harmonic Balance approach is proposed. The results of the Harmonic Balance method for single operating point is presented in Chapter 5, comparing the time-accurate, steady state and the Harmonic Balance results, as well as comparing the Harmonic Balance results with experiment. The validation of a

start-stop Harmonic Balance is presented in Chapter 6, performed on a simple
test case for a preliminary validation, followed by a real Francis-99 turbine in
Chapter 7 for which the complete shut-down and start-up processes are
investigated and the Harmonic Balance is compared with the experiment. The
work is summarised in Chapter 8 with suggestions for future work.

Chapter 2

Mathematical Model

Summary

In this chapter the mathematical model of the Harmonic Balance method is established. Along with governing equations which are presented in the Section 2.3, the discussion on different formulations of the Harmonic Balance method is given. The focus of the discussion is on the choice of the most practical formulation, mainly in terms of practicality from user point of perspective and efficiency in terms of CPU consumption and performance.

The choice of the Harmonic Balance formulation is followed by the derivation of a mathematical model for incompressible viscous turbulent flow, with segregated approach to pressure-velocity coupling. The derivation is entirely general, assuming no specific number of harmonics used or their frequency. The derived equations can be used for any variable, therefore momentum equation, turbulence equations or any other equation can be modelled in the Harmonic Balance fashion. The implementation is made simple as well, following the practice of OpenFOAM coding style, which allows simple future modifications of steady or transient equations into the Harmonic Balance form.

2.1 Harmonic Balance Forms

In this section several forms of the Harmonic Balance formulations are presented. The formulations have been reviewed by several authors previously, such as Hall et al. [43] or He [20], but will be presented here for completeness and clarification of the chosen approach. The main difference in the proposed formulations is in the treatment of temporal term and whether its evaluation is performed in the frequency or time domain. Three formulations are presented: the classic Harmonic Balance; the non–linear frequency domain Harmonic Balance; and spectral Harmonic Balance.

2.1.1 Classic Harmonic Balance

The classical approach to the Harmonic Balance method was proposed by Hall [1], by modelling the unsteady non–linear Euler equations and pseudo-marching it through time. The equations are developed into the Harmonic Balance form using the Fourier expansion and marched in pseudo time to convergence. If $f(x)$ is a function of the real variable x and it is integrable on the interval $[x_0, x_0 + P]$, where P is the repeating period of $f(x)$, then the Fourier expansion reads:

$$f(x) = a_0 + \sum_{n=1}^{\infty} \left(a_n \cos\left(\frac{2\pi n x}{P}\right) + b_n \sin\left(\frac{2\pi n x}{P}\right) \right), \qquad x \in [x_0, x_0 + P]. \quad (2.1)$$

Because of periodicity of the function, the function repeats with period P before and after the interval $[x_0, x_0 + P]$, consequently the expansion is invariant of the interval chosen. Coefficients a_n and b_n are called Fourier coefficients and can be calculated if $f(x)$ is known:

$$
\begin{aligned}
a_n &= \frac{2}{P} \int_{x_0}^{x_0+P} f(x) \cdot \cos\left(\frac{2\pi n x}{P}\right) \mathrm{d}x, \\
b_n &= \frac{2}{P} \int_{x_0}^{x_0+P} f(x) \cdot \sin\left(\frac{2\pi n x}{P}\right) \mathrm{d}x.
\end{aligned}
\qquad (2.2)
$$

However, in practical use the expansion has to be finite, therefore the basic concept is to represent the conservation variables by a truncated Fourier series:

$$\mathbf{u}(t) = \mathbf{u}_0 + \sum_{i=1}^{n} \mathbf{u}_{S_i} \sin(i\omega t) + \mathbf{u}_{C_i} \cos(i\omega t)\,. \tag{2.3}$$

In Equation 2.3 the $\mathbf{u}_{C_i}$ and $\mathbf{u}_{S_i}$ are the Fourier coefficients of the i-th harmonic for the sine and cosine term. The Fourier form of conservation variable, Equation 2.3 is substituted into momentum equation, eventually leading to a set of $2n + 1$ equations: n for cosine terms, n for sine terms and one for mean value.

Furthermore, the pseudo time τ is introduced in order to use conventional time marching methods to solve steady flow problems. The pseudo-time term of each equation is driven to zero, yielding the steady state solution.

As stated by Hall [43], for simple problems the solution to the obtained equation set is possible, however, with choice of larger number of harmonics n the computational cost grows rapidly and scales by a factor of n^3. Furthermore, in case of turbulent flow the complexity grows as well which is mainly why this form has not been used extensively in CFD.

2.1.2   Non-linear Frequency Domain Harmonic Balance

The non-linear frequency domain form of the Harmonic Balance method was developed and widely used by McMullen et al. [44, 45]. By transforming the convection and diffusion fluxes into the time domain, the efficiency of the method is increased compared to classic Harmonic Balance.

The methodology of the non-linear frequency domain Harmonic Balance is based on evaluating residuals in frequency domain, as well as the conservation variable. However, due to the non–linearity of the residual operator, the frequency domain residual cannot be computed directly from the conservation variable in the frequency domain. To alleviate this, the conservation variable has to be transformed into physical space using the inverse fast Fourier transform, yielding conservation variable in time domain in all of the $2n + 1$ time instants. The residual operator is then calculated in the time domain and further transformed into frequency domain. The new frequency domain residual is used to obtain

the new approximate of the conservation variable in frequency domain and the cycle repeats. The computational cost of this method is proportional to $(2n + 1)\log(2n + 1)$, where n is the number of solved harmonics. Thus, the proposed method is more efficient compared to classical Harmonic Balance approach.

2.1.3   Spectral Harmonic Balance

The final form of the Harmonic Balance method is the time-spectral formulation. This formulation is similar to the non-linear frequency domain form of the Harmonic Balance, with key difference being the domain in which the conservation variables are solved for. Here, the variables represent the solution in time domain equally distributed over one time period. Therefore, such equations represent mathematically steady problems as there is no time derivation term. However, the obtained equations are mutually coupled via an additional source term and the coupling term behaves as the time derivation term.

Computational efficiency of such an approach is similar to the efficiency of the non-linear frequency domain Harmonic Balance. In terms of memory requirements, this approach requires $2n + 1$ times more memory, as each conservation variable is stored at $2n + 1$ time instants. Therefore, the simulation result will be the flow fields in $2n + 1$ time instants, rather than just a single variable set. Although by reconstruction within the scope of a Fourier expansion a complete period can be obtained, i.e. any point in time regardless of the calculated time instants.

2.2   The Harmonic Balance Derivation

In this study the time-spectral form of the Harmonic Balance method is used. The derivation of the method is presented in the sequel, which will be applied to the governing equations presented in Section 2.3.

The main assumption based on which the Harmonic Balance method is formulated is that the flow is periodic in time. Such assumption allows utilizing approximation of the periodic function by superposing a number of harmonic

functions. The lowest order of approximation is the mean value, to which sine and cosine functions can be added to obtain fluctuation. Approximation series based on sum of harmonic functions is called the Fourier expansion. If the expansion contains infinite number of terms, the series is no longer an approximation. However, in common practice it is impossible to have infinite number of terms, therefore the error of the approximation is equal to the sum of uncounted terms. In most cases the value of each following term is smaller compared to the previous one, resulting in first several terms consisting the majority of the result and being the most significant. Higher harmonics account for the effects appearing with the frequency much higher than the dominant, base frequency and therefore are needed to capture fine instabilities occurring during the base period. If conservation variables are expanded in Fourier series with arbitrary number of harmonics n, periodic behaviour is assumed. Moreover, for completeness the whole derivation will be presented, with reference to [40, 42, 46].

Under assumption that the problem to be analysed is periodic, with its transport described with a convection-diffusion equation:

$$\frac{\partial \mathcal{Q}}{\partial t} + \mathcal{R} = 0\,, \tag{2.4}$$

where $\mathcal{R}$ stands for convection, diffusion and source/sink terms:

$$\mathcal{R} = \nabla_{\bullet}(\mathbf{u}\mathcal{Q}) - \nabla_{\bullet}(\gamma\nabla\mathcal{Q}) - S_{\mathcal{Q}}\,. \tag{2.5}$$

Here, $\mathbf{u}$ is the transport velocity and γ is diffusivity, the primary variable $\mathcal{Q}$ can be written as a Fourier series with n harmonics:

$$\mathcal{Q}(t) = Q_0 + \sum_{i=1}^{n} Q_{S_i}\sin(i\omega t) + Q_{C_i}\cos(i\omega t)\,. \tag{2.6}$$

As a general note, the notation of $\mathcal{Q}$ is used for the time domain, and Q for the frequency domain. The Fourier expansion for $\mathcal{R}$ is analogous to one in Eqn. (2.6),

with Q substituted by $\mathcal{R}$:

$$\mathcal{R}(t) = R_0 + \sum_{i=1}^{n} R_{S_i} \sin(i\omega t) + R_{C_i} \cos(i\omega t)\,. \tag{2.7}$$

One harmonic in the Fourier expansion refers to a sum of a single sine and cosine term. For only nth harmonic part of the solution it can be written:

$$Q_n = Q_{S_n} \sin(n\omega t) + Q_{C_n} \cos(n\omega t)\,. \tag{2.8}$$

Inserting the time derivative of Q from Eqn. (2.6), and the Fourier expansion of $\mathcal{R}$ into the original transport equation, Eqn. (2.4), yields:

$$\sum_{i=1}^{n} \left[i\omega \left(Q_{S_i} \cos(i\omega t) - Q_{C_i} \sin(i\omega t)\right) + \left(R_{C_i} \cos(i\omega t) + R_{S_i} \sin(i\omega t)\right)\right] = R_0\,. \tag{2.9}$$

Eqn. (2.9) represents the scalar transport equation in the frequency domain, where Fourier coefficients Q_{S_i} and Q_{C_i} are unknown. Note that each Q and R are fields, i.e. they represent Fourier decomposition coefficients for each point in space, assuming the same choice of base frequency. Grouping the coefficients with the same harmonic part in Eqn. (2.9) yields $2n + 1$ equations:

$$-i\omega Q_{C_i} + R_{S_i} = 0 \rightarrow n \text{ equations for sine parts, for } i = 1\ldots n\,,$$
$$R_0 = 0 \rightarrow 1 \text{ equation for mean part,} \tag{2.10}$$
$$i\omega Q_{S_i} + R_{C_i} = 0 \rightarrow n \text{ equations for cosine parts, for } i = 1\ldots n\,.$$

Eqn. (2.10) can be written in a more compact, matrix format:

$$\omega \boldsymbol{A}\,\boldsymbol{Q} + \boldsymbol{R} = \boldsymbol{0}\,, \tag{2.11}$$

where:

$$
\boldsymbol{A}=\begin{bmatrix} & & & & 0 & -1 & & & & \\ & & & & 0 & & -2 & & & \\ & & 0 & & . & & & -3 & & \\ & & & & . & & & & \ddots & \\ & & & & . & & & & & -n \\ 0 & 0 & \cdots & 0 & 0 & 0 & \cdots & 0 & 0 & 0 \\ 1 & & & & . & & & & & \\ & 2 & & & . & & & & & \\ & & 3 & & . & & & 0 & & \\ & & \ddots & & 0 & & & & & \\ & & & n & 0 & & & & & \end{bmatrix}, \; \boldsymbol{Q}=\begin{bmatrix} Q_{S_1} \\ Q_{S_2} \\ Q_{S_3} \\ \vdots \\ Q_{Sn} \\ Q_0 \\ Q_{C_1} \\ Q_{C_2} \\ Q_{C_3} \\ \vdots \\ Q_{C_n} \end{bmatrix}, \; \boldsymbol{R}=\begin{bmatrix} R_{S_1} \\ R_{S_2} \\ R_{S_3} \\ \vdots \\ R_{Sn} \\ R_0 \\ R_{C_1} \\ R_{C_2} \\ R_{C_3} \\ \vdots \\ R_{C_n} \end{bmatrix}. \quad (2.12)
$$

Solving Eqn. (2.11) would yield a set of Fourier coefficients $\boldsymbol{Q}$ for $\mathcal{Q}(t)$. However, such a procedure is not favourable since $\boldsymbol{R}$ contains differential operators that would need to be transformed into the frequency domain.

We proceed by defining a matrix representation of Discrete Fourier Transform (DFT) in order to easily switch between time and frequency domain in the discrete space. In order to have a unique one–to–one mapping, we define the discrete time-domain vector as:

$$
\boldsymbol{\mathcal{Q}}^T = \begin{bmatrix} \mathcal{Q}_{t_1} & \mathcal{Q}_{t_2} & \mathcal{Q}_{t_3} & \cdots & \mathcal{Q}_{t_{2n+1}} \end{bmatrix}, \tag{2.13}
$$

where t_n stands for time instants throughout the period T:

$$
t_i = \frac{iT}{2n+1}, \quad \text{for } i = 1\ldots 2n+1. \tag{2.14}
$$

DFT from the time-domain vector $\boldsymbol{\mathcal{Q}}$ to the frequency domain vector $\boldsymbol{Q}$ can be written in matrix form:

$$
\boldsymbol{Q} = \boldsymbol{E}\,\boldsymbol{\mathcal{Q}}, \tag{2.15}
$$

where square matrix E takes the following form:

$$E = \frac{2}{2n+1} \begin{bmatrix} \sin(\omega t_1) & \sin(\omega t_2) & \ldots & \sin(\omega t_{2n+1}) \\ \sin(2\omega t_1) & \sin(2\omega t_2) & \ldots & \sin(2\omega t_{2n+1}) \\ \vdots & \vdots & & \vdots \\ \sin(n\omega t_1) & \sin(n\omega t_2) & \ldots & \sin(n\omega t_{2n+1}) \\ \frac{1}{2} & \frac{1}{2} & \ldots & \frac{1}{2} \\ \cos(\omega t_1) & \cos(\omega t_2) & \ldots & \cos(\omega t_{2n+1}) \\ \cos(2\omega t_1) & \cos(2\omega t_2) & \ldots & \cos(2\omega t_{2n+1}) \\ \vdots & \vdots & & \vdots \\ \cos(n\omega t_1) & \cos(n\omega t_2) & \ldots & \cos(n\omega t_{2n+1}) \end{bmatrix}. \tag{2.16}$$

Multiplying Eqn. (2.15) with E^{-1} from the left, one obtains mapping from the frequency domain to the time domain:

$$\mathcal{Q} = E^{-1} Q, \tag{2.17}$$

where the inverse transformation matrix reads:

$$E^{-1} = \begin{bmatrix} \sin(\omega t_1) & \ldots & \sin(n\omega t_1) & 1 & \cos(\omega t_1) & \ldots & \cos(n\omega t_1) \\ \sin(\omega t_2) & \ldots & \sin(n\omega t_2) & 1 & \cos(\omega t_2) & \ldots & \cos(n\omega t_2) \\ & & & \vdots & & & \\ & & & \vdots & & & \\ \sin(\omega t_{2n+1}) & \ldots & \sin(n\omega t_{2n+1}) & 1 & \cos(\omega t_{2n+1}) & \ldots & \cos(n\omega t_{2n+1}) \end{bmatrix}. \tag{2.18}$$

Having defined the forward and backward transformation matrices, E and E^{-1}, respectively, we proceed to formulate the frequency domain scalar transport equation. Inserting the Eqn. (2.15) into Eqn. (2.11) yields the frequency domain

equation, expressed via the time domain vector $\boldsymbol{\mathcal{Q}}$:

$$\omega \boldsymbol{A}\,\boldsymbol{E}\,\boldsymbol{\mathcal{Q}} + \boldsymbol{E}\,\boldsymbol{\mathcal{R}} = \boldsymbol{0}\,, \tag{2.19}$$

where the same transformation has been applied to $\boldsymbol{R}$ and $\boldsymbol{Q}$.

While the (linear) equations could be solved in this form, evaluating sources and fluxes in the frequency domain is computationally expensive and inconvenient [1]. We shall therefore proceed to transform the equations back to the time domain. To achieve this, Eqn. (2.19) is multiplied with $\boldsymbol{E}^{-1}$ from the left, yielding:

$$\omega \boldsymbol{E}^{-1}\,\boldsymbol{A}\,\boldsymbol{E}\,\boldsymbol{\mathcal{Q}} + \boldsymbol{\mathcal{R}} = \boldsymbol{0}\,. \tag{2.20}$$

The resulting equation represents a temporally–coupled set of $2n+1$ steady state problems, analogous to the initial problem, Eqn. (2.4).

Comparing Eqn. (2.20) with the original scalar transport equation, Eqn. (2.4), two important features may be observed:

- $\mathcal{R}$ has been replaced with its discrete counterpart $\boldsymbol{\mathcal{R}}$, indicating that the solution is sought at a fixed number of discrete time instants only. The number of discrete time instants is defined with a specified number of harmonics n, as indicated in Eqn. (2.13).

- The solving variables are no longer continuous in time, but are discrete, representing the solution in each of the time instants.

- The time derivative term has been replaced by terms coupling the solutions at different time steps. This is equivalent to evaluating the time derivative of a harmonic signal via $2n+1$ uniformly spaced temporal snapshots, including a mean (steady) solution, where the effect of temporal distance is taken into account by the coefficients P_l (Equation 2.25), as demonstrated in Figure 2.1. It can be seen that coefficients in time instants closer to the time instant of interest are larger (in absolute value) than those farther away. As the investigated signal is periodic, the coefficients are the same, symmetrically reducing in positive and negative time direction. Therefore

the shift of three time instants in the positive time direction can be seen as a shift of four time instants in the negative time direction due to periodicity.

- The coupling term refers to temporal-coupling as it replaced the time derivative term and accounts for temporal effects. This is not related to any other forms of coupling, such as pressure-velocity coupling. Therefore, the treatment of the source term can be explicit or implicit regardless of the pressure-velocity coupling.
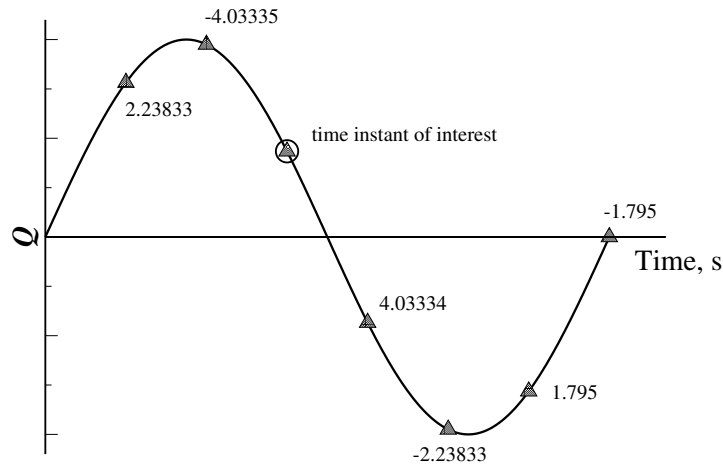
Figure 2.1: Time instants and Fourier coefficients P_l for 3 harmonics.

The matrix $\boldsymbol{E}^{-1}\,\boldsymbol{A}\,\boldsymbol{E}$ pre–multiplying $\boldsymbol{\mathcal{Q}}$ in Eqn. (2.20) has the following form:

$$
\boldsymbol{E}^{-1}\,\boldsymbol{A}\,\boldsymbol{E} = \frac{2}{2n+1}
\begin{bmatrix}
0 & P_1 & P_2 & P_3 & \dots & \dots & P_{2n} \\
-P_1 & 0 & P_1 & P_2 & P_3 & & \vdots \\
-P_2 & -P_1 & 0 & P_1 & P_2 & & \vdots \\
-P_3 & -P_2 & -P_1 & 0 & P_1 & & \vdots \\
\vdots & & & & \ddots & & P_2 \\
\vdots & & & & & \ddots & P_1 \\
-P_{2n} & \dots & \dots & -P_3 & -P_2 & -P_1 & 0
\end{bmatrix},
\qquad (2.21)
$$

where P_l is defined as:

$$P_l = \sum_{k=1}^{n} k \sin(lk\omega\Delta t)\,, \text{ for } l = 1 \ldots 2n\,, \tag{2.22}$$

where:

$$\Delta t = \frac{T}{2n+1}\,. \tag{2.23}$$

Constant coefficients P_l depend only on the base frequency and specified number of harmonics, which are defined beforehand. Therefore, P_l may be calculated and stored only once at the beginning of a simulation, with negligible memory demand compared to the cost of a CFD simulation.

Using Eqn. (2.21) in combination with Eqn. (2.20), the expanded form of the coupled Harmonic Balance scalar transport equations may be written in a more convenient form:

$$\nabla\bullet(\mathbf{u}\mathcal{Q}_{t_j}) - \nabla\bullet\left(\gamma\nabla\mathcal{Q}_{t_j}\right) - S_{\mathcal{Q}_{t_j}} = -\frac{2\omega}{2n+1}\left(\sum_{i=1}^{2n} P_{i-j}\mathcal{Q}_{t_i}\right)\,, \tag{2.24}$$

$$\text{for } j = 1 \ldots 2n+1\,,$$

where P_{i-j} is defined as:

$$P_{i-j} = P_l = \sum_{k=1}^{n} k \sin(lk\omega\Delta t)\,, \quad \text{for } l = -2n \ldots 2n\,. \tag{2.25}$$

P_{i-j} term takes into account the temporal distance between solution time instants, therefore yielding small coupling coefficient for distant time instants making them less important compared to temporally-close time instants which become more significant. Due to this, the temporally closer neighbouring solutions affect the current solution more than those farther away, as demonstrated in Figure 2.1. It should be noted that no less then $2n + 1$ time

instants should be solved, as that could cause the aliasing errors. A set of $2n + 1$ equations is the smallest required number of time instants for a chosen number of harmonics, n, for which an accurate solution can be obtained. As the coupling of solutions at different time instants t_j is achieved through P_{i-j} coefficient, it is clear that the time derivative term is now modelled as additional source terms. Q_{t_j} represents the solution in time instant t_j and all of the $2n + 1$ time instants are solved simultaneously as a closed set of equations. Hence, a single transient equation given by Eqn. (2.4) is transformed into a set of $2n + 1$ coupled steady state problems, Eqn. (2.24), obtaining the solution in $2n + 1$ time instants. As the temporal term is replaced by a HB-coupling term, the equation has become a mathematically steady equation, although due to the nature and origin of the coupling term it can be considered a quasi–steady equation.

2.3   Governing Equations

This section covers the governing equations solved within the scope of the thesis. Equations include the continuity equation, the momentum equation and the pressure equation, forming the pressure-velocity equation set for the incompressible viscous turbulent flow. Continuity equation states that the amount of fluid entering the domain is equal to the amount of fluid exiting the domain:

$$\frac{\partial \rho}{\partial t} + \nabla \boldsymbol{\cdot} (\rho \mathbf{u}) = 0 \,, \tag{2.26}$$

where $\mathbf{u}$ is a velocity field, ρ is density and t is time. In case of incompressible flow the equation Eqn. (2.26) gets reduced as there is no change in density:

$$\nabla \boldsymbol{\cdot} \mathbf{u} = 0 \,. \tag{2.27}$$

The momentum equation is of the form:

$$\frac{\partial \mathbf{u}}{\partial t} + \nabla \boldsymbol{\cdot} (\mathbf{u} \mathbf{u}) - \nabla \boldsymbol{\cdot} (\nu \nabla \mathbf{u}) = -\frac{\nabla p}{\rho} + Su \,, \tag{2.28}$$

where ν denotes kinematic viscosity, p the pressure field and Su is a source term, if exists. The momentum equation can as well be written in condensed form, which is the form that will be used in the following sections:

$$\frac{\partial \mathbf{u}}{\partial t} + \mathcal{R} = 0 \,, \tag{2.29}$$

where $\mathcal{R}$ stands for convection and diffusion terms and any existing source or sink terms.

Terms in Equation 2.28 from left to right are:

- Temporal derivative accounting for inertia of the system.

- Convection term, representing transport with the fluid velocity field. It is hyperbolic in nature and the information is propagated based on the direction of velocity.

- Diffusion term, representing transport due to gradient of a passive scalar. It is elliptic, therefore every point in the domain feels any disturbance within the domain instantaneously.

- Source term.

The governing equations solved in this work are the Navier–Stokes equations for incompressible fluid flow. The momentum equation is transformed into HB form following the procedure presented in the previous subsection, while continuity equation remains unchanged as it does not have the temporal term:

$$\nabla\bullet\mathbf{u}_{t_j} = 0 \,, \tag{2.30}$$

$$\nabla\bullet(\mathbf{u}_{t_j}\mathbf{u}_{t_j}) - \nabla\bullet\left(\nu\nabla\mathbf{u}_{t_j}\right) = -\frac{\nabla p_{t_j}}{\rho} - \frac{2\omega}{2n+1}\left(\sum_{i=1}^{2n} P_{i-j}\mathbf{u}_{t_i}\right) \,, \tag{2.31}$$

for $j = 1 \ldots 2n + 1$.

Equations 2.30 and 2.31 represent a coupled pressure-velocity system of $2n + 1$ equations defined by dominant frequency ω, resolved with accuracy corresponding to n harmonics. The solution obtained is always perfectly time-periodic, which would not be the case in the equivalent transient simulation. Additionally, by calculating the Fourier coefficients and performing a reconstruction, the solution can be obtained at any time instant within a period.

2.4 Closure

A general overview of the governing equations and the Harmonic Balance method, followed by its interpretation has been presented. Three main Harmonic Balance techniques have been briefly presented, with explanation on why the spectral form was selected for development. The Harmonic Balance treatment and derivation is then outlined, with notes on temporal coupling and interpretation of the transformation from single time-accurate equation into a set of coupled steady equations. Finally governing equations are presented covering the fluid flow problem in this study.

The overhead that conventional transient simulation poses compared to the Harmonic Balance method comes from solving a large number of time steps in order to propagate the unsteadiness throught the system and obtain periodic steady state. For periodic problems, obtaining a periodic steady state solution is mandatory, as otherwise the solution should not be referred to as periodic. Therefore, reaching periodic steady state means solving a number of periods until the achieved difference between a number of successive periods is within the proposed tolerance for a significant variable. This can mean solving from several periods up to several dozen periods. The main benefit of the Harmonic Balance method is that a set of steady state equations is solved, meaning that solution is converged in a steady state manner for all of the equations. As Fourier series is the core of the Harmonic Balance method, the number of steady state equations depends on the number of harmonics, n. Simple problems can be solved accurately with one harmonic, while for more complex problems larger number of harmonics should be resolved. The number of Harmonic Balance equations scales with number of harmonics by a factor of $2n + 1$.

Chapter 3

Numerical Model

Summary

The governing equations for viscous, turbulent, non-linear flow in the final
Harmonic Balance form were presented in Chapter 2. Choice of the most
suitable Harmonic Balance form was made, with a brief overview of different
formulation possibilities. The derivation of the Harmonic Balance equations
shows the transformation from a single temporally resolved equation into a set
of $2n + 1$ coupled mathematically steady equations for n harmonics.

In this chapter the numerical treatment of governing equations in physical
space is presented. Within the Section 3.1 the transformation from general
equations to finite volume equations is presented, with notes on implicit or
explicit treatment of each term. The Section 3.4 deals with interpolation
procedures in case of solving multiple domains with adjacent boundaries. In
turbomachinery, it is a common case for each blade row to be its own domain -
yielding a number of interconnected domains which exchange information over
the numerical interface in a specific manner, based on a chosen interpolation
algorithm. Section 3.3 briefly introduces two steady state approaches, multiple

reference frame (MRF) and single reference frame (SRF) models that are used in this work for comparison, but as a method are not of interest here.

3.1   Discretisation

Discretisation of equation terms refers to adapting the mathematical form of the governing equations into a numerically suitable form for iterative solving in the framework of finite volumes (cells). The spatially continuous equation is transformed into a finite volume configuration, such that physical space is no longer continuous, but discrete and divided into cells. Therefore, the domain consists of cells, internal faces and boundary faces. A cell has a finite number of neighbours sharing a common face, whereas a single internal face is shared only by two cells. Collocated grids are commonly used in CFD, meaning that the solution variables are stored at cell centres, while flux is evaluated on cell faces. The arrangement of both pressure and velocity variables located in cell centres can in case of incompressible flow solved on uniform mesh lead to odd-even cell decoupling [47], characterised by checkerboarding in the resulting flow field. In order to avoid odd-even cell decoupling on uniform meshes, the Rhie and Chow procedure is used [48]. Rhie and Chow proposed interpolating the velocity onto faces without accounting for the pressure gradient, while performing separate interpolation of the pressure gradient onto faces. Such procedure preserves the local influence of each cell, without the possibility of odd-even decoupling to occur.

In the following subsections the finite volume discretisation of momentum and pressure equations is presented, as well as the treatment of each term in the equation. The numerical discretisation of governing PDEs, using second-order accurate, collocated finite volume method for arbitrary polyhedral (unstructured) grids is presented [49] and used in this work. Collocated, polyhedral framework is preferred due to its simplicity regarding grid generation for complex geometries often encountered in turbomachinery. However, the methodology presented here is general regardless of type of grid used, polyhedral or block structured.

The integral form of the governing equations is obtained by integrating over the control volume faces. Additional details on finite volume discretisation in

collocated grids can be found in [50, 47, 49, 51, 52].

3.1.1   Spatial Discretisation

Prior to solving the governing equations, the solution domain should be spatially discretised. By discretising the solution domain in terms of finite volumes, a computational mesh consisting of control volumes is produced. A typical control volume is shown in Figure 3.1, where P denotes the cell centre and N stands for a neighbouring cell centre. $\mathbf{s}_f$ represents the face area vector: pointing in the direction normal to face with its magnitude equal to face area. Control volumes (or cells) are bounded by an arbitrary number of faces, thus making it a general polyhedron. Faces are flat and each face is shared with only one neighbouring control volume. Furthermore, control volumes do not overlap and fill the computational domain completely. Finally, the discretised mesh holds the variables in the cell centroid, P, while N denotes neighbour cell centre. The computed value is considered constant for the whole cell, although a representation of a continuous field can be obtained by interpolating between cell centres. Obviously, the smaller the control volumes, the smaller parts of space are considered to have a constant value. Thus, finer field distribution is obtained. In general, the size of the cell should be chosen based on the problem, so that phenomena with large gradients is discretized with smaller cells. Within the finite volume method, PDE's are solved for cell centres in case of collocated grid and in cell centres and faces for staggered.

3.1.2   Temporal Discretisation

Temporal discretisation refers to dividing the physical continuous time into discrete instants in which the solution is sought. In conventional time-accurate simulations, the time is discretised by prescribing the size of the time step that will be used during the calculation. The solution is then obtained by marching from the prescribed initial condition, propagating in increments of time which are of size of prescribed time step. Based on the problem and temporal variation of the flow, the time step size should be chosen so that fluctuations can be captured. Furthermore, one should have in mind the restriction of CFL
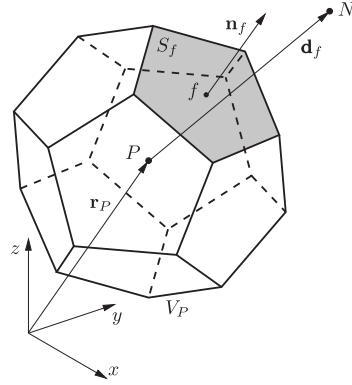
Figure 3.1: Finite volume polyhedral cell [53].

number in terms of stability for explicit codes, so that information does not propagate more than one cell per time step. The CFL criterion relates cell size, velocity within cell and time step. However, in case of the Harmonic Balance method the discretisation of time is performed in a different manner: one period is perceived as a total physical time which is split into a $2n + 1$ equidistant time instants. Time step can be thought of as $\delta t = \dfrac{T}{2n + 1}$, where T is the complete period and n is the number of harmonics used.

However, stemming from the fact that in the Harmonic Balance method the solution is not marched in time, the time increment does not have the same interpretation as in the time-accurate simulations. Moreover, the impact of the temporal distance between the time instants is expressed through the Harmonic Balance coupling term, without marching from one time instant to another. The coupling coefficient in the Harmonic Balance source term becomes larger as the temporal distance is smaller, thus accounting for the temporal closeness, which can be thought of as the influence coefficient of the phenomena appearing closer in time and having greater impact or farther in time with smaller impact.

Figure 2.1 shows the temporal discretisation in the Harmonic Balance simulation. The error of the Fourier approximation, Equation 2.1, can clearly be noticed: for small number of harmonics, n, the time steps are rather large, whereas in case of infinite number of harmonics, the time would no longer be discretised, but would become continuous (with infintesimal time steps).

3.1.3   Discretised Momentum Equation

The momentum equation expressed in Equation 2.31 is briefly discussed here in terms of discretisation and treatment. This section briefly presents the finite volume implementation of the Harmonic Balance variant of the pressure–velocity system. The resolution of coupling the Harmonic Balance equations will be discussed to a somewhat greater extent.

Following the notation by Vukcevic [54], we use $[\cdot]_i$ to denote implicit finite volume discretisation and $[\cdot]_e$ for explicit. Details on finite volume discretisation may be found in Jasak [49] and will not be presented here. Since the convection, diffusion and source terms remain unchanged compared to conventional discretisation, the discretised the Harmonic Balance pressure-velocity system, Eqn. (2.31), reads:

$$\left[\nabla\bullet(\mathbf{u}_{t_j}\mathbf{u}_{t_j})\right]_i - \left[\nabla\bullet\left(\nu\nabla\mathbf{u}_{t_j}\right)\right]_i = -\left[\frac{\nabla p_{t_j}}{\rho}\right]_e - \left[\frac{2\omega}{2n+1}\left(\sum_{i=1}^{2n}P_{i-j}\mathbf{u}_{t_i}\right)\right]_e , \quad (3.1)$$
$$\text{for } j = 1\ldots 2n+1 \, ,$$

where the source term arising from the Harmonic Balance treatment of the time derivative term is treated explicitly. Hence, a segregated, iterative solution algorithm for successive $\mathbf{u}_{t_j}$ is employed.

The pressure equation in the finite volume framework is used to create conservative fluxes for incompressible fluid flow. Following Patankar and Spalding [55] the pressure-velocity coupling algorithm is derived, with Rhie and Chow correction procedure taken into account as well. In its final form, the discretised pressure equation reads:

$$\left[\nabla\bullet\left(\frac{1}{a_{Pt_j}}\nabla p_{t_j}\right)\right]_i = \left[\nabla\bullet\left(\frac{\mathbf{H}(\mathbf{u}_{t_j})}{a_{Pt_j}}\right)\right]_e , \text{ for } j = 1\ldots 2n+1 \, , \qquad (3.2)$$

where a_{Pt_j} is the diagonal coefficient of the momentum equation at time instant t_j, and $\mathbf{H}(\mathbf{u}_{t_j})$ is the flux operator as defined by Jasak [49]. Following the Rhie

and Chow correction, the pressure gradient term is not included in the $\mathbf{H}(\mathbf{u}_{t_j})$ operator. $\mathbf{H}(\mathbf{u}_{t_j})$ term consists of:

$$\mathbf{H}(\mathbf{u}_{t_j}) = \left[-\sum_N a_{Nt_j} \mathbf{u}_{Nt_j} \right]_i + \left[\frac{\mathbf{u}_{t_j}}{\Delta t} \right]_e . \qquad (3.3)$$

The Harmonic Balance pressure equation, Eqn. (3.2) is obtained from the Harmonic Balance continuity equation, Eqn. (2.30), using standard procedure for segregated solution algorithms. This is possible, as the continuity equation must hold for every point in time, i.e. for all $2n + 1$ time instants. For the pressure equation at time t_j, the accompanying variables for time t_j have to be used. Due to lack of temporal term, the final pressure equation does not contain the coupling source term. As discussed, the Harmonic Balance variant of a transient transport equation yields $2n + 1$ coupled steady state problems. Hence, the SIMPLE [55] algorithm is employed to resolve the pressure–velocity coupling at each time instant t_j.

3.2 The Harmonic Balance Pressure-Velocity Coupling

Following the analogy with the Gauss–Seidel iterative solution algorithm [56], each $\mathbf{u}_{t_j}$ is solved once per outer iteration during a forward sweep ($j = 1 \ldots 2n+1$). Latest available $\mathbf{u}_{t_i}$ is always used in source terms for other equations ($j > i$), preventing additional memory requirements. Outer iterations are continued until convergence.

Within the Harmonic Balance simulation, inner and outer coupling appears. Outer coupling refers to a standard simple loop for resolving the $\mathbf{u} - p$ coupling. However, in case of Harmonic Balance the corresponding variables have to be coupled depending on the time instant: $\mathbf{u}_{t_j} - p_{t_j}$. Inner coupling refers to $\phi_{t_j} - \phi_{t_i}$ coupling of a single conservative variable in different time instants, performed through the source term. Therefore, in addition to pressure–velocity coupling at each time step, velocity fields at different time instants are coupled via Harmonic

Balance source terms on the right hand side of Eqn. (3.1). $\mathbf{u}_{t_j}$ coupling is resolved during a forward sweep, using the latest available $\mathbf{u}_{t_j}$, while each time instant demands its own SIMPLE loop. However, only one SIMPLE iteration is sufficient for each t_j in order to simultaneously resolve $\mathbf{u}_{t_j} - p_{t_j}$ and $\mathbf{u}_{t_j} - \mathbf{u}_{t_k}$ coupling.

3.3 Domain Treatment

Steady state turbomachinery simulations can be performed regardless of the missing rotational motion. Such approach is usually referred to as a *frozen rotor approach*, namely due to the captured flow field resembling a snapshot during continuous operation. Such simulations offer reasonable accuracy, with good estimate of power, torque or efficiency, for only a fraction of transient simulation CPU time.

In order to obtain the rotating flow field which accurately represents the physical behaviour even though a steady simulation is run, the additional source terms accounting for rotation are added into momentum equation. Furthermore, it is clear that the rotating blade velocity is of magnitude different from zero and therefore the mesh flux has to be included as well [57].

The source term that is added in the momentum equation represents the Coriolis force and centrifugal force:

$$Su = 2\omega \times \mathbf{u}_R + \omega \times \omega \times \mathbf{r} \tag{3.4}$$

Two variants of steady state simulations are possible: Single Reference Frame (SRF) or Multiple Reference Frame (MRF) simulations [58]. SRF is used when the whole domain is rotating with the single angular velocity. Therefore, this is where the name comes from - only one frame of reference is used and it is valid for the whole domain. Example of SRF simulations include rotor-only configurations such as single rotor blade passage or propellers and fans without non-rotating parts, Figure 3.2.

(a) Full annulus SRF.   (b) Single blade passage SRF.
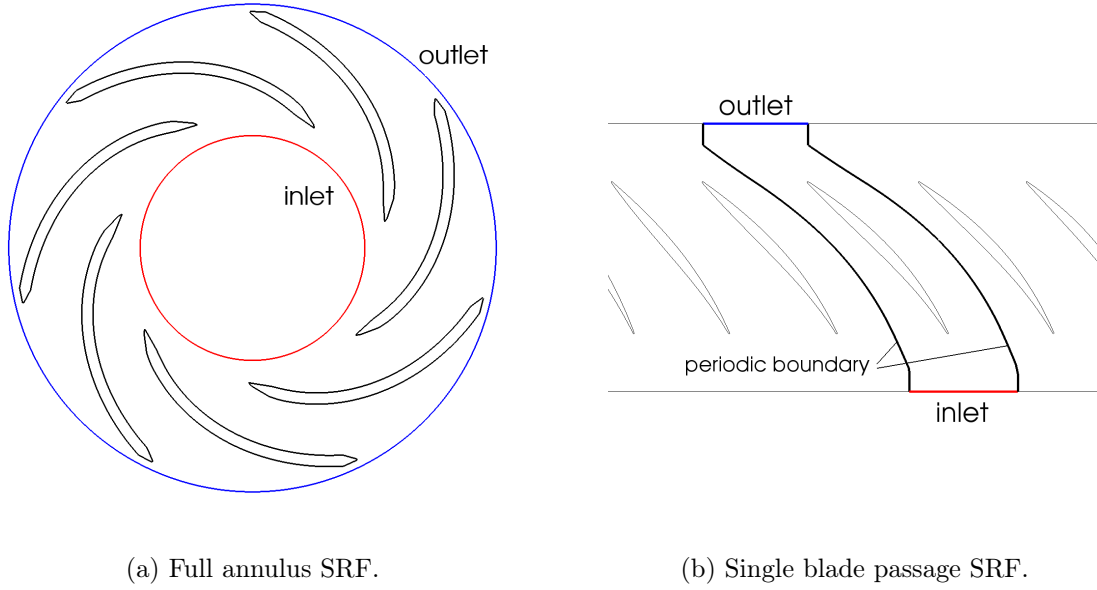
Figure 3.2: Single reference frame (SRF) domains.

MRF is applied when several different frames of reference are to be used due to different angular velocity. MRF approach is common in multistage turbomachinery simulations due to multiple stationary and rotating blade rows which should be accounted for. Moreover, in case of different angular velocities between moving regions, each region should have its own reference frame, i.e. MRF-zone.

SRF and MRF can be implemented choosing either the absolute or relative velocity formulation. Within `foam-extend`, the MRF implementation is performed with relative convective velocity and absolute velocity as a conservative variable. The final momentum equation after collapsing appropriate terms is of the form:

$$\nabla_{\bullet}(\mathbf{u}_R \otimes \mathbf{u}_I) + \Omega \times \mathbf{u}_I - \nabla_{\bullet}(\nu \nabla \mathbf{u}_I) = -\frac{\nabla p}{\rho} \qquad (3.5)$$

MRF can be used for any rotating objects, such as spinning wheels, propellers, fans, mixers, where both rotating and stationary parts exist. Due to flux conservation, the MRF zone should not have the mesh flux through its

boundaries, therefore it has to be cylindrical. Although it is possible to define the MRF zone as a selection of cells in which the rotation will be accounted for, a more common way is to define and mesh separate domains, connected with the aid of interface boundary condition. Possibilities for interface treatment and possible interpolation schemes are presented in the following passage, Section 3.4.

3.4   Interface Treatment

In this section the methods of the interface treatment between adjacent domains are covered. In CFD, many applications can require solving a multiple-domain problem for two reasons:

- Split complex geometrical parts from less complex in order to perform separate meshing and simplify the pre-processing step.

- Different parts of domain may require different treatment, for instance one part is moving while the other is stationary.

Having in mind that meshing is a highly important part of preparation, the meshing procedure should be performed with great care and attention. As good mesh will improve the quality of the results [59, 60], so will the bad mesh decrease the convergence rate or even lead to divergence [61, 62, 63]. Therefore, it is necessary to obtain the sufficiently good mesh in terms of common mesh criteria [64, 65, 66]. The requirement to fit all regions with a single mesh or conformal matching interfaces is often very difficult or leads to geometric compromises that affect the numerical quality of the simulation results.

In cases of complex geometry, such as turbomachinery, it is convenient to split the mesh into several parts, based on complexity. The interblade passage is usually chosen as one region, the inlet casing the second and the outlet draft tube the third. This allows using coarse grid in inlet and outlet parts and fine grid for the blades in order to describe the blade geometry accurately, as well as capture the appearing boundary layer. Moreover, if the turbomachine consists of both rotor and stator blades, then the domains have to be split as well in

order to allow rotation only of the rotor parts. The presented cases are solved using the interface on the adjacent boundaries to allow flow propagation from one domain into another. In order to accommodate physically split domain, in terms of matrix representation the domain should be unified before solving. This is performed using the interface boundary conditions which perform implicit or explicit domain coupling. In `foam-extend` these boundary conditions are called General Grid Interface (GGI), Overlap General Grid Interface [67] and Mixing Plane [68]. GGI, Overlap GGI and Mixing Plane are implicit techniques.

The main challenges that turbomachinery simulations impose are linked with the need to study the relative motion of multiple rotors and stators. Depending on the transient or steady state approach, the rotation can be handled in two ways: directly by moving the mesh or indirectly by using a static mesh and modifying the equations to take into account the rotation. The first way is only appropriate for transient simulations, whereas the static-mesh approach is suitable for SRF, or MRF.

The interface between stationary and rotating parts can be treated in several ways: for transient simulation with topological changes, sliding mesh technique is commonly used, whereas the available methods are: General Grid Interface (GGI), where a weighted interpolation is performed to evaluate and transmit flow values across a pair of conformal or non-conformal coupled patches [69]; the partial Overlap GGI for cases where some of the interface faces are not physically covered by their counterpart; and the Mixing Plane interface that performs the circumferential averaging of the solution at the rotor-stator interface [70].

3.4.1   General Grid Interface

The General Grid Interface (GGI) is a region coupling boundary condition available in `foam-extend` used for connecting the two neighbouring domains [71]. The adjacent boundaries affect the internal cells by acting as a prescribed fixed boundary condition. The conservative variables from one domain are interpolated over the interface onto the second domain. The interpolation is performed by taking into account the face area weights in order to obtain the conservative field. The interpolation is not done explicitly in-between the

iterations, but implicitly by adding the coefficients in the solving matrix equation. The main advantage of the GGI comes from the ability to adjust the topology of the mesh between the two non-conformal domains, Figures 3.3 and 3.4. Based on that, a set of weighting factors is evaluated in order to properly balance the flux at the GGI. Interpolation is fully conservative irrespective of the face shape, provided that full overlap of surfaces is achieved.

For time–accurate turbomachinery simulations with rotating runner, it is inevitable to have non-conformal interfaces between the fixed and moving domain during the mesh motion. This is easily handled via GGI, which performs the re-evaluation of the GGI weighting factors at each time step and interpolates the variables accordingly. The GGI weighting factors are computed as a percentage of surface intersection between two overlapping faces, performed using an efficient 2D face-to-face Sutherland-Hodgman intersection algorithm [67].
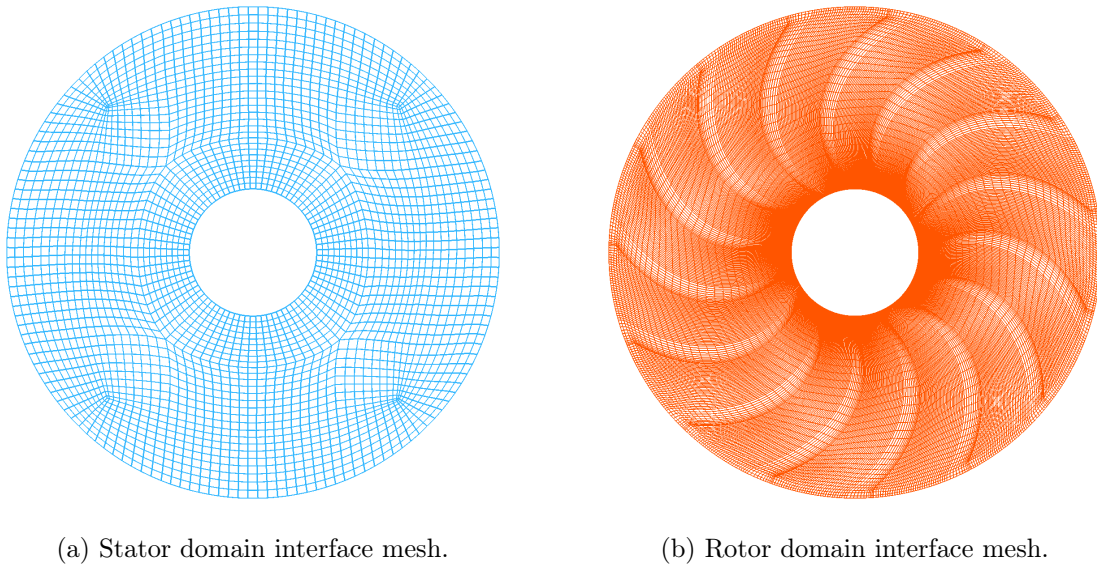

(a) Stator domain interface mesh.   (b) Rotor domain interface mesh.

Figure 3.3: GGI non-conformal interface set.

3.4.2   Overlap and Cyclic General Grid Interface

In case of axisymmetric problems, common in turbomachinery, only a portion of domain can be used. Instead of solving for the complere circumference of
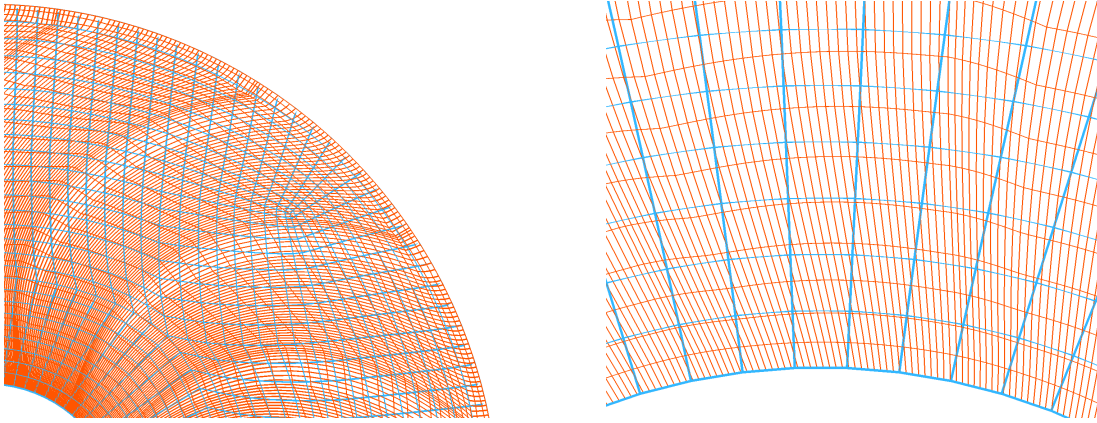
Figure 3.4: Non-conformal rotor and stator overlapping.

the blade row, the effect of spatial periodicity can be taken into account, thus reducing the domain size. For example, if the investigated propeller has n blades, the solved domain can consist of only $1/n$ of the whole annulus, containing just a single blade (or blade passage). In turbomachinery this is extremely useful, as blade rows can have large number of blades, meaning that the reduction in simulation CPU time will scale with the number of blades, making the simulation significantly more efficient.

If such case is considered and only a single blade passage is simulated, two important boundary conditions should be used: periodic boundary condition for meridional boundaries and overlap GGI for domain coupling. The use of the periodic boundary condition is presented in Figure 3.6. The flow field variables are interpolated from one meridional plane onto another, creating an effect of repeating domains, i.e. spatial periodicity. In cases where meridional boundaries are non-conformal, the GGI interpolation is utilized, while for the conformal boundaries the values do not have to be interpolated. Communication between multiple domains is achieved using the overlap GGI functionality. The overlap GGI is a variant of regular GGI, which is capable of running only a portion of annulus, while performing interpolation as if the whole annulus is present. Furthermore, for vectors and tensors the appropriate coordinate transfomation is applied as well.

The overlap GGI is presented in Figure 3.5 between stationary and rotating domain. The non-overlapped parts could not be evaluated and interpolated using

a standard GGI approach due to the lack of shadow interface. Within the overlap
GGI, this is handled by doing copy-and-rotate of both rotor and stator interfaces
to obtain the whole annulus. Once the whole annulus is paved, both the rotor
and stator interface are fully covered and a regular variant of GGI interpolation
can be performed. The last step after interpolation is reduction of the complete
annulus back to the original portion of the interface.

Such a procedure allows running both transient and steady simulations, as the
non-overlapped part is no longer an issue. In specific cases it is not possible to
have all parts of the domain cut within a proposed circular interval, for instance
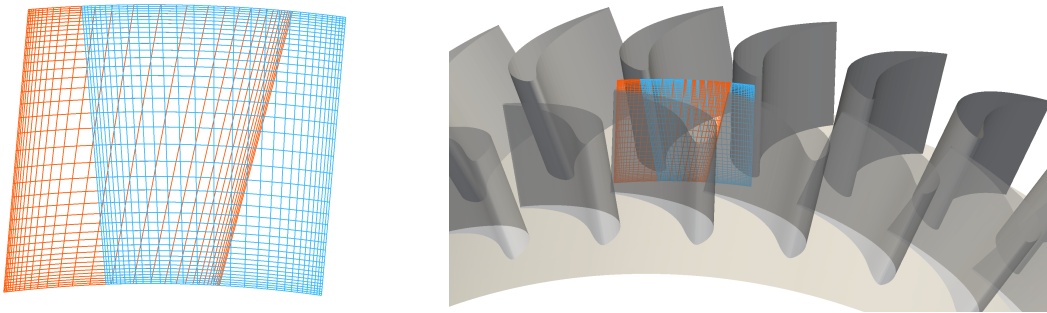in case of bent draft tube.

Figure 3.5: Non-conformal mesh detail with overlap GGI. Coupled interface set (left) and
complete annulus (right) created by copying a single blade passage domain.

However, if the GGI between the rotating part and draft tube is far enough from
the bend so that it is not affected by it, the overlap GGI can be used as well:
only the rotating part will be paved a number of times, thus using single blade
passage, while draft tube will be in its complete form.

The situation which should not be handled using the overlap GGI is a
turbomachine with non-multiple number of blades. The domain can not be split
such that per one rotor blade m stator blades are simulated. This could happen
if rotor has 17 blades and stator has 19 blades, therefore using single rotor and
single stator blade would not be accurate, as the spatial periodicity would not
be satisfied. Relative position of rotor-stator blades would in that case be
different for each paved instance, yielding inaccurate results as if the spatial
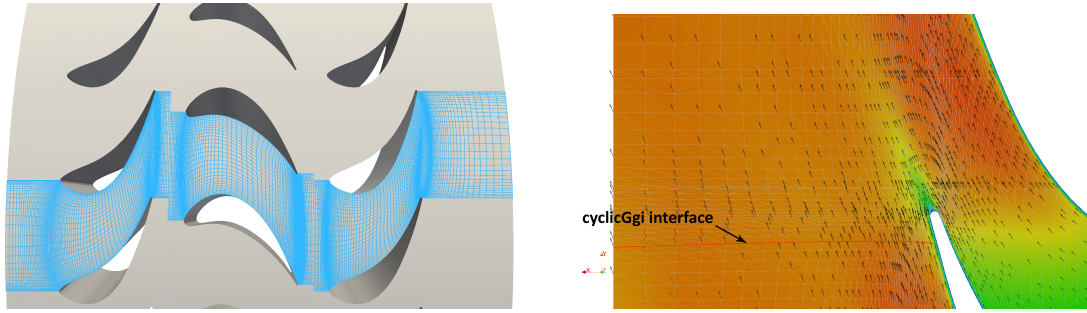periodicity is satisfied.

Figure 3.6: Non-conformal mesh detail with cyclic GGI periodic boundary.

The problem of non-multiple number of blades can be alleviated in two ways if just a portion of domain wants to be used. Depending on the wanted outcome, the user should choose a preferable option. First solution is to modify the given geometry such that spatial periodicity is assumed: in case of 17 rotor blades and 19 stator blades, single blade passages are 21.1765° and 18.9474°, respectively. The angular difference is 2.229°, meaning that one domain could be expanded by ≈1° and the other contracted by ≈1° in order to achieve spatial periodicity. This would give reasonably accurate results in terms of power, torque, efficiency [72, 73, 46], as well as a modified rotor-stator interaction. The second solution for non-matching blade count is a Mixing Plane approach, which is described in the following section.

3.4.3   Mixing Plane

Mixing Plane is the implicit interface interpolation approach used only in turbomachinery, due to its mathematical model and basic idea which was derived with turbomachinery in mind [68]. Mixing Plane interpolation mimicks the temporally averaged flow on the interface by performing the circumferential averaging. Therefore, the flow from the rotor side of the interface is circumferentially averaged and yet then it is transferred to the stator side and vice versa, Figure 3.7. This is extremely useful in cases where wake propagation is not of main interest, but general flow field and performance is required. One of the most common usage is for single blade passage simulations with non-matching blade count between adjacent blade rows. If Mixing Plane is used, the exchanged variables between rows are smeared, passing on the other

side variables in a temporally averaged fashion. Therefore, due to circumferential averaging the relative position between rotor and stator becomes irrelevant. Furthermore, no wakes are propagated through the interface due to the averaging (smearing).

The comprehensive comparison of GGI, overlap GGI and Mixing Plane approach on the same case was performed by [74]. The authors compare the three methods with the transient results for a single blade passage in a rotor-stator configuration. All three methods give similar results in the majority of the domain, with largest differences at the interface when using the Mixing Plane interpolation. However, a comparison of interpolation methods was performed against the time-averaged transient simulation, for which all three methods gave results of the similar accuracy. This states that regardless of Mixing Plane's inability to propagate wakes over the interface, the global flow field will resemble the time-averaged transient flow as well as the remaining two methods, GGI and overlap GGI.
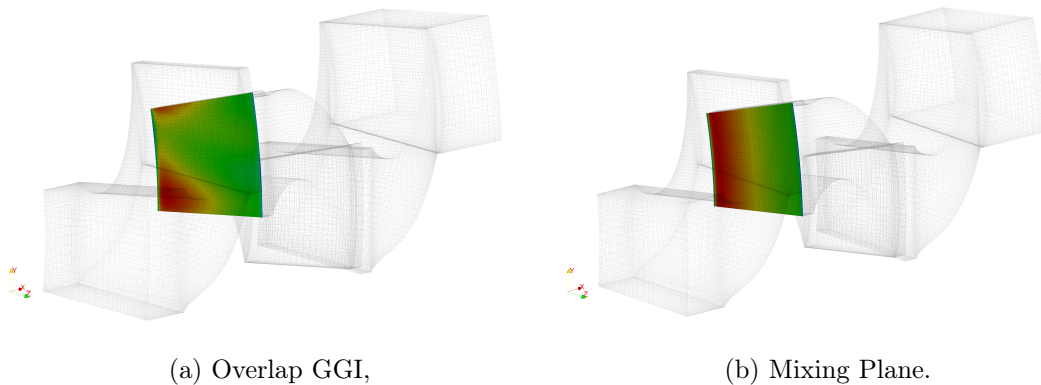

(a) Overlap GGI,   (b) Mixing Plane.

Figure 3.7: Different interpolation procedures on the interface.

3.5   Closure

Numerical concerns related to treatment of equations in terms of finite volume method; domain treatment and interface treatment have been presented in this chapter. Discretised forms of equations presented in Chapter 2 have been covered and followed by discussion on the pressure-velocity coupling and

iterative procedure employed. Although in the Harmonic Balance form a number of steady equations are simultaneously solved, the SIMPLE algorithm is used with inter-equation coupling resolved in a Gauss-Seidel sweep. A SIMPLE iterative procedure is performed for each time instant separately.

The treatment of the domain should be considered if only a portion of domain wants to be simulated. This is possible in case of spatial periodicity, such as in turbomachinery so that a single blade passage per rotor or stator row is simulated. If the complete considered domain is part of a single frame of reference, an SRF steady state model can be used. In case of several frames of reference, MRF steady state model should be used. Furthermore, in case of single blade passage simulations, additional boundary treatment has to be performed, thus applying periodic boundary conditions which account for spatial periodicity. However, for the coupling between two regions, for instance rotor and stator, a suitable interface interpolation method should be chosen between GGI, overlap GGI and mixing plane. Figure 3.8 presents a case of single blade passage with notes on boundary conditions which should be prescribed.
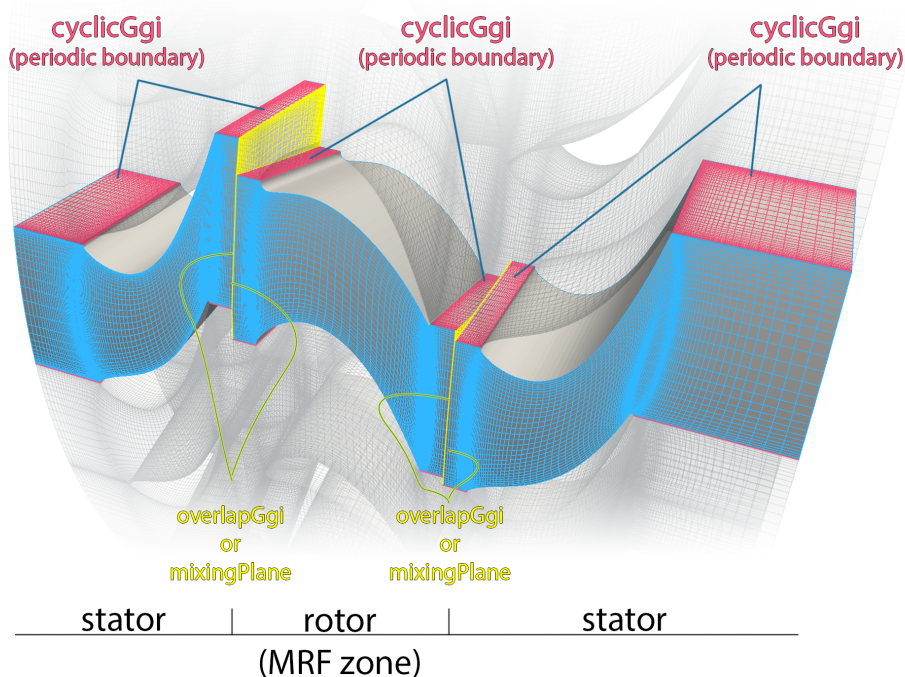

Figure 3.8: Single blade passage consisting of stator, rotor and stator with interface boundary conditions.

Chapter 4

Start-up and Shut-down Handling

Start-up and shut-down present a challenging change of operating conditions in turbomachines. For instance, due to varying power demand through time, a change of operating conditions should be performed for the output to adjust to the demand. The turbomachine should be designed with flexibility in mind, ensuring that a machine is not efficient only in one operating point, but at a whole range of operating points. Additionally, flexibility means more frequent load variations and load rejection events as well as off-design operation at prolonged time. Load variations cause significant volatile events due to change of runner speed, excessive unsteady pressure loading, mass flow rate variations and large pressure fluctuations on blade surfaces. Such events cause asymmetric stresses on surfaces [75] and even resonance conditions, eventually leading to significantly reduced operating life of the runner [76]. However, most hydroturbines, especially those of Francis type are not designed with unsteady operation in mind.

Undoubtedly, the increase of flexibility and efficiency is therefore in the spotlight of turbomachinery development. The only way of affecting flexibility is designing a machine for a whole range of operating points and optimizing its operation. This is especially valid for start-up and shut-down as the transients

impose the largest load variation. Depending on the type of turbomachine, different start-up and shut-down procedures are used [77], and can be performed at constant rotor speed by changing the mass flow rate, or by changing the rotor speed.

In case of a gas turbine, during start-up it undergoes a sequence of increasing the compressor spin until reaching the firing speed. Sequence consists of ignition, turbine acceleration to self-sustaining speed, synchronization, and loading. Since turbines cannot produce torque at zero speed, the starting-system is used to start the gas turbine rolling, accelerate it to firing speed and assist the fired turbine to reach the self-sustaining speed. That is accomplished by a motor or a generator. This arrangement provides the needed torque for turbine start-up as well as during shut-down when it continues to rotate the turbine rotor at slow speed until it cools down [78]. There are numerous thermo-mechanical constraints during the start-up of the gas turbine, including limits on the airflow velocity through the compressor blades to prevent stall, vibrational limits, and combustion temperature limits to prevent turbine blade fatigue. Conversely, in case of a pump start-up, the pump must be filled with liquid up to the level where the impeller and casing are flooded since the pressure rise created by the impeller operating in air is virtually zero due to low density. Depending on the size of the turbomachine, start-up and shut-down processes can last from a few seconds up to a few hours.

4.1   CFD in Start-up and Shut-down

As presented in previous section, start-up and shut-down processes consist of a number of transient phenomena and flow variations which is why simulating a single operating point is not enough. However, if a whole process was to be simulated, it would require extensive computational resources due to numerical limitations. One of the main limitations for running a time-accurate simulation is the CFL (Courant-Friedrichs-Levy) number. CFL number defines the relation between cell size, timestep and velocity in that cell, limiting the timestep in such a way that the information does not spread more than one cell per timestep. In case of turbomachinery, the most sensitive area of the domain is the blade tip, due to

the highest velocities in that region, while the smallest cells are used for capturing the boundary layer. This forces the time step to be extremely small (order of 10^{-6} s). Furthermore, for practical turbine simulations, of the order of 100 time-steps per one blade pitch passage are needed. On the other hand, if turbine shut-down to be simulated lasts for several minutes, this means running approximately 10^7 time-steps. Furthermore, as simulation start and initial conditions should not affect the final solution, a number of periods should be run prior to performing the regime change, so that periodic steady state is reached as a starting point. In case of a standard turbomachinery simulation with several million cells, this means running a simulation which would take several weeks time on a reasonable size cluster. As a possibility for speeding up this process, the idea of Harmonic Balance method appeared – with the goal of turning the time-accurate start-up simulation into a Harmonic Balance one.

4.2   Harmonic Balance Start-up and Shut-down

In order to alleviate the problems noted in the previous section, a modified version of the Harmonic Balance method is developed, where the solution procedure is adjusted. The main idea is to run a small number of steady-state problems, which form the Harmonic Balance simulation and describe the problem at one scale with sufficient accuracy. Additional Harmonic Balance treatment is performed on top of that, creating a nested structure with two coupling levels. In general, the change of regime cannot be described using a Harmonic Balance method, as it requires a periodic problem. However, if a change of operating conditions is made periodic by returning to the initial operating condition, the Harmonic Balance method is applicable.

4.2.1   Introduction

The Harmonic Balance method is deployed here as a quasi-steady method in order to reduce the simulation time and capture the behaviour during regime change. Non-periodic processes such as start-up or shut-down are made periodic by considering both start-up and shut-down as a complete process, Figure 4.1.

The period then consists of two complementary regime changes, with $2n + 1$ simulations throughout the period of start-up and shut-down. Due to two distinctive time-scales of the rotor period (inner) and complete start-up/shut-down period (outer), a nested Harmonic Balance structure is deployed. Therefore, the $2n + 1$ Harmonic Balance simulations for $2n + 1$ time instants are interconnected with additional Harmonic Balance source term for the outer coupling.

4.2.2   Approach

In terms of the turbine regime change, the periodicity is created by adding a complementary regime change so to return to initial operating point. Therefore, if the first regime change is from operating point OP1 to operating point OP2, the complete considered period is OP1-OP2-OP1. This period can be further deconstructed to following parts, Figure 4.1:

a Steady-state operation at OP1, followed by

b a change from OP1 to OP2,

c OP2 maintained for a number of periods to reach periodic steady-state,

d change from OP2 to OP1,

e reaching OP1 periodic steady-state.

Figure 4.1 presents a general schematic overview of how the problem should be decomposed and a similar variation will be used in the following parts of this work. As two regime changes do not commonly ocurr immediately one after another, the steady operation plateaues (a, c, e) are added to provide an adequate starting point for regime change, but also to flush out the phenomena from the previous regime change. The length of these parts should be arbitrarily chosen according to the problem, but sufficient number of periods must be permitted. However, based on results, if no fluctuations exist in those sections, then satisfactory number of periods are run.
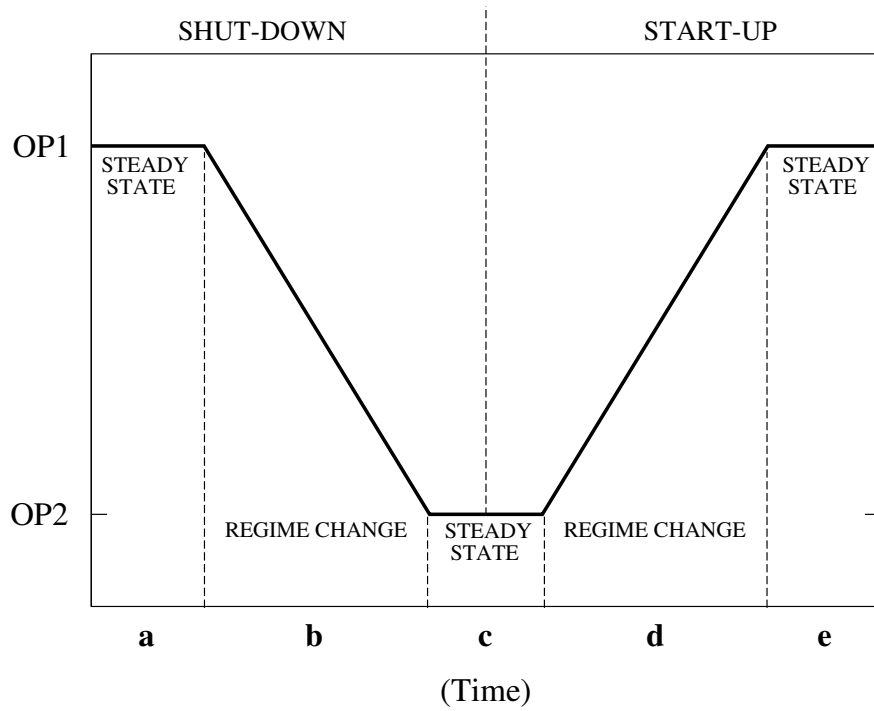
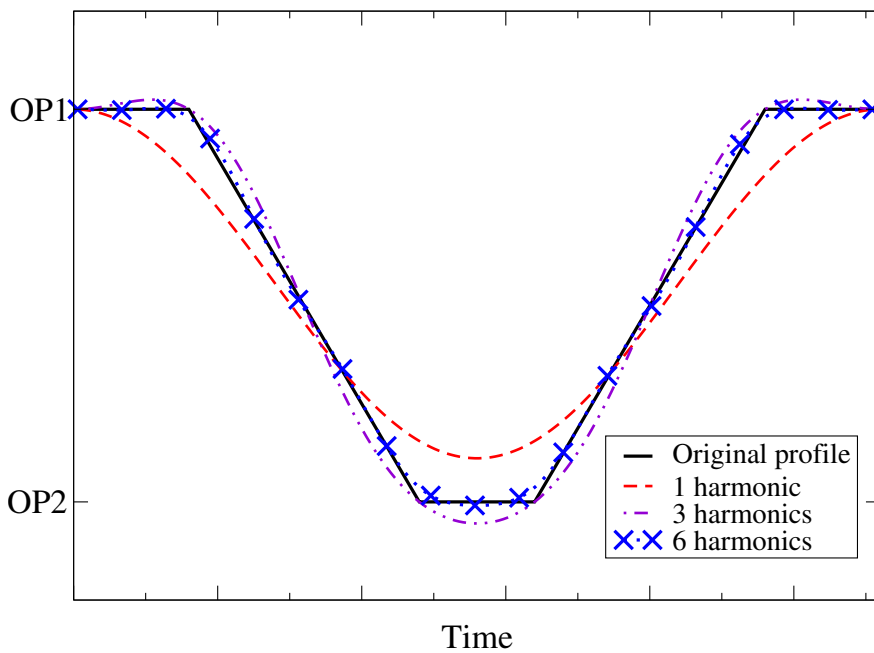Figure 4.1: Stages of a complete shut-down and start-up period.

Figure 4.2: HB approximation functions.

In terms of Harmonic Balance, it is necessary to determine a sufficient number of harmonics m so that a Harmonic Balance curve follows the original profile

closely. Figure 4.2 shows an approximation of the original profile using different number of harmonics. The nested structure is then obtained by running a $2m + 1$ coupled Harmonic Balance simulations where each simulation resolves rotor-stator interaction, while the coupling between the simulations resolves temporal influence of start-up and shut-down. For m harmonics the period consists of $M = 2m + 1$ time instants, while for accuracy in each of the $2m + 1$ time instants an additional single-harmonic Harmonic Balance simulation is run. Therefore, the outer (single) HB loop accounts for changes related to regime change, while the inner $2m + 1$ HB loops account for rotor-stator interaction and rotor rotation. The two loops are interconnected over mutual source term. However, as it will be shown in the sequel, the outer loop can be seen as a larger Harmonic Balance simulation consisting of smaller Harmonic Balance simulations. Although it is referred to as a *simulation*, no additional equations are solved but only the coupling source term is added into the smaller simulations.

4.2.3   Mathematical Aspect

The nested Harmonic Balance simulation consists of two layers, based on time-scales (frequencies) to be resolved. The outer layer is based on the start-up/shut-down period and corresponding frequency, which is of the order from several seconds to few minutes, depending on the problem. Figure 4.3 shows the outer layer scheme for $m = 6$ harmonics for a period T_o. The horizontal axis denotes time, the vertical axis is a function of start-up/shut-down feature, such as stator blade pitch (opening), rotor speed or mass flow rate. A change from a starting operating condition OP1 to final a operating condition OP2, and then back to OP1 is presented.

With adequately chosen number of harmonics (see Figure 4.2), the outer Harmonic Balance layer will closely match the prescribed function. However, due to large fundamental frequency, only large fluctuations can be captured, without small fluctuations on a turbulence or blade interaction level. This is handled by nesting the additional layer with fundamental Harmonic Balance frequency set to rotor frequency. This layer will be referred to as the *inner layer*
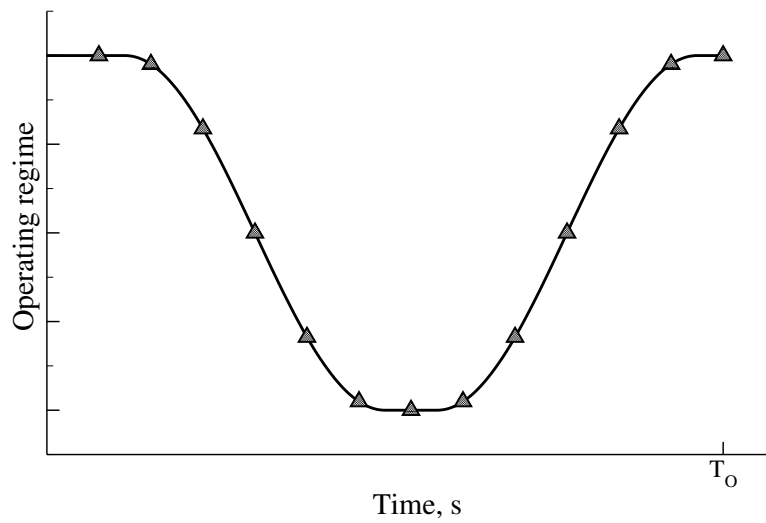
Figure 4.3: Outer layer.

with inner period and inner frequency.   The inner layer is responsible for rotor-stator interaction, small disturbances and similar phenomena. The scheme of the inner layer is shown in Figure 4.4.
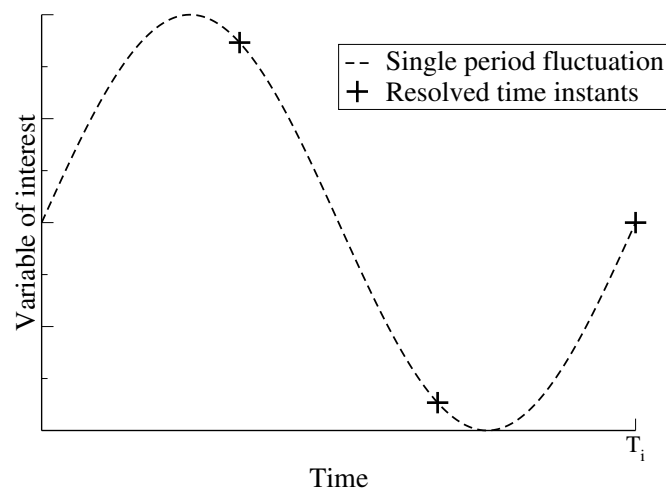

Figure 4.4: Inner layer.

In the presented scheme, a number of Harmonic Balance simulations are run through a number of operating points. As it will be shown in Chapter 5, the one-harmonic Harmonic Balance simulation offers good accuracy compared to computational cost. Therefore, for efficiency reasons, each of the inner Harmonic Balance simulations is set to solve a single harmonic, i.e. $n = 1$ harmonic.

However, in order to assemble a nested two-layer approach, there should be $2m+1$ inner simulations, where m is the number of harmonics in the outer layer. In terms of the equations, the same equations would be solved for the inner and outer layer, with different base frequency and number of harmonics. If inner simulations are calculated in exact time instants as the outer time instants, these two solutions coincide and should be the same, one having a time-history (Su_o coupling term) of a complete period T_o and the other of an inner period T_i (Su_i). This is the base for assembling joined equations. Figure 4.5 shows the scheme of two coinciding layers with inner and outer time instants. Each triangle represents one solved time instant. Larger trangles (on curve) are coupled over complete period source term Su_o, while the inner layer (small) triangles are coupled over inner period source term Su_i.
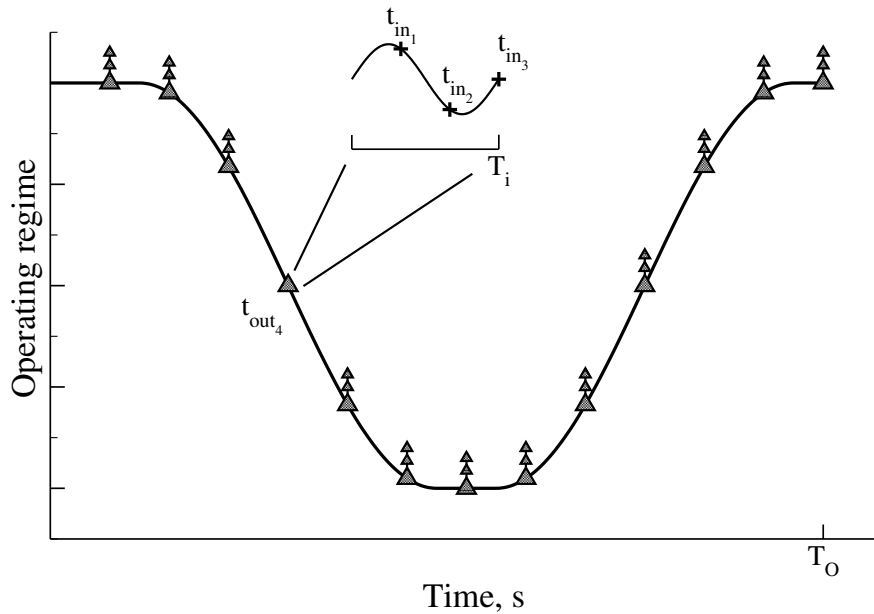

Figure 4.5: Inner and outer layer.

If one were solving for time instant t_{out_4}, based on the two layers, this point would redundantly be solved twice, once within the scope of the outer layer as t_{out_4}, and once within the scope of inner layer as t_{in_3}. Therefore, it is clear that it is sufficient to solve them once for a single layer, with the addition of temporal history arising from the other layer. The final equation is assembled for the inner layer, with an additional coupling source term for the outer layer. This

is equivalent to performing the Harmonic Balance procedure (Chapter 2) twice with different fundamental frequencies:

$$\nabla_{\bullet}(\mathbf{u}_{kl}\mathbf{u}_{kl}) + \nabla_{\bullet}(\nu\nabla\mathbf{u}_{kl}) = Su_k + Su_l, \text{ where}$$

$$Su_l = -\frac{2\omega_i}{2n+1}\left(\sum_{i=1}^{2n} P_{i-l}\mathbf{u}_{ki}\right) \tag{4.1}$$

and

$$Su_k = -\frac{2\omega_o}{2m+1}\left(\sum_{i=1}^{2m} P_{i-k}\mathbf{u}_{iN}\right),$$

$$\text{for } k = 1...2m+1 \quad \rightarrow \text{outer loop}$$
$$\text{and } l = 1...2n+1 \quad \rightarrow \text{inner loop},$$
$$\text{with } N = 2n+1.$$

Eqn. (4.1) is valid for solving inner layer simulations with a coupling term which interconnects the inner simulations into a single outer. The inner source term is assembled as in a regular Harmonic Balance simulation, while the outer contains solutions for the same rotor position throughout outer time instants. In terms of Harmonic Balance simulations, only the $\mathbf{u}_{t_{2n+1}}$ is collected for coupling in each t_n.

In this approach it is assumed that start-up and shut-down last for a large number of periods, so that when a single time instant is observed (t_{out_i}) it can be considered as a steady operating point. This approximation allows having constant boundary conditions for the whole inner simulation, therefore t_{in_1}, t_{in_2}, t_{in_3} have the same boundary conditions, without accounting for the small change during a single rotor period. However, if short start-stop was considered, which lasts only for several rotor periods than the change of operating conditions would be too significant during one rotor period and this approach would not be valid. This is the reason why in Figure 4.5 the inner time instants are schematically placed above outer time instants, to denote that they are taking place approximately at the same time.

In the work on Francis turbine presented in Chapter 7, one rotor period lasts 0.18018 s, while shutdown lasts 9.23 s, which is 51.2 rotor periods. As the shutdown and start-up are regulated by the mass flow rate, in the experiment the mass flow rate changed ≈1.5% during one rotor rotation, while in the numerical model this variation was neglected.

4.2.4   Additional Notes

In this work, once the start-up and shut-down curves were assembled, the whole period is adjusted in time so that it is symmetric with respect to the middle time instant, i.e. $t = (n+1)\dfrac{T}{2n+1}$. This allows a significant numerical reduction – only one half of the time instants can be calculated and projected as an opposite-side solution. This can be done as opposite time instants at a symmetrically positioned curve have the same boundary conditions, same rotor speed, and blade angle, but different flow history. However, flow history, or temporal coupling, is governed by the Harmonic Balance term, which is not affected.

In the case of Francis-99 test case, which is presented in Chapter 7, the flow rate is regulated by opening and closing guide vanes. The blades are closing linearly through time between the best efficiency point (BEP) and minimum load (ML) operating points, which would require mesh morphing or some other advanced technique, such as Immersed Boundary Method [79, 80, 81] or overset grid [82, 83] in the simulation. In case of symmetrical Harmonic Balance, only $n+1$ blade positions and meshes are needed, thus allowing to fine-tune each of the $n+1$ grids if needed.

4.3   Closure

The approach for dealing with efficient turbomachinery shut-down and start-up simulations was proposed in this chapter. Due to a number of phenomena appearing during regime change or start-up and shut-down, this topic is of special interest. However, CFD simulations using conventional time-accurate approach are still quite CPU time demanding and therefore expensive. The method proposed here expands the existing time-spectral Harmonic Balance

method to handle regime changes, thus providing results faster but with reduced accuracy. As opposed to time-spectral Harmonic Balance, additional source term is added to account for additional time-scale. Therefore, two time scales defined by two dominant frequencies are taken into account: rotor frequency and start-stop frequency. Rotor frequency is defined as $f = \frac{rpm}{60}$, while start-stop frequency is a reciprocal value of the total shut-down and start-up time $f = \frac{1}{T_{SD}+T_{SU}}$ where subscripts SU stands for start-up and SD for shut-down. The validation using two test cases is presented in Chapter 6, with validation of the Harmonic Balance for single operating point given in the following chapter.

Chapter 5

Best efficiency point simulations of the ERCOFTAC Centrifugal Pump

Summary

The mathematical model, numerical tools and treatment of solution procedures was discussed in previous chapters. The Harmonic Balance method was established mathematically and the algorithm was described with notes on Harmonic Balance coupling. In this chapter the validation of the method is presented, followed by investigation of turbomachinery start-up and shut-down in Chapters 6 and 7.

The Harmonic Balance validation is performed using the ERCOFTAC centrifugal pump test case. Prior to investigation of significant flow phenomena, validation of the code has to be performed. Comparison process of the Harmonic Balance method with experimental data should give insight into accuracy of the method and its implementation and whether it is considered validated. Based on proper validation, confidence in achieved results is obtained and the CFD results can be considered relevant and reliable without the

experimental data or any other measured data from the real existing machine.

ERCOFTAC Centrifugal Pump is a 2D test case, consisting of a rotor and stator in a full-annulus configuration. Rotor consists of 7 blades and stator of 12 blades with a 6% vaneless radial gap. The domain is discretised using 93 886 hexahedral cells with the GGI interface between the rotor and stator domain. The domain is depicted in Figure 5.4. Rotational speed is 2000 rpm, operating at the nominal operating condition, with $k - \varepsilon$ model used for turbulence.

There have been a number of numerical studies of both the 2D and 3D ERCOFTAC centrifugal pump. A 3D analysis of transient flow features was performed by Combes et al. [84], proving that their computational finite element method was able to reproduce unsteady flow effects. Their results closely matched the ones obtained by Ubaldi et al. [85], however, they proceeded with running 2D steady and unsteady simulation using finite element Navier–Stokes code [86]. Still, majority of work relates to solving simplified or reduced problems. 2D results with satisfactory agreement were published by Ubaldi et al. [85], while Sato and He [87, 88, 89] presented 3D unsteady results obtained using a single blade passage. Based on incompressible Navier–Stokes equations with dual time stepping and pseudo-compressibility, the predicted unsteady results showed good agreement with experimental data. Furthermore, unsteady 2D simulations were presented by Page et al. [90], showing accurate prediction of the rotor-stator interaction. Page and Beaudoin [91] and Xie et al. [92] showed that OpenFOAM can produce similar results as other CFD codes.

5.1   Geometry

The ERCOFTAC centrifugal pump presented here was first introduced by J.F. Combes [93] within the ERCOFTAC Seminar and Workshop on Turbomachinery Flow Prediction. The pump consists of an unshrouded impeller of 7 blades with a rotatable diffuser of 12 vanes. The centrifugal impeller is 420 mm in diameter and the radial vaned diffuser is 664 mm in diameter. Details and parameters of the impeller blade and the construction details of the diffuser vane are given in Ubaldi et al. [85, 94, 95]. The impeller blades are untwisted constant thickness backswept blades with a 6% vaneless radial gap between the impeller and diffuser.

The tip clearance is set to a value of 0.4 mm, corresponding to 1% of the blade span, Figure 5.1.
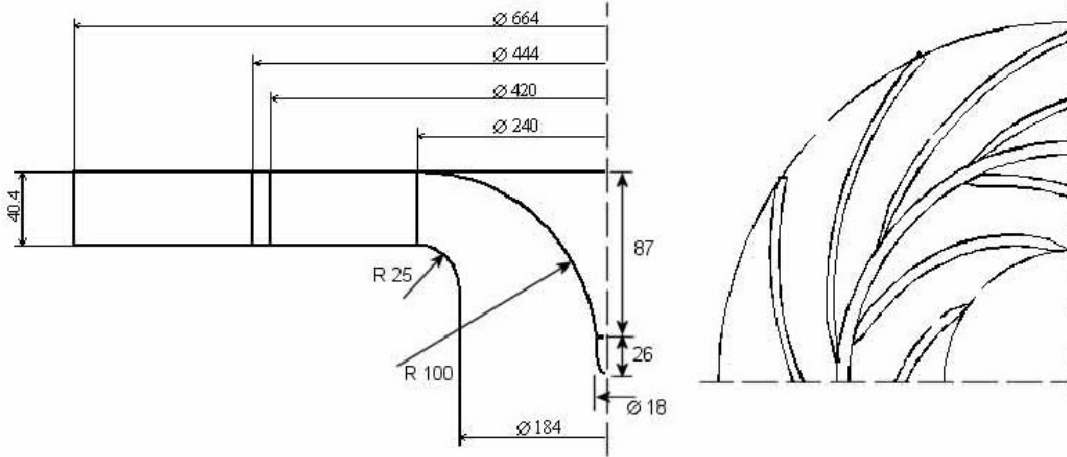

Figure 5.1: ERCOFTAC Centrifugal Pump geometry [85].

5.2   Experimental Setup

Experimental measurements of the ERCOFTAC centrifugal pump were performed by Ubaldi et al. [85] at the University of Genova by obtaining the phase locked ensemble averaged velocity components. Static pressure was measured at the impeller front end. The impeller was directly driven by a DC motor, with the model operating in an open circuit. The air is fed to the impeller through a long straight pipe and discharged into the atmosphere directly from the radial diffuser. In order to provide a uniform inflow velocity, the inlet pipe is equipped with a honeycomb, a cloth filtering element, and a throttling valve.

The measurements were taken by means of a constant-temperature hot-wire anemometer with single sensor probes and flush-mounted miniature fast response pressure transducers at the impeller outlet. Furthermore, the impeller outflow was observed by means of hot-wire probe between impeller blade trailing edge and vane leading edge (at $D_m/D_2 = 1.02$). The measured signal showed existence of a periodic part superposed with random non-repeating fluctuation. Periodic part appears due to circumferential repeating and is related to the blade passing

frequency, while the random part is usually referred to as unresolved unsteadiness
[96]. The unresolved unsteadiness denotes flow turbulence, vortex shedding, flow
separation and other unsteady phenomena. The periodic signal was separated
from unresolved unsteadiness by phase-locked sampling and ensemble-average
technique [97, 98] of a hot-wire instantaneous signal. The experimental setup is
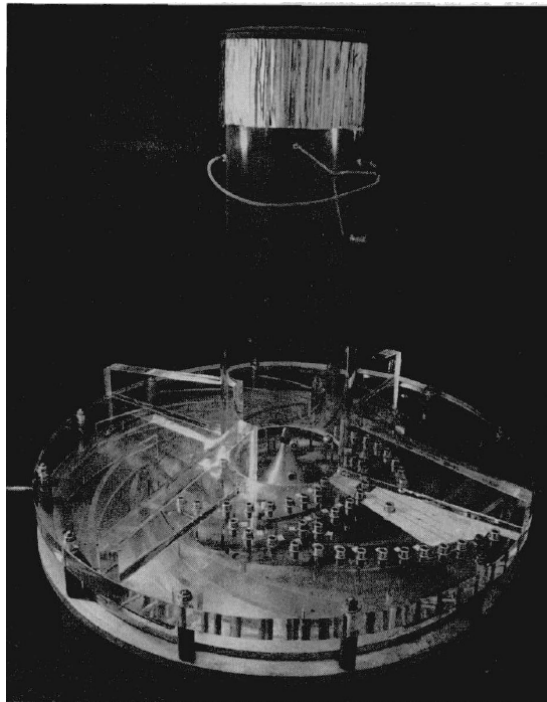shown in Figure 5.2. Detailed information regarding the experimental setup is
given in Ubaldi et al. [85].

Figure 5.2: ERCOFTAC Centrifugal pump experiment setup [85].

Overall, the velocity in the axial direction at the impeller outlet was obtained
using 17 measuring points. The distribution of the static pressure was obtained
using 10 radial measuring locations from impeller inlet to outlet through one
blade passage.

5.3   Numerical Setup

The ERCOFTAC centrifugal pump has been discretised using a block structured
mesh consisting of 93 886 hexahedral cells. The domain consists of two regions,

rotor (inner ring) and stator (outer ring), coupled with the means of a GGI interface (see Section 3.4). Although the complete geometry was available in 3D, a 2D version is used due to simplicity and conclusions brought by [86], that relevant information could be recovered from 2D simulations, although the real flow has 3D features. Therefore, the 2D approach is capable of resolving flow features with sufficient accuracy for good agreement with experimental data. Details of the mesh used are presented in Figure 5.3, showing both the complete mesh and the mesh region at the GGI interface.
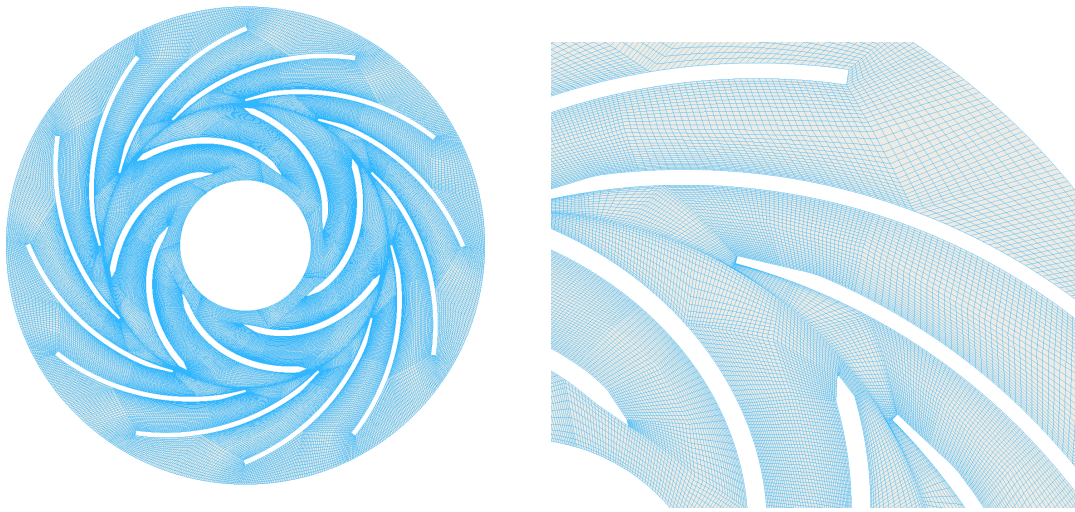

Figure 5.3: ERCOFTAC mesh. Complete mesh (left), mesh detail with blade boundary layers and GGI (right).

5.4   Validation

To prove that Harmonic Balance approach is beneficial over a conventional transient simulation, three aspects will be presented: local flow field, forces and CPU time comparison. Along with the transient simulation, the MRF steady state simulation is performed as a cheaper alternative in terms of CPU time with less accurate results. MRF is a Multiple Reference Frame method (*frozen rotor approach*) with additional source terms in steady state equations accounting for rotation, but no mesh is rotated, as described in Section 3.3. The computational domain is presented in Figure 5.4.
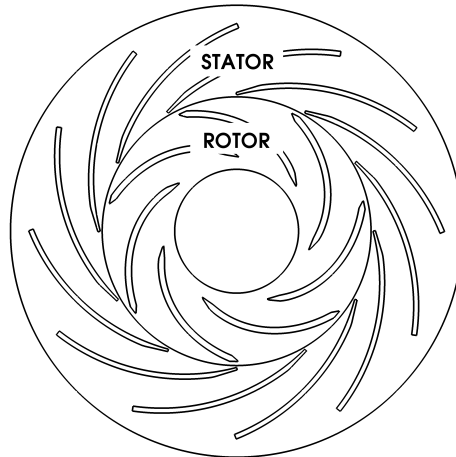
Figure 5.4: ERCOFTAC Centrifugal Pump domain.

Figure 5.5 shows the comparison of pressure contours over a single rotor blade in three time instants for solutions obtained using one and two harmonics. The two harmonics solution agrees with the transient one the most closely, which is expected. The 1 harmonic solution and MRF give similar results, with a major difference in approach, as MRF is solved for a single rotor position, thus giving no insight into different rotor-stator interaction occurrences and Harmonic Balance solving for 3 rotor-stator positions in a coupled manner. It is clear that there are no strong transients on a single frequency.

Interblade transient effects are presented in Figure 5.6, where the level of resolving the transient flow features can be noticed with an increase in the number of harmonics. The Harmonic Balance simulations exhibit wakes in the stator blade passage, as well as the transient simulation, although it is clear that a larger number of harmonics could be used to describe the flow pattern more accurately. The MRF simulation shows no wakes as the rotor is stationary.
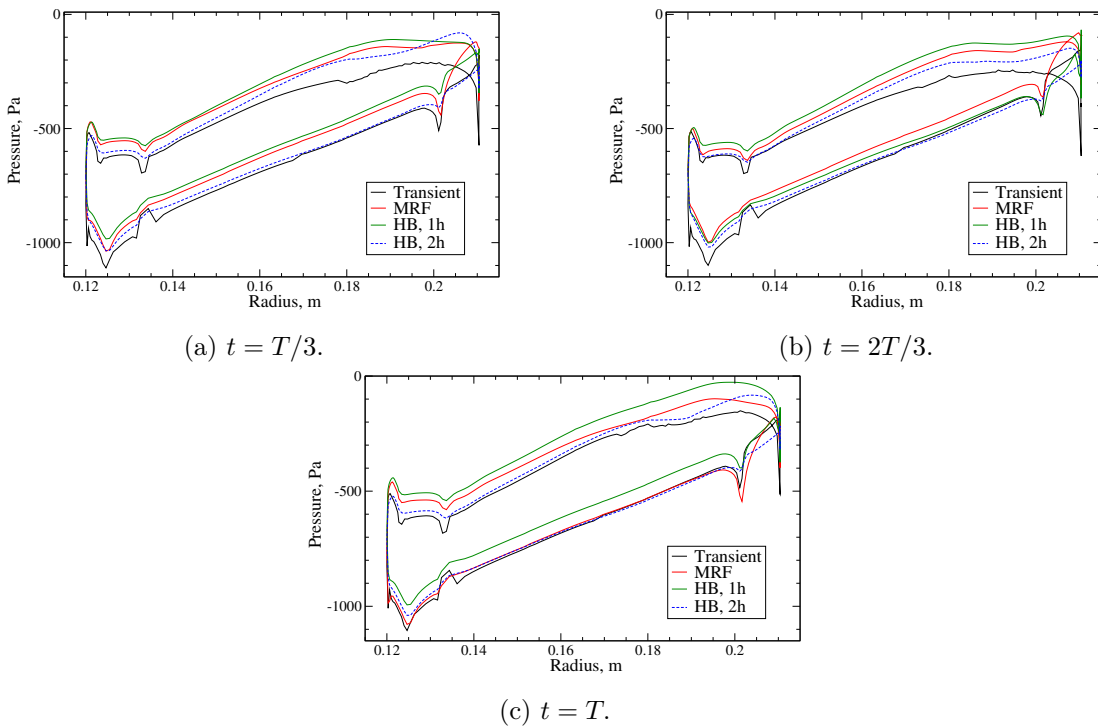
(a) $t = T/3$.

(b) $t = 2T/3$.

(c) $t = T$.

Figure 5.5: Pressure contours on rotor blade at different time instants.

(a) Transient simulation.

(b) Harmonic Balance with 1 harmonic.

(c) Harmonic Balance with 2 harmonics.
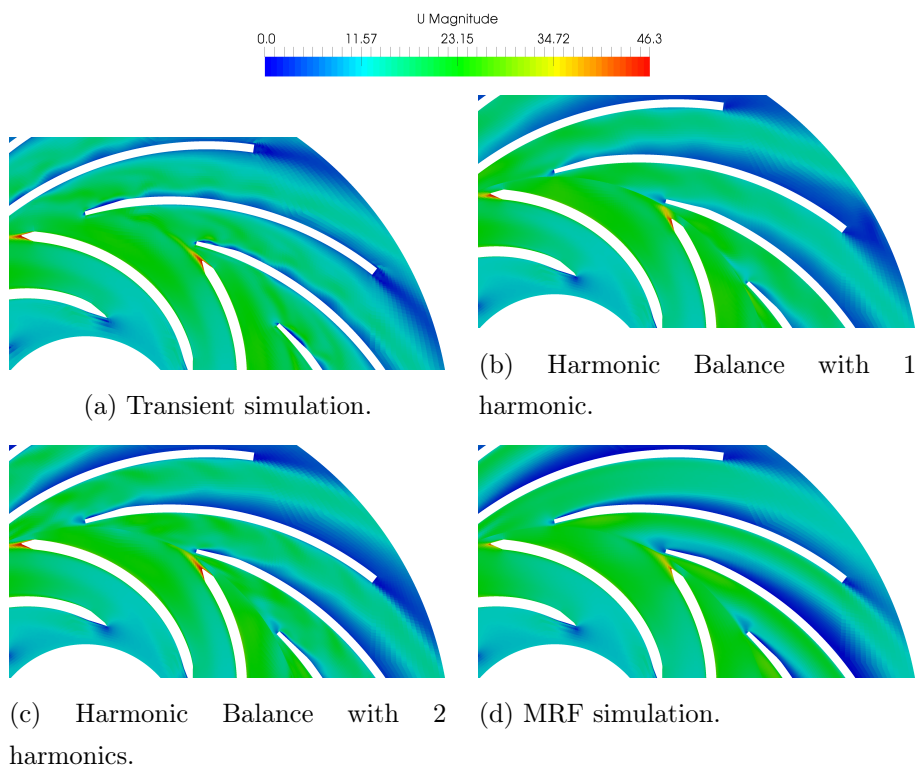
(d) MRF simulation.

Figure 5.6: Local transient effects comparison, velocity field.

Torque, head and efficiency of the pump for the MRF and various Harmonic Balance simulations are compared in table 5.1. Due to the fact that values oscillate throughout the period, the results are compared in three time instants. Lowest error of 1.3% in the Harmonic Balance simulation compared to the transient simulation denotes the significant level of accuracy with as few as 2 harmonics used.

Table 5.1: Global pump parameters comparison.

		Transient solver	HB, 1h	error, %	HB, 2h	error, %	MRF	error, %
	Efficiency	89.72	88.80	1.0	89.76	0.0	89.65	0.1
$t = \frac{T}{3}$	Head	81.48	81.80	0.4	80.45	1.3	84.12	3.1
	Torque	0.0297	0.0302	1.7	0.0294	0.9	0.0308	3.6
	Efficiency	89.92	88.78	1.3	89.81	0.1	89.65	0.3
$t = \frac{2T}{3}$	Head	81.48	81.85	0.4	80.6	1.1	84.12	3.2
	Torque	0.0296	0.0302	2.0	0.0295	0.4	0.0308	4.1
	Efficiency	89.83	88.85	1.1	89.71	0.1	89.65	0.2
$t = T$	Head	81.49	81.79	0.4	80.39	1.3	84.12	3.2
	Torque	0.0297	0.0302	1.6	0.0294	1.0	0.0308	3.7

In the remainder of this chapter, comparison of the Harmonic Balance CFD with experimental data is presented. The Harmonic Balance data is taken from the case solved with 1 harmonic. Measurements have been performed in several probing points for three variables: tangential velocity u_t, radial velocity u_r and pressure coefficient. However, velocity measurements were provided in a non-dimensional form, normalised with the measured velocity U_2, which is the velocity at $R_2 = 0.21$ m. The pressure coefficient is obtained from the following relation:

$$C_p = 2(p - p_0)\frac{\rho}{U_2^2} \tag{5.1}$$

In this study the comparison is performed against the probe located at $R/R_2 = 1.01905$ at four different time instants. Figures 5.7-5.14 show angle versus normalized velocity and pressure coefficient for each time instant. The symbols of square and triangle at top and bottom horizontal axes represent rotor and stator blade positions, respectively. This is given for reference only,

and it can be seen that the complete measured angle spans two rotor blade passages. The Harmonic Balance results are presented with a dashed line and experimental data with the solid line.   In terms of the general order of magnitude, good agreement can be reported. However, for specific rotor-stator positions or measuring angles, a more significant discrepancy may appear. If a greater level of accuracy is needed, a larger number of harmonics should be used, as for $n = 1$ only time instants $T/3$, $2T/3$ and T are solved for, while the solution in other time instants is obtained by the reconstruction from the Fourier series. Exactly these time instants ($t = 0.126$, 0.226, 0.326, 0.426 s) were not solved in that rotor position, but obtained as a harmonic interpolate of the solved time instants $t = 0.01$, 0.02, 0.03 s.
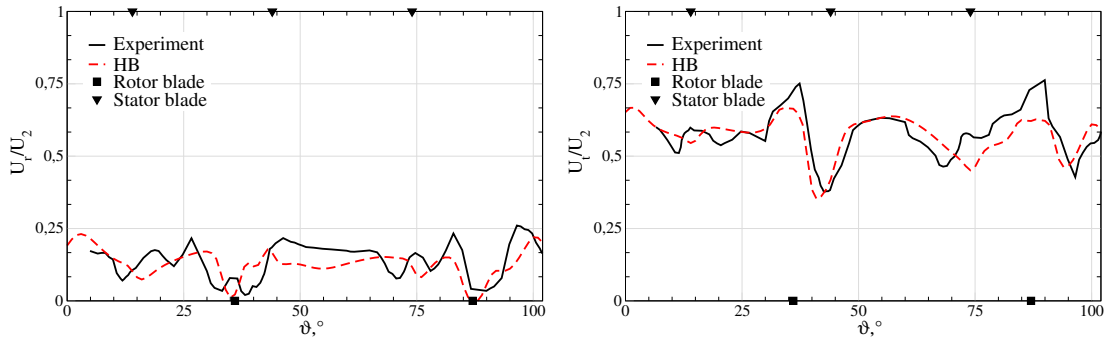

Figure 5.7: Radial (left) and tangential (right) velocity comparison at $t = 0.126$ s.
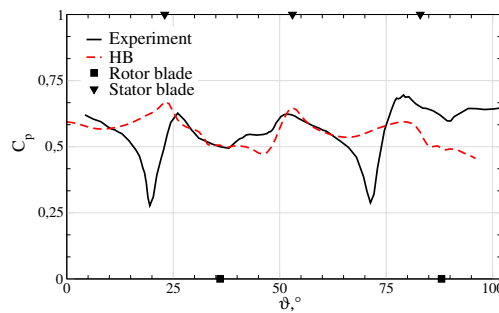

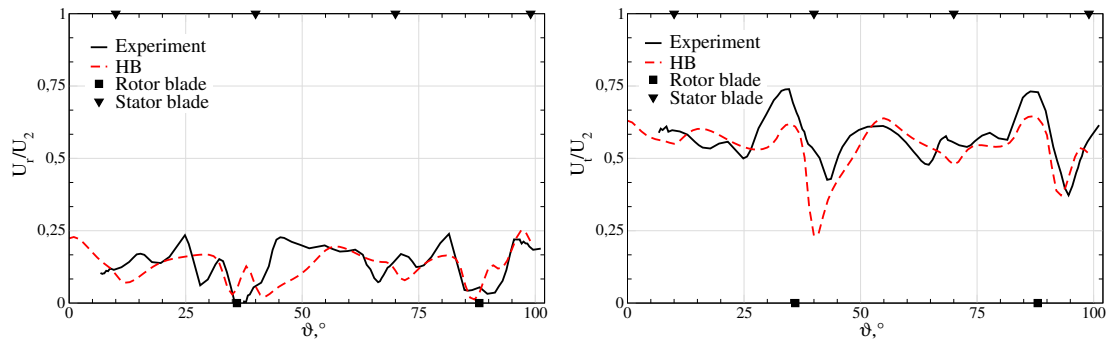Figure 5.8: Pressure coefficient comparison at $t = 0.1$ s.

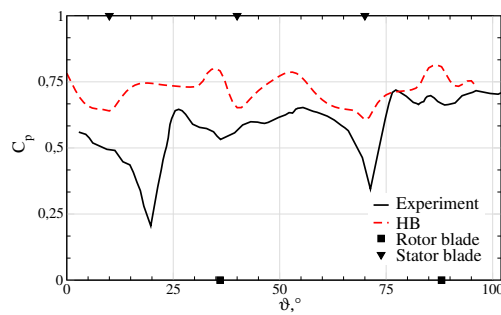Figure 5.9: Radial (left) and tangential (right) velocity comparison at $t = 0.226$ s.

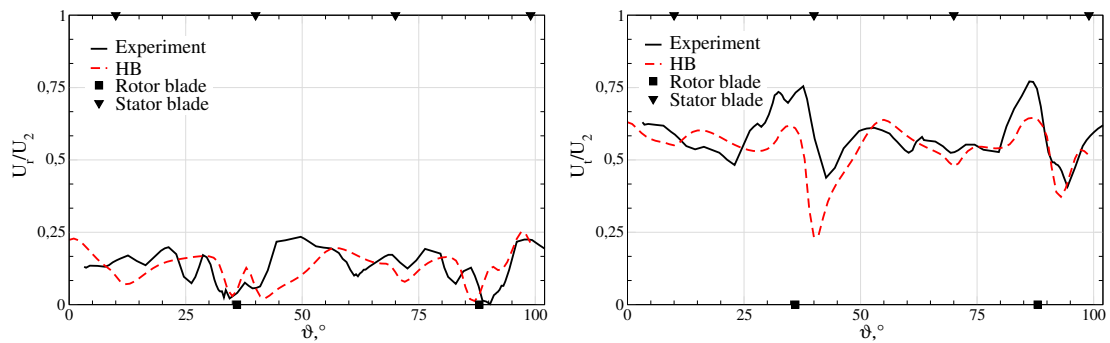Figure 5.10: Pressure coefficient comparison at $t = 0.2$ s.

Figure 5.11: Radial (left) and tangential (right) velocity comparison at $t = 0.326$ s.
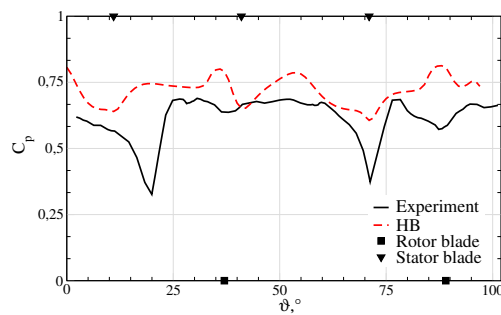

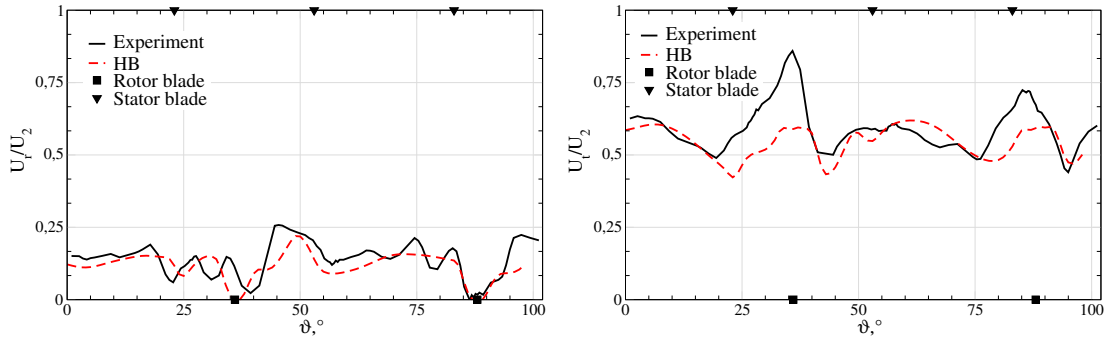Figure 5.12: Pressure coefficient comparison at $t = 0.3$ s.

Figure 5.13: Radial (left) and tangential (right) velocity comparison at $t = 0.426$ s.
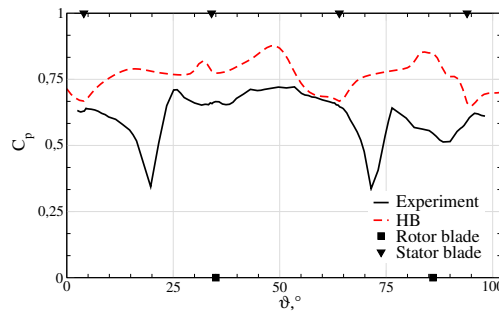

Figure 5.14: Pressure coefficient comparison at $t = 0.4$ s.

The CPU time comparison between transient, MRF and two Harmonic Balance simulations is presented in table 5.2. All of the simulations were run in serial on an Intel Core i5-3570K, 3.4 GHz computer with the same setup and mesh. The transient simulation was run at a maximum Courant-Friedrich-Lewy number equal to 0.5 and 600 time steps per period. In order to conclude the transient simulation, a periodic steady state has to be reached. In this case 8 periods were needed, yielding 40 hours of CPU time. The Harmonic Balance simulation with 2 harmonics converged in approximately 78 minutes, being 30 times faster than transient simulation.

Table 5.2: CPU time comparison for transient simulation, MRF and HB.

Transient	1 period = $\sim$ 5 hours, 8 periods = 40 hours
MRF	3100 iterations, $\sim$ 20 minutes
HB, 1h	3000 iterations, $\sim$ 52 minutes
HB, 2h	2400 iterations, $\sim$ 78 minutes

5.5   Closure

The Harmonic Balance simulation for ERCOFTAC centrifugal pump best efficiency point operation has been presented. The comparison with conventional time-accurate and steady state methods shows the advantage of the Harmonic Balance over other methods, due to accuracy and efficiency backed by flexibility in choice of harmonics resolved. Good agreement with time-accurate simulation for 1 and 2 harmonics gives additional reliability in the method, even at lower number of harmonics. Measured by wall-clock time, the CPU time comparison is performed, culminating in Harmonic Balance being approximately 30 times faster than the conventional time-accurate simulation. Based on the observed accuracy, this shows that relevant results can be obtained in a fraction of time needed by the time-accurate simulation.

Finally, the comparison of Harmonic Balance with experimental data is performed in four time instants throughout the period. Investigated variables include radial and tangential velocity and pressure coefficient and a similar level of accuracy was achieved as in the results presented by several other authors [85, 90, 92, 99].

Based on this work, a general numerical accuracy of the method has been assessed and is therefore expected in the following analyses. A number of aspects have been covered: integral quantities (head, torque, efficiency), local flow features, pressure fluctuations on the blade, compared with other numerical methods and experimental data.

Chapter 6

Start-up and Shut-down Prediction with Harmonic Balance: 2D Pump

Summary

Validation of the general Harmonic Balance method was presented in Chapter 5 using the ERCOFTAC centrifugal pump, a 2D test case with available experimental results. The Harmonic Balance method is validated against conventional time-accurate and steady state MRF approach. After the validation of the conventional Harmonic Balance, a novel application is presented for simulations of turbomachinery transients, such as start-up and shut-down, or any other regime change (e.g. load acceptance and load rejection investigation). The Francis turbine is chosen since experimental data is publicly available for several steady flow regimes (PL, BEP, HL) and two regime changes (start-up and shut-down) and the comparison of Harmonic Balance with experimental results is performed. The main reason for using Harmonic Balance to investigate the regime change is the significant amount of CPU time saved, as regime change can last for up to 100 periods, followed and preceded by the

requirement for reaching the periodic steady-state. In terms of transient simulation, this means running a number of periods in order to reach periodic steady state, followed by periods involving the regime change and then reaching the periodic steady-state to eliminate any occurring flow changes. On the other hand, the Harmonic Balance method converges directly to periodic steady state, thus significantly reducing the CPU time.

The presented approach of nested Harmonic Balance is validated on a preliminary 2D pump test case. The test case presents a smaller and simpler version of general problems to be solved using this technique. Therefore, the results could be easily obtained in a fraction of time compared to large industrial cases, and thoroughly compared based on reduced size of the data gathered. This allowed running a complete time-accurate simulation of shut-down and start-up followed by a detailed comparison with nested Harmonic Balance. Efficiency and accuracy of the model are assessed by comparing the nested Harmonic Balance results to conventional time-accurate simulation performed with the same boundary conditions, on the same domain with equal number of cells and on the same computer. Therefore, the comparison can be performed both in terms of resulting flow field and in terms of computational time. The presented results give pressure and velocity fluctuations throughout time in four probes for the Harmonic Balance and time-accurate simulations. If good agreement is achieved, the method can then be further deployed on the Francis 99 test case in Chapter 7.

6.1   Geometry

The geometry is a simplified model of a centrifugal pump in a rotor-stator configuration. The blades are arbitrarily thin and straight with no profile. Rotor consists of 4 blades and stator of 3 blades with the aim of obtaining and observing the rotor-stator interaction on a larger time scale. The geometry is presented in Figure 6.1.

The inner ring represents the stator, with a radius from $r = 0.2$ m to $r = 0.5$ m. Stator blades are 0.145 m long and 0.015 m thick. The outer ring is a rotor, from $r = 0.5$ m to $r = 1$ m, with blades 0.29 m long and 0.029 m thick.

Vaneless space between rotor and stator blades is 0.18 m or 62% of the rotor blade.

6.2   Numerical Setup

The computational domain is a 2D annulus consisting of two parts: stator and rotor. The domain is discretised with 12 580 hexahedral cells, as presented in Figure 6.1. The interface between rotor and stator regions is modelled using the overlap GGI boundary condition (see Section 3.4), allowing for contiguous flow between regions regardless of numerical boundary. Due to GGI, the master and shadow sides of the interface do not have to have conformal mesh points as cell weighted implicit interpolation is performed, thus allowing easier mesh generation.
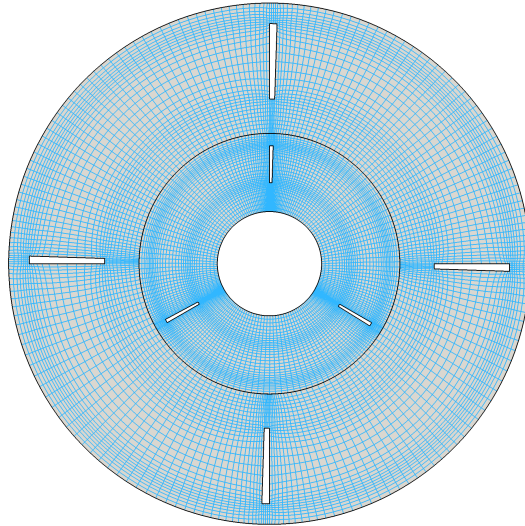

Figure 6.1: Test case mesh and geometry.

The change of operating conditions is performed between two operating points, OP1 and OP2, by regulating the inlet velocity (inlet flow rate) at a constant rotor speed. Rotor speed is set to 60 rpm at all times, with OP1 characterized by inlet velocity $u = 8$ ms^{-1} and OP2 by inlet velocity $u = 0$ ms^{-1}, resembling a closed inlet valve. The start-up and shut-down curve is assembled arbitrarily with complete period set to $T = 130$ s. The curves describing the change of the regime are parts of a sine function, described with the equation:

$$y = 4 + 4\cos(\frac{2\pi}{T}t) \tag{6.1}$$

The complete period can be divided into 5 parts as shown in Figure 4.1. The initial steady state at OP1 is kept unchanged from $t = 0$ s to $t = 15$ s. This is to reach the periodic steady state prior to shut-down, followed by shut-down lasting from $t = 15$ s to $t = 65$ s, during which the inlet velocity is reduced to $u_{inlet} = 0$ ms^{-1}. The closed condition, at constant rotor speed of 60 rpm is maintained for 10 s, to clear out the effects of shut-down. Closed condition is followed by the pump start-up from $t = 75$ s to $t = 125$ s during which the pump gets to the initial, fully open operating point OP1 with inlet velocity $u = 8$ ms^{-1}. This final state is kept for 5 s until the end of the period, $t = 130$ s. The overview of the complete period is shown in Figure 6.2.
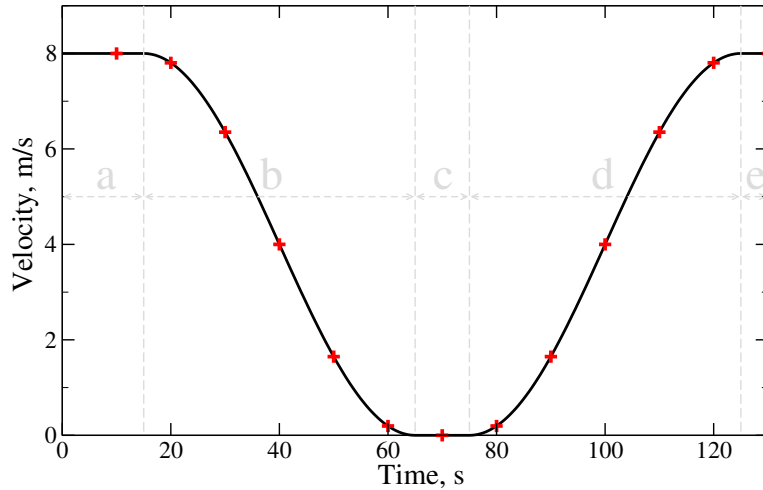

Figure 6.2: Inlet velocity profile and time instants of the inner simulations.

For the time-accurate simulation the inlet velocity curve presented in Figure 6.2 is set as the inlet velocity boundary condition. Simulation is run for one complete period, $T = 130$ s and compared with the Harmonic Balance. The Harmonic Balance simulation is run using $n = 6$ outer and $m = 1$ inner harmonics, which are denoted by red crosses in Figure 6.2. As the inlet velocity curve is symmetrical in time with respect to $t = 70$ s (the points left from $t = 70$ s have the same operating conditions as those to the right) only 7 time instants can be calculated

and projected to its matching part, offering additional reduction in computational cost.

6.3   Results

The comparison between Harmonic Balance and time-accurate simulation for the changes of operating point is presented in this section. The comparison consists of velocity and pressure analysis in several probes, followed by a visual comparison of a 2D flow field. Pressure and velocity samples were taken through time in four probing points at different parts of the domain. The probing points are presented in Figure 6.3.
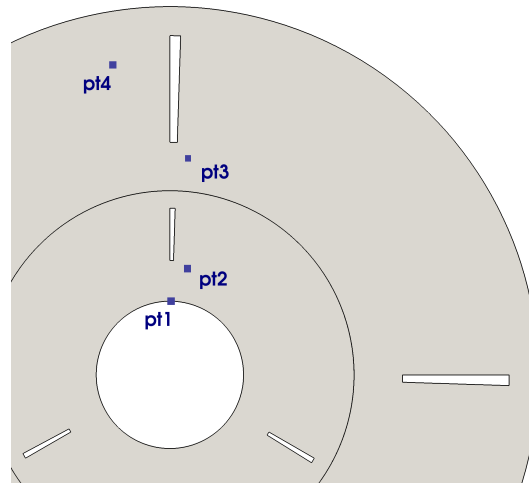

Figure 6.3: Location of probes.

2D flow field in terms of velocity and pressure is presented in a number of time steps in Figures 6.4 and 6.5. Figures show that the overall trend and flow features were successfully captured, with minor discrepancies between the Harmonic Balance and time-accurate simulations. Therefore, the Harmonic Balance approach gives accurate results for a simple case and should be tested against experimental results once the numerical accuracy has been assessed. Comparison in terms of efficiency is covered in the following section.

(a) HB, $t = 13$s

(b) Transient, $t = 13$s

(c) HB, $t = 32$s

(d) Transient, $t = 32$s

(e) HB, $t = 40$s

(f) Transient, $t = 40$s

(g) HB, $t = 48$s

(h) Transient, $t = 48$s

(i) HB, $t = 70$s

(j) Transient, $t = 70$s

Figure 6.4: Velocity fields over time.

(a) HB, $t = 13$s

(b) Transient, $t = 13$s

(c) HB, $t = 32$s

(d) Transient, $t = 32$s

(e) HB, $t = 40$s

(f) Transient, $t = 40$s

(g) HB, $t = 48$s

(h) Transient, $t = 48$s

(i) HB, $t = 70$s

(j) Transient, $t = 70$s
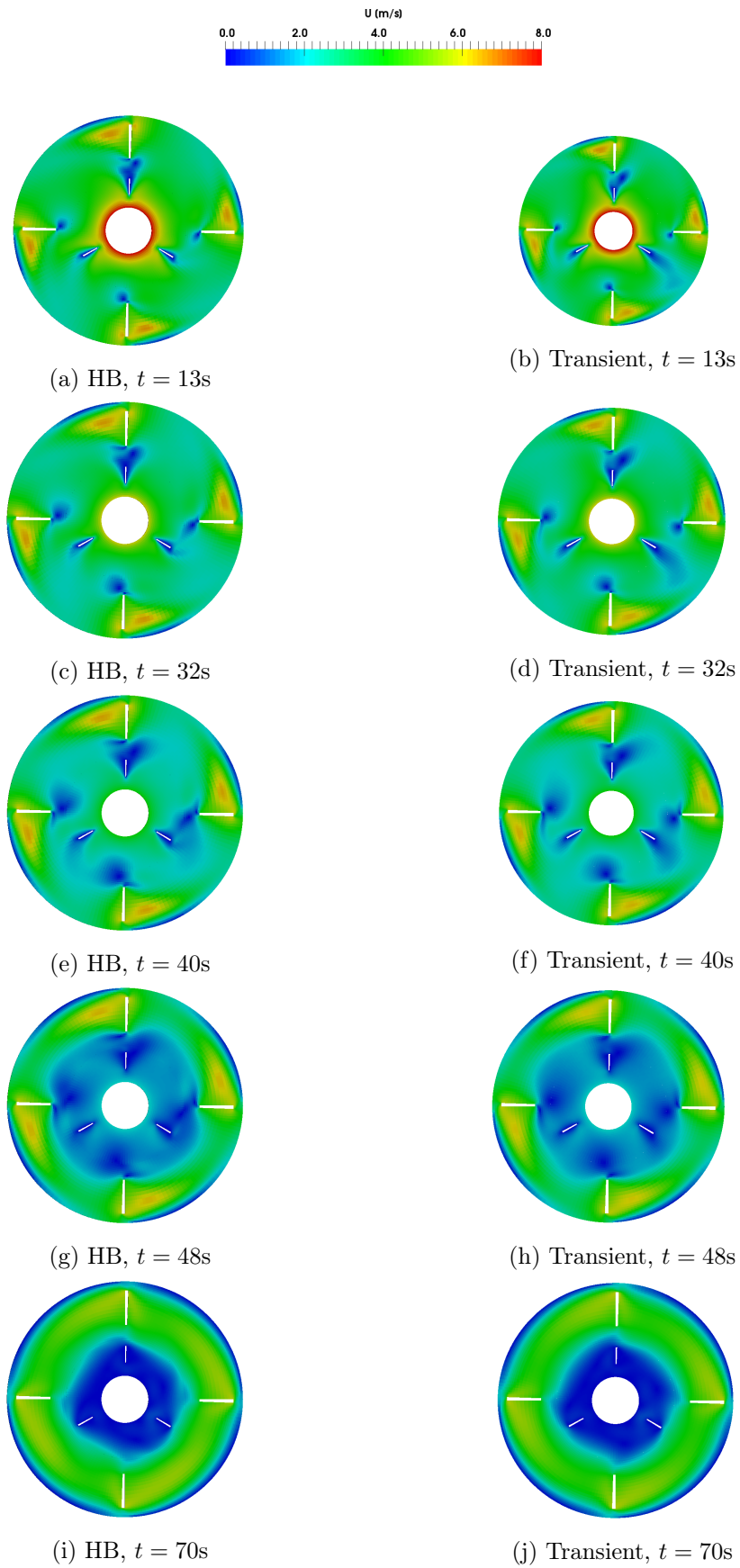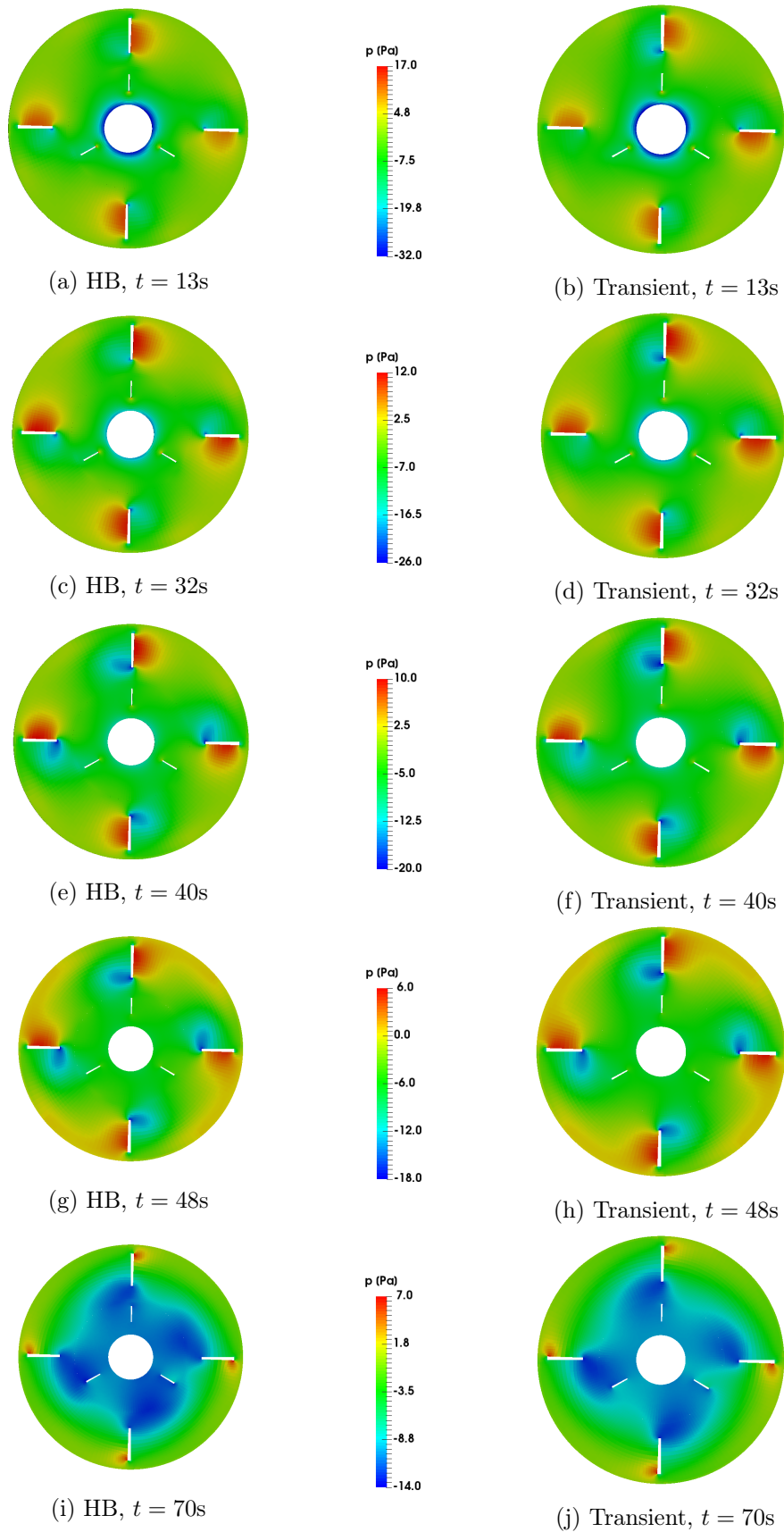
Figure 6.5: Pressure fields over time.

Probe 1 is the inlet probe which will show how well the boundary conditions were captured. Inlet velocity should be captured exactly, as this is a prescribed boundary condition, while pressure is expected to exhibit some fluctuations. Probe 2 is located just before the stator blade, while probe 3 is positioned in the vaneless space between the stator and rotor blade. Probe 4 is located next to the rotor blade, such that the rotor–stator interaction can be captured. Figure 6.6 shows pressure and velocity probes comparison between the Harmonic Balance and time-accurate simulation. Figures on the left show time versus velocity, while figures on the right show time versus pressure. The thin black line represents time-accurate simulation and thick red line represents the Harmonic Balance simulation.

Good agreement can be observed, although the Harmonic Balance results do not exhibit each blade passing fluctuation as the time-accurate simulation does. Moreover, the Harmonic Balance solution resembles the averaged time-accurate measurements. Figure 6.6a shows that the inlet profile is matched exactly between the two simulations, as expected.

The obtained results show that the approximation that the boundary conditions are not changing significantly during one rotor period (Section 4.2) is valid for these types of problems. At full period being 130 s and rotor speed of 60 rpm, the inlet velocity should change 1.6% per rotor rotation, which is neglected in the Harmonic Balance simulation. However, compared with the time-accurate simulation where boundary conditions change gradually, this approximation did not show any deterioration in results.

(a) Velocity in point 1,

(b) Pressure in point 1,

(c) Velocity in point 2,

(d) Pressure in point 2,

(e) Velocity in point 3,

(f) Pressure in point 3,

(g) Velocity in point 4,
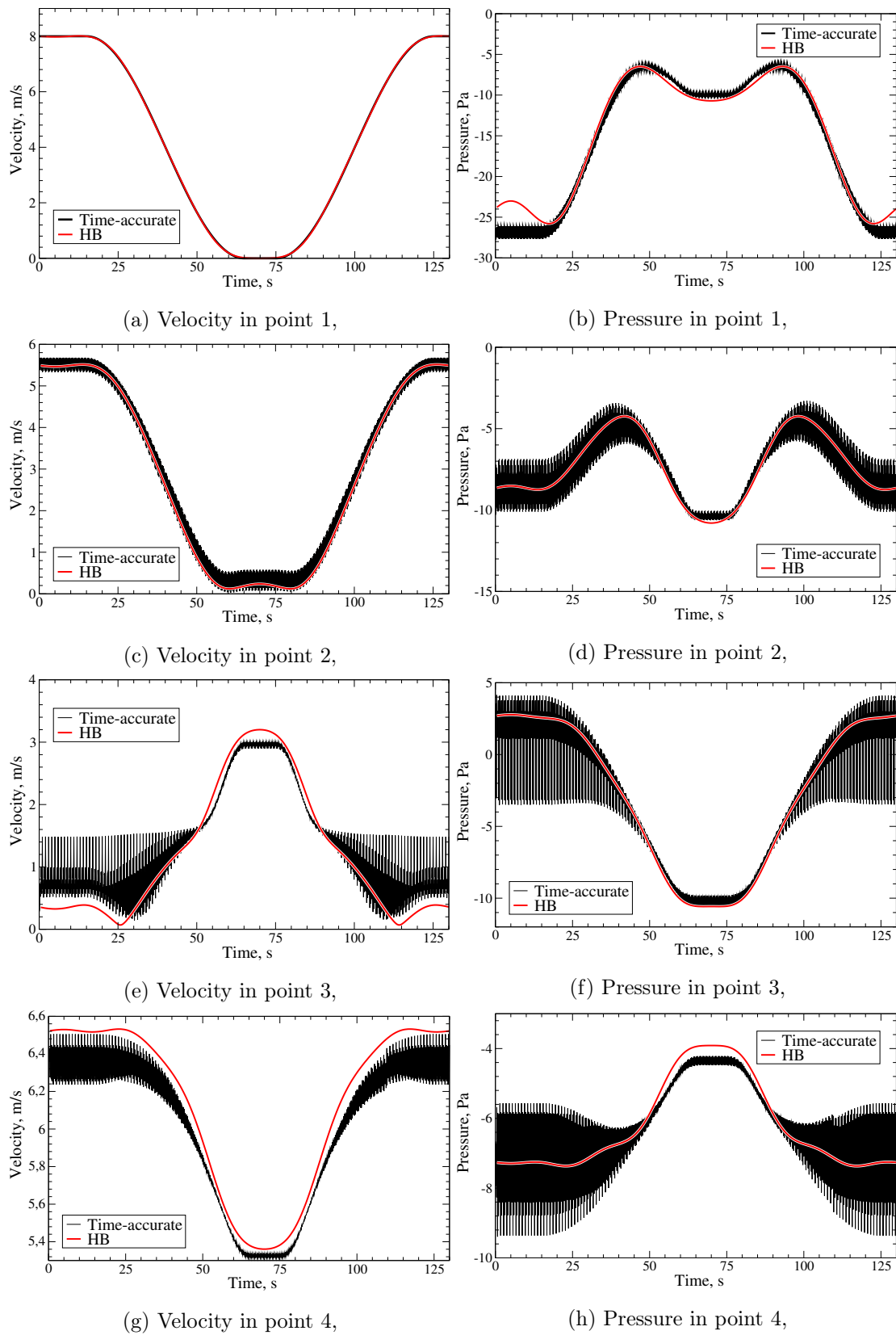
(h) Pressure in point 4,

Figure 6.6: Velocity and pressure over time in measured probes.

6.4   CPU Time Comparison

The main idea behind the Harmonic Balance approach for turbine shut-down and start-up was the reduction of CPU time for prediction of flow features. CPU time comparison is performed for the Harmonic Balance and time-accurate simulations and presented in this section. For the comparison to be valid, all of the settings were the same, as much as the distinctive nature of the two methods allowed. The computational domain was exactly the same, with all simulations run on a single Intel Core i5-3570K CPU @ 3.40 GHz and 8Gb RAM computer, using only one core. The time-accurate simulation was run based on CFL number limited to 0.5, resulting in variable time step between $4 - 8 \cdot 10^{-4}$ s. The Harmonic Balance simulation was run with $n = 6$ outer and $m = 1$ inner harmonics, yielding overall 18 steady state equations, which is negligible compared to the number of time steps in time-accurate simulation. This is well demonstrated by the measured wall-clock time for both simulations, as presented in Table 6.1. Convergence criterion for the Harmonic Balance simulation was that residuals of all equations fall below 10^{-5}. Both simulations started from uninitialized flow field. Time-accurate simulation took 18.7 hours to finish the whole 130 s period, which is quite long for a simple 2D case with $\approx$12000 cells. On the other hand, the Harmonic Balance simulation took $\approx$40 minutes to reach convergence. This is a reduction of almost 30 times meaning that significant savings in terms of computational resources can be achieved. The presented comparison proves the initial goal of the method is fulfilled, which is to create a less time consuming approach with good accuracy compared to conventional numerical methods. With time-accurate simulation lasting almost 19 hours and Harmonic Balance simulation being more that 28 times faster by converging in 40 minutes, this approach is beneficial for future use.

Table 6.1: Calculation time.

	Full HB simulation	Transient simulation	Reduction (Transient/HB)
Time	0.66 h	18.7 h	**28.3**

6.5   Closure

The application of the Harmonic Balance method for turbomachinery start-stop simulations was presented in this chapter. The change of operating regime from arbitrary operating point OP1 to closed condition OP2 is demonstrated, as well as the start-up from closed-valve mixing regime to OP1. The comparison of nested Harmonic Balance with the time-accurate simulation shows good agreement in terms of pressure and velocity measured in four probes, however, the Harmonic Balance does not exhibit the blade passing fluctuations . CPU time comparison reveals the main strength of the Harmonic Balance, as the simulation took 30 times less time compared to time-accurate one. The comparison of the Harmonic Balance with experimental data is presented in the following chapter.

Chapter 7

Start-up and Shut-down Prediction with Harmonic Balance: Francis-99

Summary

Francis test case and experiment, based on the Francis-99 Workshop [100] is presented in this section. Organizers of the Workshops provided a large amount of technical documentation concerning the geometry and operating regime of the turbine, which is what this work is based on and the authors gratefully acknowledge the NTNU - Norwegian University of Science and Technology for the significant amount of valuable publicly released data. Francis turbine is a water turbine consisting of a spiral inlet, followed by 14 stay vanes, 28 guide vanes and 30 runner blades, ending with the draft tube outlet. Within the Workshop, data for best efficiency point (BEP), minimum load (ML), high load (HL), start-up and shut-down are provided. In this study only the BEP, start-up and shut-down are considered. Simulations are performed using the Harmonic Balance approach

presented in Chapter 4 and compared with experimental data. Start-up and shut-down are regulated by changing the inlet mass flow rate, which is achieved in the experiment by changing the guide vanes angle, i.e. by opening and closing the flow channels with blade rotation. During start-up and shut-down, the rotational velocity is held constant. The same start-stop process is modelled here, however, if a different procedure was undertaken in the experiment, it could have been modelled differently in the simulation as well. Comparison includes pressure fluctuation measurements in two probing points and power measurement for the whole shut-down and start-up cycle. As noted by the experimentalists from the Workshop, certain inconsistencies related to experimental data exist, which are analysed in the following sections.

7.1   Experimental Setup

The experimental setup for the Francis turbine, provided within the Francis-99 Workshop [101, 102] is presented in this section. The model of a turbine, in a scale of 1 : 5.1 was used in the experiment as a part of an open loop hydraulic system. Both steady state and transient measurements were performed. Steady state measurements were conducted for three operating points:

- part load (PL),

- best efficiency point (BEP),

- high load (HL),

defined by a guide vane angle and mass flow rate. The transient measurements correspond to change of operating conditions:

- load acceptance from PL to BEP,

- load reduction from BEP to PL,

- turbine start-up,

- turbine shut-down.

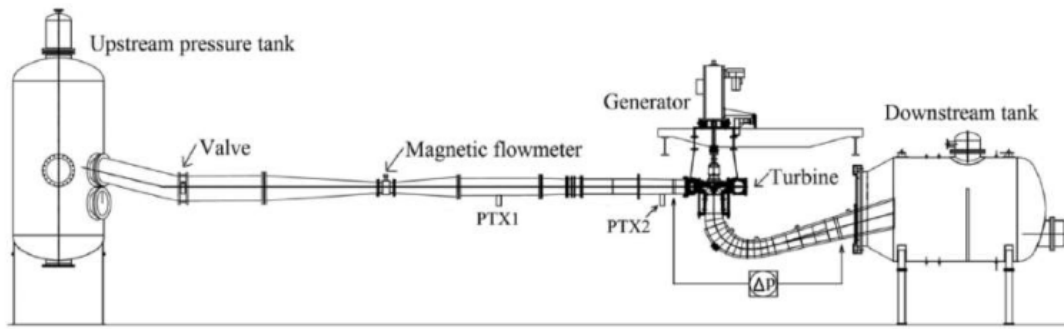The experimental setup is presented in Figure 7.1.

Figure 7.1: Francis 99 model test rig [103].

Pressure probes were mounted at three locations: pressure sensor VL2 at the vaneless space and sensors DT5 and DT6 at the draft tube cone. Exact locations of the probes are given in Table 7.1.

Table 7.1: Coordinates of the pressure probes.

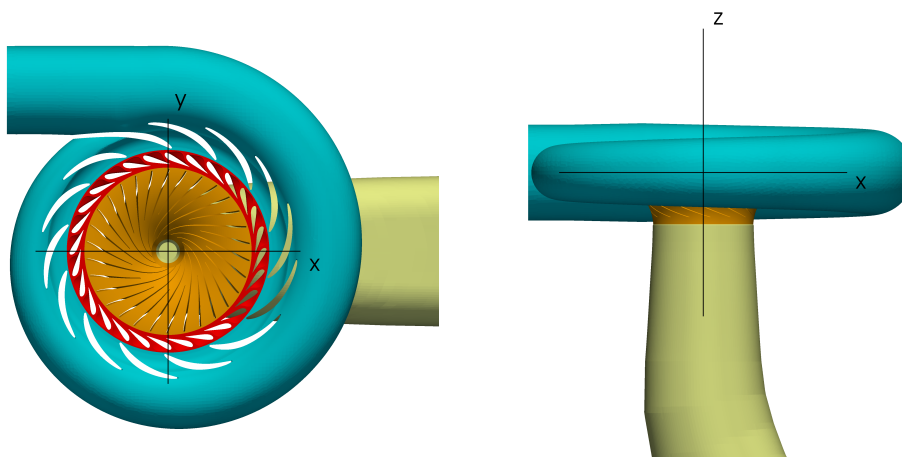| Sensor	VL2	DT5	DT6
x[mm]	-320.0	-149.1	149.1
y[mm]	62.2	-100.6	100.6
z[mm]	-29.4	-305.8	305.8
Uncertainty[%]	±0.01%	±0.1%	±0.1%

Figure 7.2: Global coordinate system for the measurement locations.

The definition of global coordinates is given in Figure 7.2.   The pressure fluctuations were gathered at a sampling rate of 5 kHz. The uncertainties for

VL2 probe is $\pm 0.01\%$ and for the remaining two is $\pm 0.1\%$. Uncertainty was estimated following the procedure available in IEC 60193 [104] and the measurement uncertainty was measured by repeating the test several times.

Velocity measurements were performed along three lines, two horizontal and one vertical in the draft tube cone. The horizontal lines were acquired using the laser doppler anemometry (LDA) and the vertical one is measured in a PIV plane, Figure 7.3. Sampling rate for the velocity measurements is 40 Hz. The exact locations of the lines L1, L2 and L3 are given in Table 7.2.
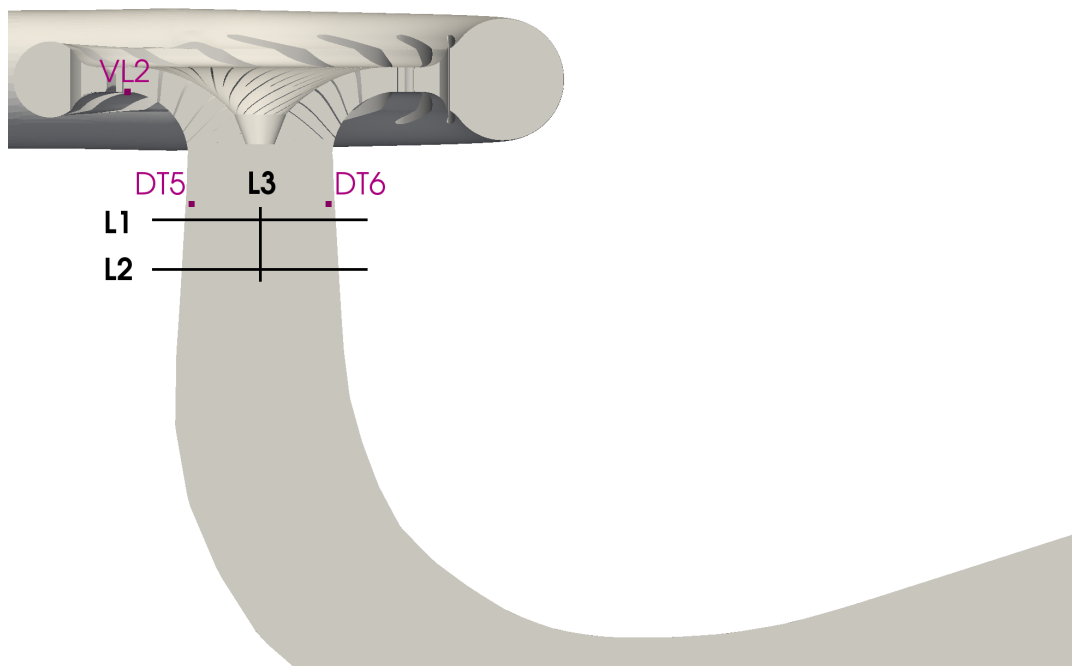

Figure 7.3: Positions of the pressure sensors and velocity measurement lines.

Table 7.2: Coordinates of the velocity lines.

Velocity lines	L1 start	L1 end	L2 start	L2 end	L3 start	L3 end
x[mm]	25.96	-25.56	25.96	-25.56	0	0
y[mm]	133.55	-131.49	133.55	-131.49	0	0
z[mm]	-338.60	-338.60	-458.60	-458.60	-488.6	-308.6
Total points	28		28		28	

Due to a difference between the experimental setup and numerical model, the

measurements provided for the inlet and outlet do not physically match the location of inlet and outlet in the numerical model. Details of the experimental model inlet and outlet are included here, to allow data calibration for the numerical model.   Cross sectional areas of the inlet and outlet pressure measurement locations are 0.0962 m² and 0.236 m². The outlet cross sectional pressure measurement location is 1.58 m before the draft tube outlet in the numerical model. The height difference between the inlet and outlet pressure measurement is 1.0715 m, with the remaining data given in Table 7.3.

Table 7.3: Acquired flow parameters and setup for PL, BEP and HL.

Parameter	PL	BEP	HL
Guide vane angle (°)	6.72	9.84	12.43
Net head (m)	11.87	11.94	11.88
Discharge (m^3s^{-1})	0.13962	0.19959	0.24246
Runner angular speed (rpm)	332.84	332.59	332.59
Casing inlet pressure - absolute (kPa)	218.08	215.57	212.38
Hydraulic efficiency (%)	90.13	92.39	91.71
Water density (kg m^{-3})	999.8	999.8	999.8
Kinematic viscosity (m^2 s^{-1})	$9.57 \cdot 10^{-7}$	$9.57 \cdot 10^{-7}$	$9.57 \cdot 10^{-7}$

7.2   Data Manipulation

As reported by the experimentalists [103], the provided pieces of data for the transient operation measurements were not fully accurate.   For transient operation, four transient conditions were measured: load acceptance from PL to BEP; load reduction from BEP to PL; start-up and shut-down. However, the provided measurement of the mass flow rate variation is not correct as the flowmeter response time was too slow, yielding delay in the measurements of ≈2 s. As the working medium is water (with constant density), the mass flow rate is a linear function of guide vane angle, therefore the mass flow rate variation can be reconstructed based on initial and final mass flow rate and guide vane angle variation. It was stated on the Workshop website [103] that

the used flowmeter response time was too slow for valid readings and was causing a significant discrepancy between blade angle and measured mass flow rate. Experimentalists suggest using linearized mass flow rate based on guide vane angle (openness). The linearized data was used by Minakov et al. [105] who obtained good agreement. Therefore, the same approach was adopted here.

Flow rate was considered to change from 0.202 m^3s^{-1} at 9.84° blade angle to 0.018 m^3s^{-1} at 0.8° blade angle. In order to assess the complete experimental curve, values from the reached steady-state points are used, as flow meter response time is ≈2 s and other readings cannot be used. Therefore, the real mass flow rate variation curve could be constructed based on the provided steady state measurements taken prior to the load variation, and afterwards. Figure 7.4 shows the comparison of originally provided mass flow rate (triangles), reconstructed mass flow rate (solid line) and guide vane angle (dots). Normalized curves are presented for shut-down mass flow rate (measured and linearized) and blade angle against time. The same variation is used for start-up as well. Therefore, the reconstructed mass flow rate shown in Figure 7.4 is used in the remainder of this work.
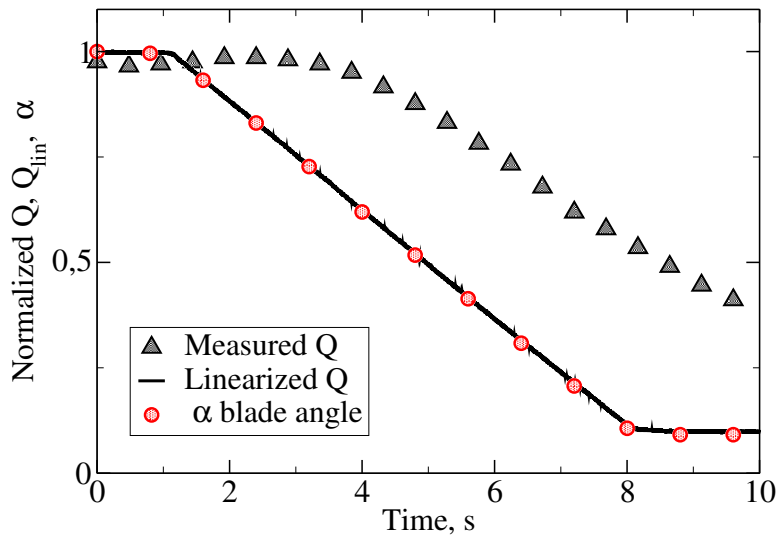

Figure 7.4: Normalized flow rate as measured (Q), linearized (Q_{lin}) and blade angle (α).

The provided experimental data needs to be configured to match the numerical model and prescribed boundary conditions. Therefore, reference pressure at the referent height needs to be established prior to the comparison. In this study,

most of the relations are based upon the measured variation of guide vane angle in time. As in the experiment both the inlet and outlet variations exist, but only the inlet measurement is provided, the outlet pressure and total pressure difference through the turbine is calculated based on the measurement of head. The calculation of pressure difference was needed due to a fixed pressure value boundary condition at the outlet in the numerical simulation. This allowed the comparison of measurements in pressure probes. Power variation during the change of operating regime is then calculated using the reconstructed mass flow rate and measured head:

$$P = QH\rho g\eta \tag{7.1}$$

7.3   Geometry

The geometry of the Francis turbine provided by the Francis-99 Workshop [101] consists of a spiral inlet casing with 14 stay vanes, shown in Figures 7.5 and 7.6, followed by 28 guide vanes responsible for regulating the mass flow rate by opening or closing, further followed by the runner. The runner consists of main blades and shorter splitter blades, overall counting 15 of each. The blades are twisted at 180° from inlet to the outlet of the runner. The end of the runner is continued by a draft tube cone followed by a draft tube.

The experiment and the provided data and geometry refer to the model of a turbine, scaled $1 : 5.1$ to a prototype operating at a Tokke power plant in Norway. Therefore, all of the data provided are valid at model scale. The size of a spiral casing is $r = 0.73$ m at the outer radius, with stay vanes located between radius $r_1 = 0.388$ m and $r_2 = 0.5$ m. The short guide vanes are positioned close to the stay vanes and rotate between 0.8° at closed condition, to 12.43° for high load. Best efficiency point is obtained at 9.84° and 333 min^{-1}. Runner inlet and outlet diameters are 0.63 m and 0.349 m, respectively. The runner inlet height is 0.06 m. Draft tube is 5.45 m long with total height difference of 0.5 m. The comparison between model scale and prototype is given in Table 7.4.
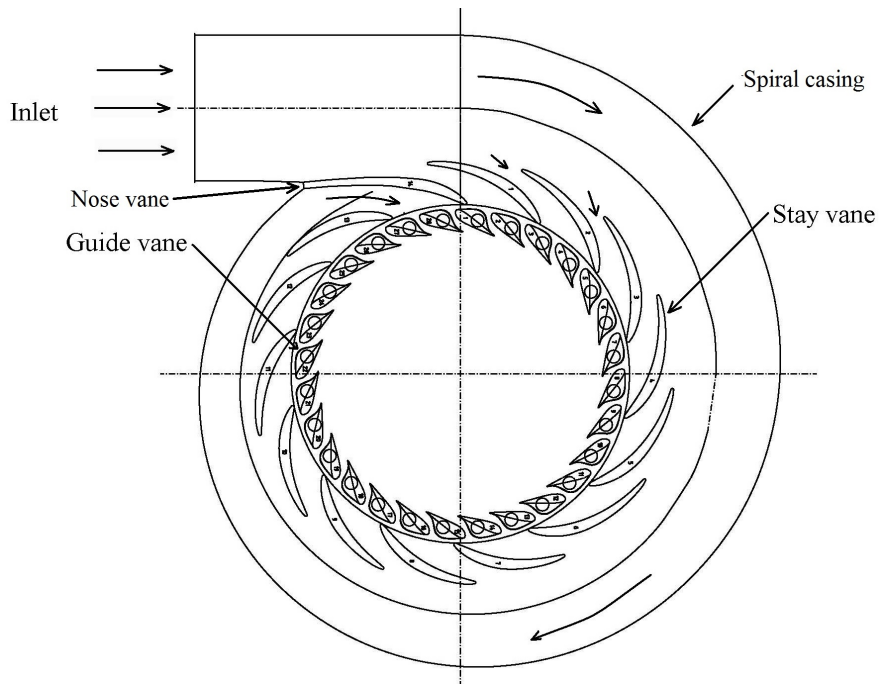
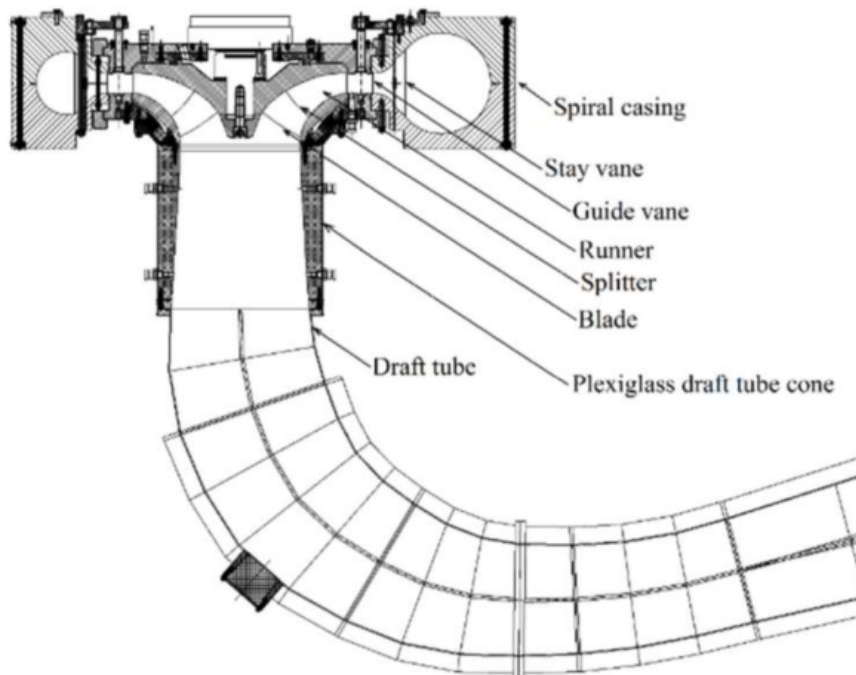Figure 7.5: Top view of the Francis-99 turbine model [101].

Figure 7.6: Cut view of the Francis-99 turbine model [101].

Table 7.4: Francis 99 model and prototype parameters at BEP.

	$H[m]$	$d_{inlet}[m]$	$d_{outlet}[m]$	$n[min^{-1}]$	$Q[m^3 s^{-1}]$	$P[kW]$	$Re[-]$
Model	12	0.630	0.349	335	0.2	22	$1.8 \cdot 10^6$
Prototype	377	3.216	1.779	375	31.0	110000	$4.1 \cdot 10^7$

7.4   Numerical Setup

In this section the details regarding the numerical setup of the Francis-99 case are presented. Although the mesh was provided within the Workshop along with the geometry, a new mesh was generated for this study. Software used for meshing is Pointwise [106] and several meshes were created. Pointwise is a commercial meshing software for manual mesh generation with various types of finite volume elements available (tetrahedra, hexahedra, prisms, pyramids). Meshes used in this study are fully structured. For the best efficiency point simulation, a mesh consisting of full-annulus guide vanes, runner and draft tube was created. For shut-down/start-up simulations, a set of identical meshes was created, with each having a different guide vane angle. The start-stop set of meshes was done using a single blade passage.

7.4.1   Best Efficiency Point Mesh

BEP mesh was done in a full-annulus configuration, consisting of guide vanes followed by a runner and a draft tube. The spiral casing inlet was not taken into account. The domain was discretised with 6 242 679 hexahedral cells in three numerical regions: guide vanes, runner and draft tube, Figure 7.7. Regions were numerically connected using the appropriate boundary conditions, with the aid of the overlap GGI (see Chapter 3). For BEP operating conditions, the guide vanes were set to 9.84° angle. Figures 7.8 and 7.9 present the mesh used for BEP simulations.
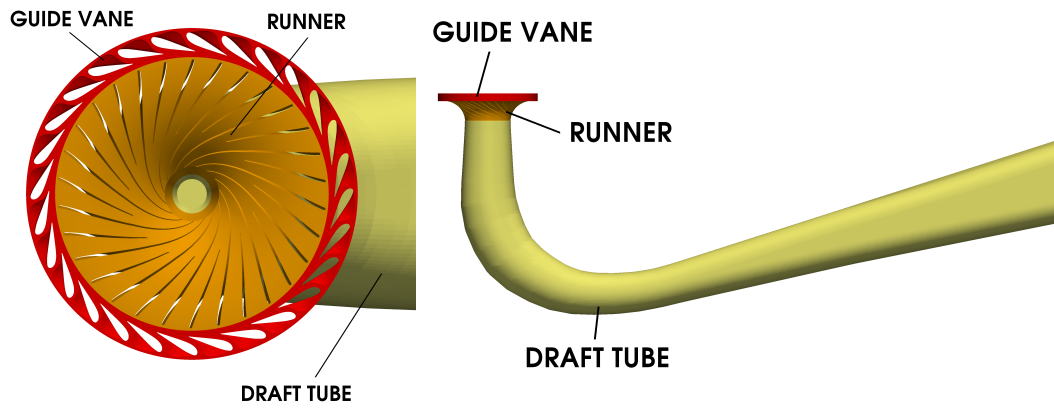
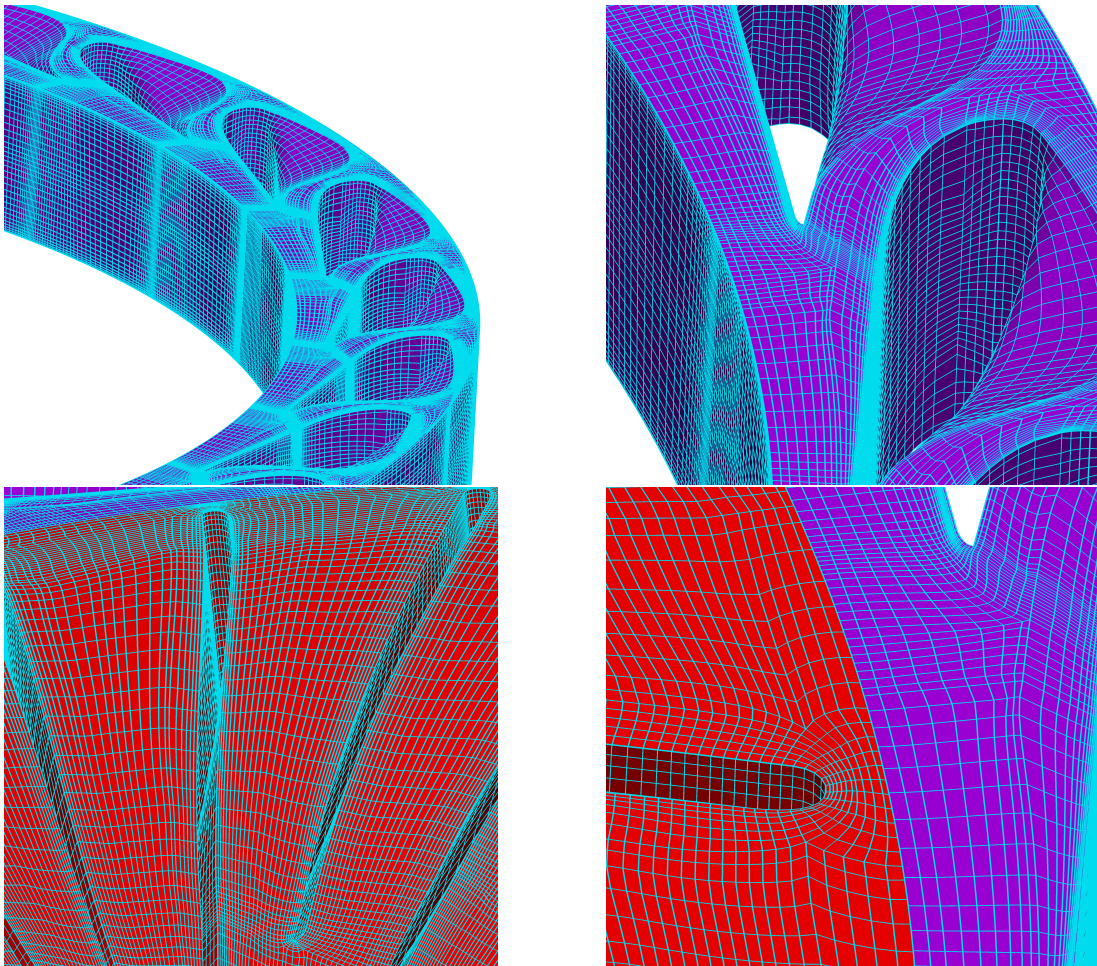Figure 7.7: BEP simulation numerical domain.

Figure 7.8: BEP mesh details. Guide vane annulus (top left), guide vane boundary layer (top right), runner blades (bottom left) and non-conformal GGI interface between the guide vane and the runner (bottom right).
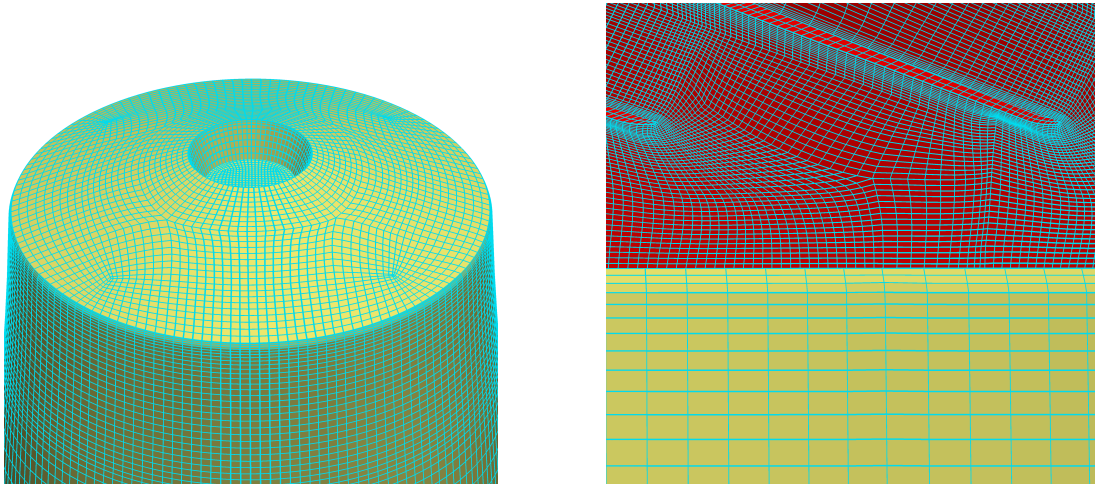
Figure 7.9: BEP mesh details. Draft tube (left) and non-conformal GGI interface between the runner and the draft tube (right).

7.4.2   Shut-down/Start-up Mesh Set

As presented in Section 4.2, the Harmonic Balance shut-down/start-up simulations require different guide vane angle position for each time instant, whereas the symmetrical time instants have the same operating conditions and guide vane angle. Therefore, $n + 1$ guide vane positions are needed. This is treated by creating a set of meshes, for each time step beforehand, which allows inspecting them for any modifications needed. If mesh skewness, non-orthogonality or aspect ratio was exceeding a prescribed threshold, this was fixed in advance, prior to running the simulations, yielding $n + 1 = 7$ meshes with satisfactory quality.

For the shut-down/start-up simulation, additional model reduction was performed by reducing the geometry to a single blade passage. With blade count of 28 guide vanes and 30 runner blades, the single blade passage cannot be unambiguously matched between the regions, unless the regions have equal number of blades. Otherwise, the flow conditions on the master side of a periodic patch should not be the same as on the shadow side of the periodic patch, meaning that periodic boundary condition would then require more than just interpolation between patches. The runner blade passage was reduced for 6.666% to match the opposing number of blades, i.e. both regions are set to

have 28 blades. Running a single blade passage proves great benefit in terms of computational cost as 28 times less cells are simulated, but consequently forces spatially aperiodic effects to be neglected. Furthermore, Francis turbine is known to exhibit vortex rope instabilities in the draft tube, which cannot be recreated by running a single slice of the draft tube. When investigating rotating instabilities, vortex rope and other aperiodic effects, the complete annulus has to be used.

A single mesh for shut-down and start-up consists of 574 431 hexahedral cells. Figures 7.10-7.12 show the geometry and mesh used for shut-down and start-up simulations.
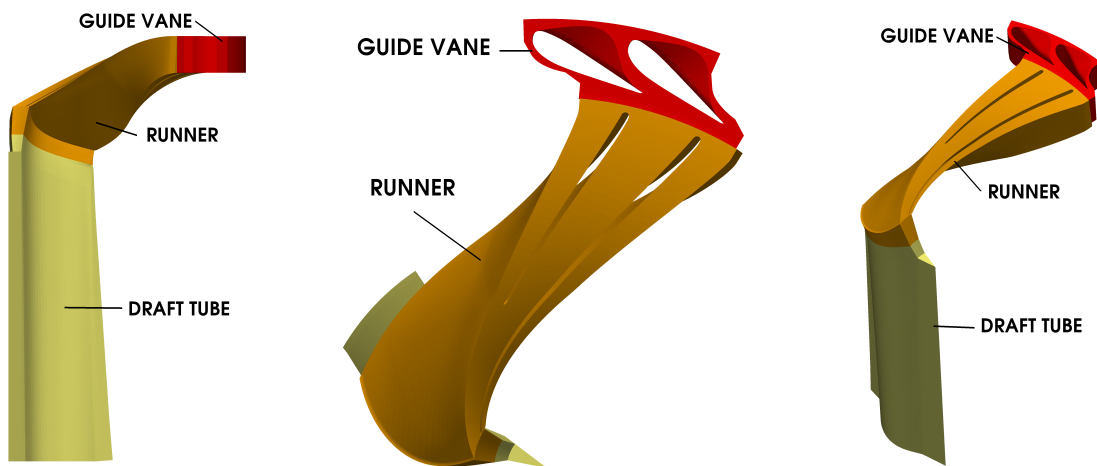

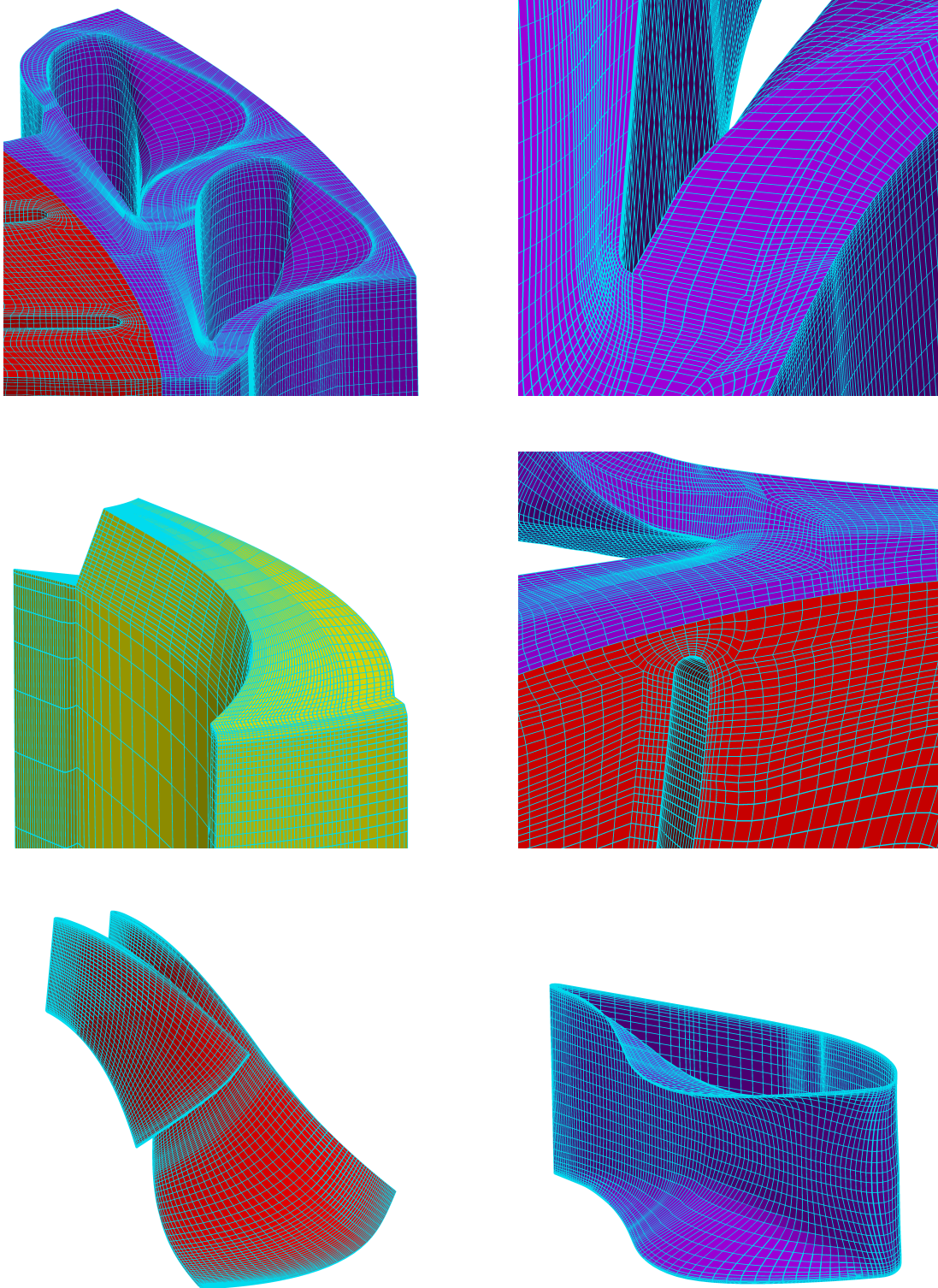Figure 7.10: Numerical domain for start-stop simulations.

Figure 7.11: Start-stop simulation mesh details.   Guide vane mesh (top left), guide vane boundary layer (top right), draft tube (middle left) and non-conformal overlap GGI interface between guide vane and runner (middle right), runner main blade and splitter blade (bottom left), single guide vane (bottom right).
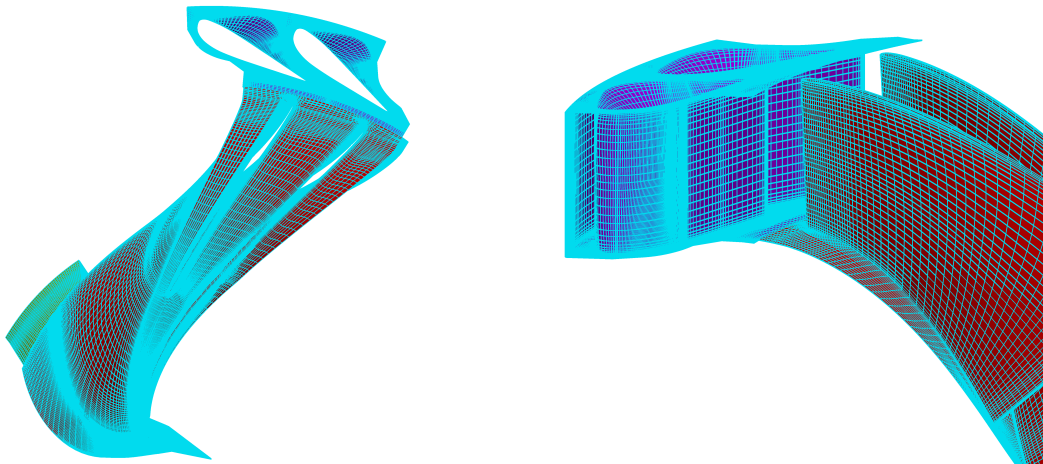
Figure 7.12: Start-stop simulation mesh details. Top view of a single blade passage assembly (left), and guide vane and runner blade (right).

The details of the guide vane mesh for different opening angles is presented in Figure 7.13. Based on the Harmonic Balance requirement for equidistant time instants, 7 different guide vane positions correspond to these time instants:

- times 1.42 s and 18.46 s: $9.84°$,

- times 2.84 s and 17.04 s: $8.936°$,

- times 4.26 s and 15.62 s: $7.128°$,

- times 5.68 s and 14.2 s: $5.32°$,

- times 7.1 s and 12.78 s: $3.512°$,

- times 8.52 s and 11.36 s: $1.704°$,

- times 9.94 s: $0.8°$.

(a) 9.84°

(b) 8.936°

(c) 7.128°

(d) 5.32°

(e) 3.512°

(f) 1.704°

(g) 0.8°
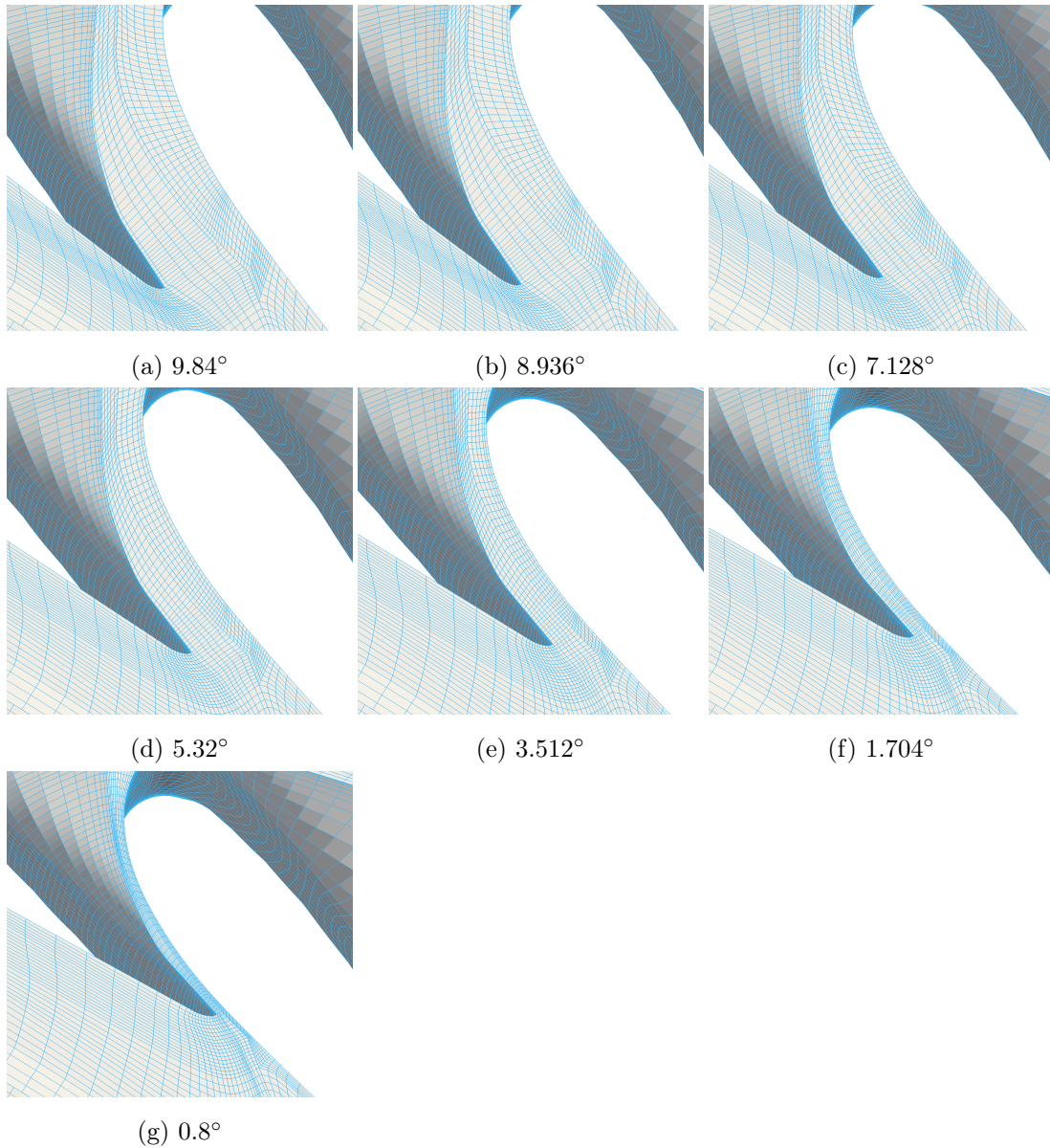
Figure 7.13: Guide vane blade passage mesh detail for different guide vane angles.

7.5   Best Efficiency Point Results

Best efficiency point simulation and results are presented in this section. BEP is used to assess the accuracy of a single harmonic simulation in case of a periodic steady state problem with non-changing operating conditions. BEP is characterized by the rotor rotational speed of 333 rpm at 202 kgs^{-1} mass flow

rate and 9.84° guide vane angle.   These operating conditions yield head of 11.94 m at efficiency 92.39%.   The experimental data for power, head and efficiency are compared to Harmonic Balance in Table 7.5, showing the error margin of 4%. This shows that global prediction is achieved quite accurately by Harmonic Balance.

Table 7.5: Comparison of integral quantities.

	P [W]	H [m]	η [%]
Experiment	21 617	11.94	92.39
Simulation	22 457	11.53	94.40
Error	3.74%	3.43%	2.13%

For greater confidence in Harmonic Balance results, local effects such as rotor–stator interaction should be observed. Within the experiment, measurements at several probing points were provided: probes VL2, DT5 and DT6. Probe VL2 is located in the vaneless space between the guide vane and runner, Figure 7.3. Probes DT5 and DT6 are positioned in the draft tube just at the runner exit. The measured pressure values in probes VL2, DT5 and DT6 are presented in Table 7.6 and compared with Harmonic Balance.   Again, the error margin is slightly over 4%, showing both local and global accuracy of the method.

Table 7.6: Comparison of pressure values in three different points.

Measurement locations	VL2	DT5	DT6
Experimental pressure, [kPa]	173.60	105.01	104.80
Simulation pressure, [kPa]	170.43	109.53	109.15
Error	1.80%	4.12%	3.98%

The overview of pressure and velocity fields at different sections of the domain is presented in Figure 7.14. Figure 7.15 shows the pressure field at the runner and guide vane section, followed by the velocity field for the same section in Figure 7.16.

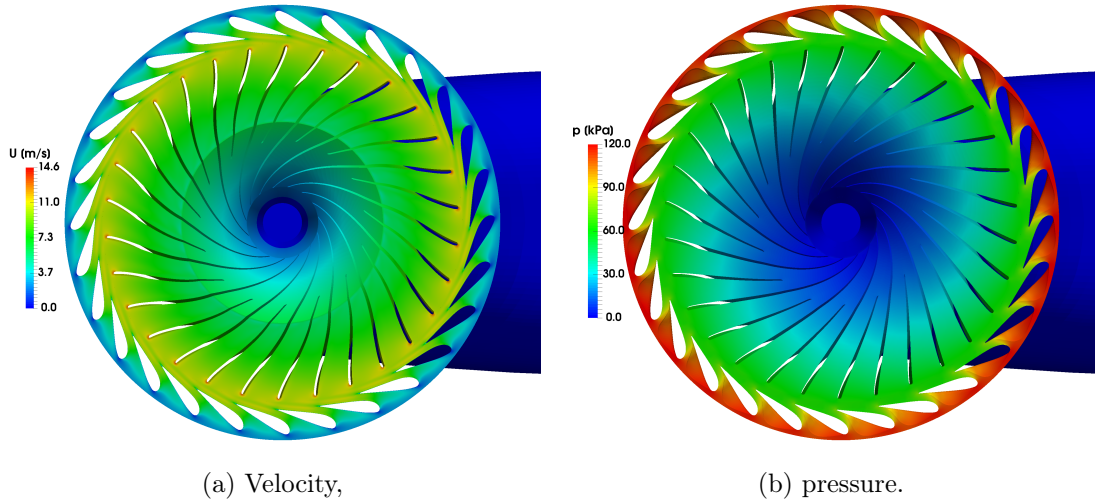(a) Velocity,   (b) pressure.
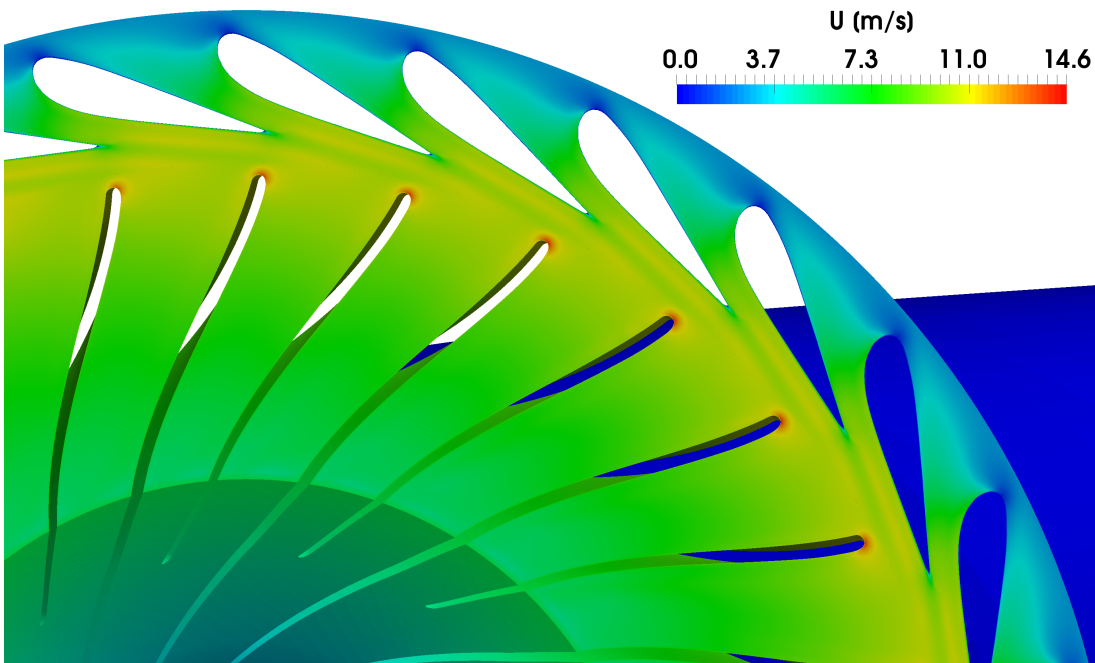
Figure 7.14: BEP runner flow field.

Figure 7.15: BEP operating point guide vane wake propagation, velocity field.
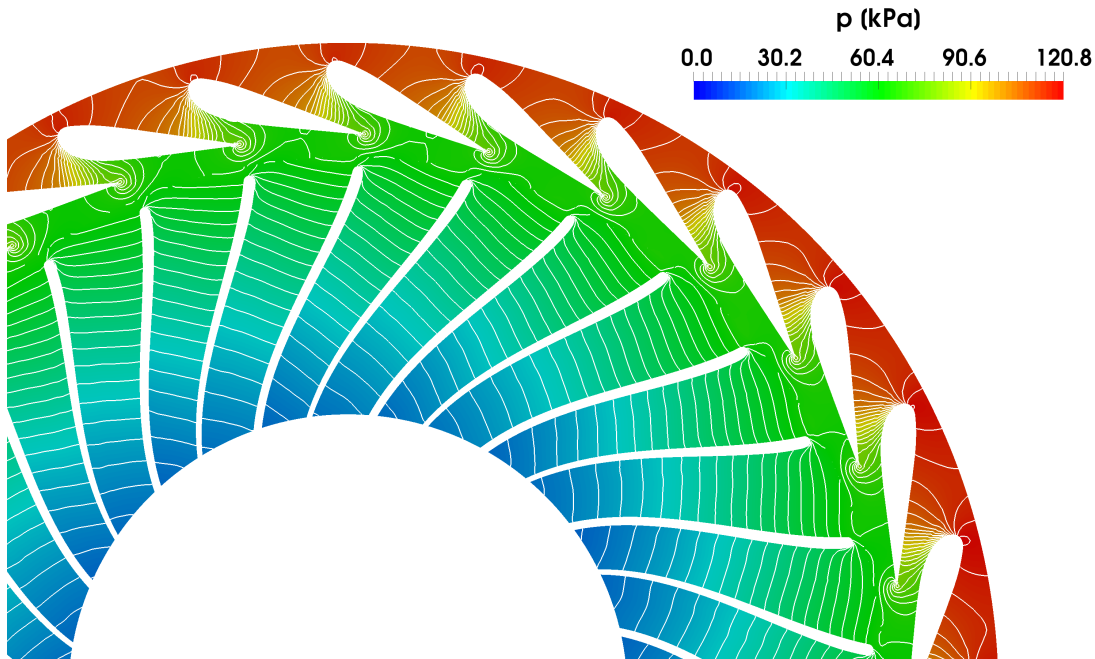
Figure 7.16: Guide vane and runner pressure field and iso contours.

7.6   Start-up and Shut-down Prediction

Based on the assessment from BEP obtained in the previous section, with error margin of 4% compared to the experiment, similar discrepancy is expected for the start-stop simulation and can be considered as a limitation of the method with a single harmonic. However, based on the experience, the error of 4% is deemed sufficiently accurate.

In this section comparison of the Harmonic Balance with experimental data is given. The Harmonic Balance simulation is performed using only a portion of geometry due to spatial periodicity. Impeller blade passages were modified to accommodate the guide vane pitch, so to have 14 main and 14 splitter blades, allowing the use of periodic boundary conditions and overlap GGI. Therefore, two blade passages were simulated both in the guide vane region and impeller region, as outlined in Section 7.4. The nested Harmonic Balance simulation was run solving $n = 6$ outer harmonics and $m = 1$ inner harmonic, which was sufficient to accurately model the imposed inlet flow rate function. In Figure 7.17 the imposed mass flow rate is denoted with a solid black line and the Harmonic

Balance approximation is shown using red lines and time instants denoted with crosses.

The start-stop conditions provided by the experiment, state that the impeller is held at constant speed of 333 min^{-1} during shut-down and start-up, therefore the same behavior is prescribed in the simulation. Corresponding to varying the inlet mass flow rate, the guide vane angle had to be adjusted for the current operating conditions, changing from 0.8° for closed condition to 9.84° for BEP. Therefore, a number of guide vane positions were necessary to fully model the flow. Turbulence was modelled using the $k - \varepsilon$ model with wall functions [107].

Based on the procedure described in Chapter 4, the Francis-99 case is valid for nested Harmonic Balance approach. At 333 min^{-1}, duration of one period is 0.18018 s, which counts up to 51.2 periods during start-up or shut-down. Operating regime change is performed by varying the mass flow rate through the machine, changing from 0.202 m^{3}s^{-1} to 0.018 m^{3}s^{-1} or vice versa. Divided through 51 periods, the change of mass flow rate is 1.5% per period. Within the scope of this approach, 1.5% is considered sufficiently small, therefore the operating conditions are held constant during one inner simulation.
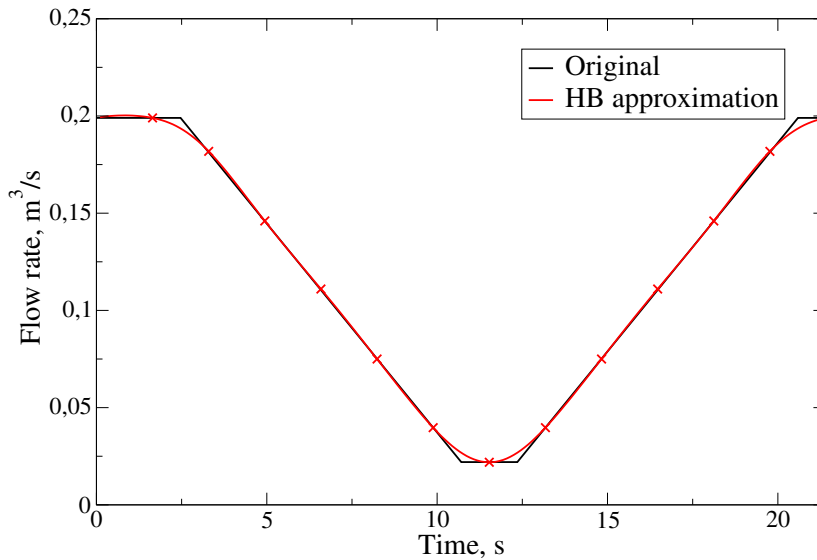

Figure 7.17: Start-stop simulation mass flow rate variation.

Since it is possible to arbitrarily change the steady-state stages of the curve (stages **a, c, e** in Figure 4.1), it was used to assemble a symmetric function. As

the regime change is dictated by guide vane angle, 6 harmonics would require meshes with 13 blade positions for each time instant. By making the function symmetrical, only 7 blade positions were needed, yielding additional savings in terms of man-hour in mesh generation. In Figure 7.17 red crosses represent $2m+1$ time instants in which 7 Harmonic Balance simulations are run due to symmetry with respect to $t = 9.94$ s. In each of the time instants, the inlet velocity is prescribed to achieve the correct mass flow rate and guide vane angle is modified accordingly. Pressure is held fixed at the outlet and the remaining boundary conditions are left unchanged.

Having in mind that Harmonic Balance is based on Fourier expansion, the solution from 13 obtained time instants can easily be reconstructed to form a complete period. The reconstructed solution is presented in the following figures. Pressure comparison in probing point VL2 is presented in Figure 7.18. Results are presented as a pressure variation through time for the complete shut-down and start-up period, with black solid line representing the experimental measurement and red line denoting Harmonic Balance simulation. The Harmonic Balance solution can be seen as the mean value of the experimental measurement, as the agreement is very good, though the Harmonic Balance curve does not exhibit blade-passing fluctuations that appear in experimental measurements. Figure 7.19 shows the pressure fluctuation comparison, measured in probing point DT5 which exhibits similar behavior. However, the pressure variation in this probing point is quite small (4 kPa) compared to total pressure variation through the complete turbine (120 kPa). It can be concluded that the pressure field from simulations shows good agreement with the experimental data as the trend in pressure drop matches between the two, suggesting the qualitative agreement between the simulated and real physical processes. It should be noted that the relative difference in results is approximately 4%, matching those in BEP simulation.
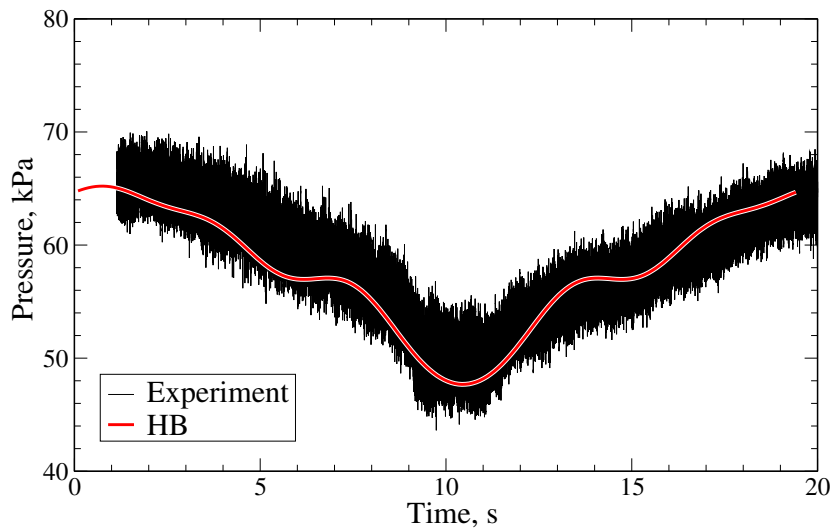
Figure 7.18: HB against experimental pressure measurements in probe VL2.
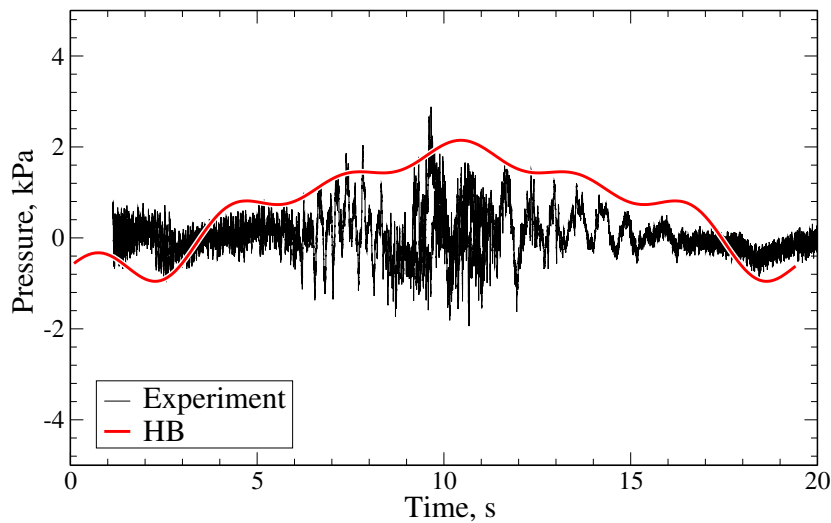
Figure 7.19: HB against experimental pressure measurements in probe DT5.

Figure 7.20 shows the power curve in time, during shut-down and start-up. Good agreement between Harmonic Balance and experiment can be observed, with the largest discrepancy at ≈ 19 s, at the end of the Harmonic Balance period. However, the value at the beginning of the Harmonic Balance period ($t = 0$ s) is equal to the value at the end of the period ($t = 19.5$ s), while experimental data differs significantly. In both cases, the first and last point represent BEP, therefore similar experimental measurements would be expected, which is not the case here.

Figure 7.20: HB against experimental measurement of power for start-stop conditions.

The presented start-stop approach closely followed the experimental setup and procedure of closing/opening the guide vanes at constant rotor speed. However, the presented approach is not limited to constant rpm, as each time instant can have different boundary conditions. The only limitation is that the complete start-stop period lasts sufficiently long, i.e. that the flow conditions are changing gradually so that constant flow can be assumed in one time instant, during one rotor period.
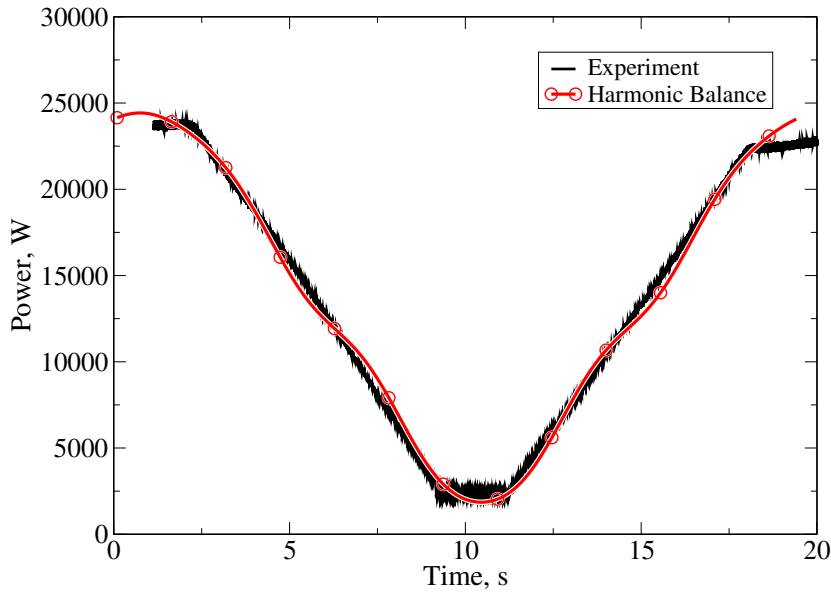
Flow fields through the turbine are presented in Figures 7.21-7.24. Runner in different time instants is presented in Figures 7.21 and 7.22, showing the process of closing the guide vanes from BEP to fully closed condition. In the last two time instants, for $1.704°$ and $0.8°$ the turbine behaves mainly like a mixer, due to the closed inlet at constant rotor speed. Draft tube flow in the same time instants, Figures 7.23 and 7.24, shows the change of flow structure and direction as the inlet closes. Fully developed flow is shown in Figure 7.23a, while the flow structure deteriorates in the following time instants. The central cylindrical flow shape gradually spreads into a cone, having majority of the flow rotating at the edges. Finally, due to mixing regime, the flow starts to circulate vertically, which can be seen in the right hand side of Figure 7.24, showing the u_z, a vertical velocity component (positive z-direction is upwards).

(a) $t = 1.42$ s, $9.84°$

(b) $t = 2.84$ s, $8.936°$

(c) $t = 4.26$ s, $7.128°$

(d) $t = 5.68$ s, $5.32°$

(e) $t = 7.1$ s, $3.512°$

(f) $t = 8.52$ s, $1.704°$
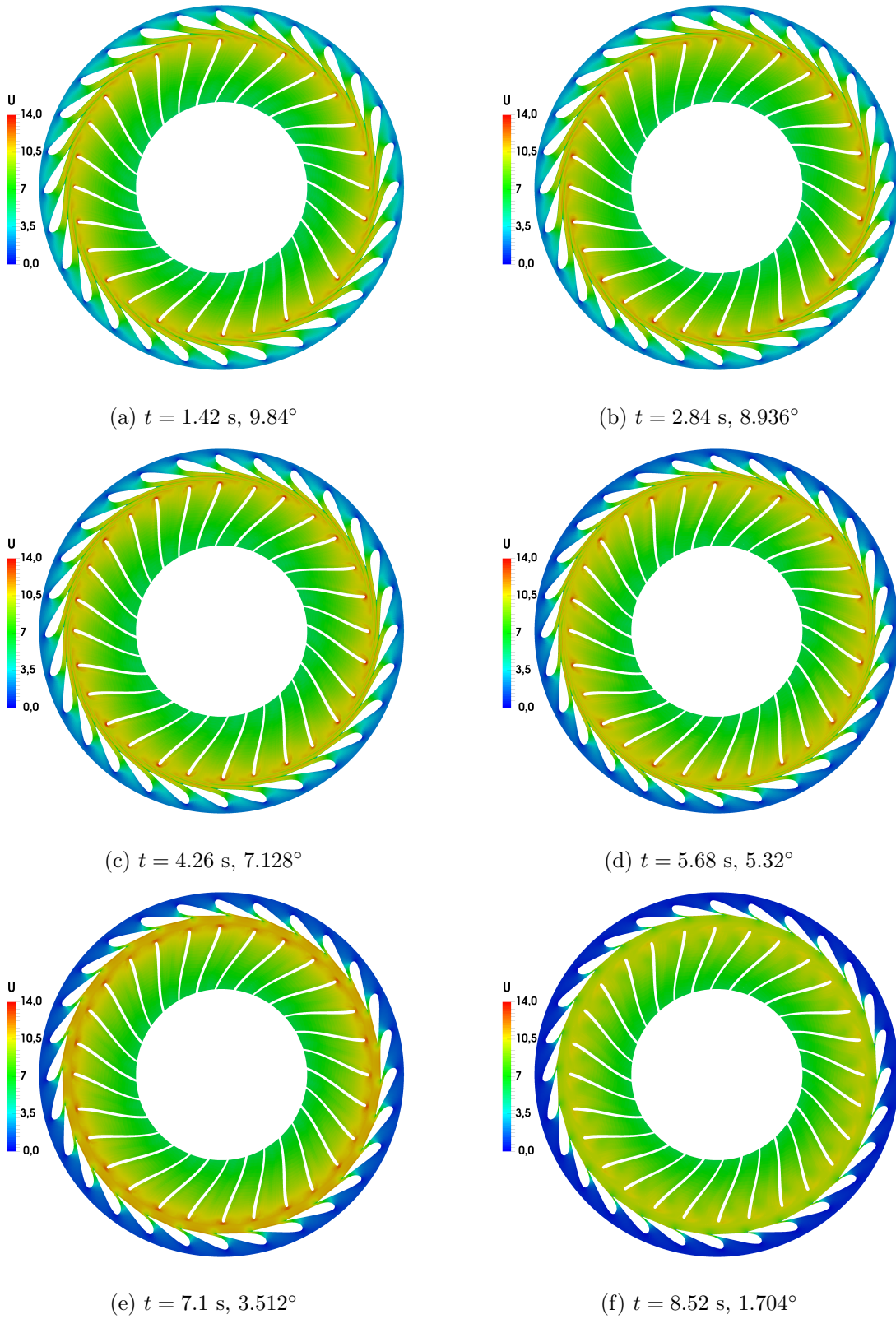
Figure 7.21: Velocity field in the runner over time.
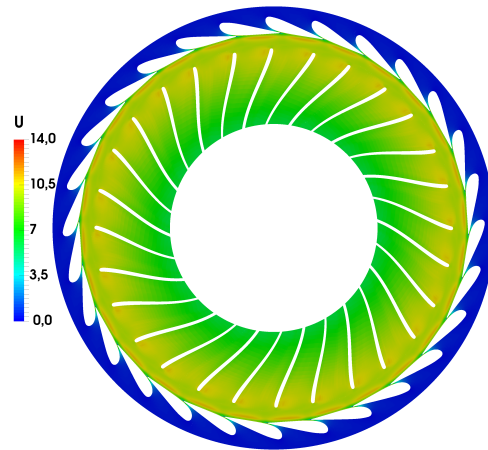
(a) $t = 9.94$ s, $0.8°$

Figure 7.22: Velocity field in the runner over time.
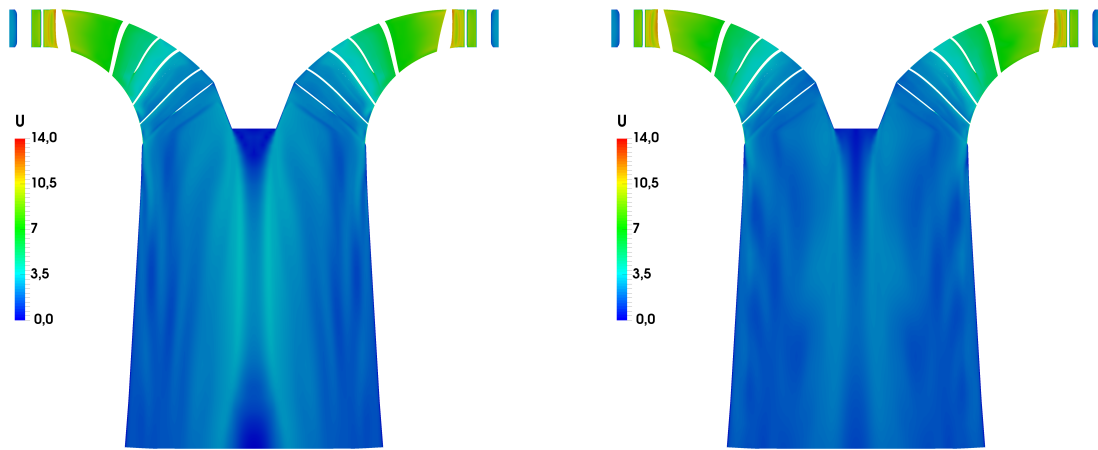
(a) $t = 1.42$ s, $9.84°$

(b) $t = 2.48$ s, $8.936°$
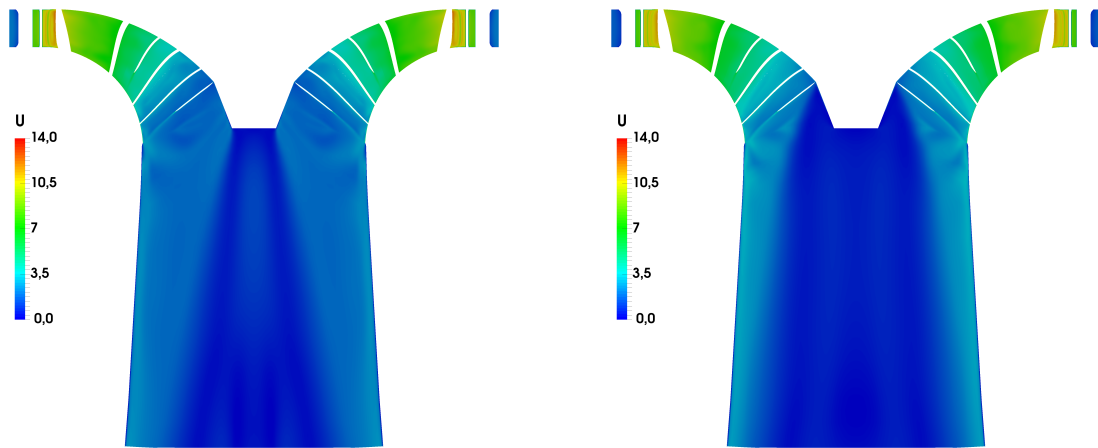
(c) $t = 4.26$ s, $7.128°$

(d) $t = 5.68$ s, $5.32°$

Figure 7.23: Velocity field in the draft tube over time.

(a) $t = 7.1$ s, $3.512°$

(b) $t = 7.1$ s, $3.512°$, u_z component

(c) $t = 8.52$ s, $1.704°$

(d) $t = 8.52$ s, $1.704°$, u_z component

(e) $t = 9.94$ s, $0.8°$

(f) $t = 9.94$ s, $0.8°$, u_z component
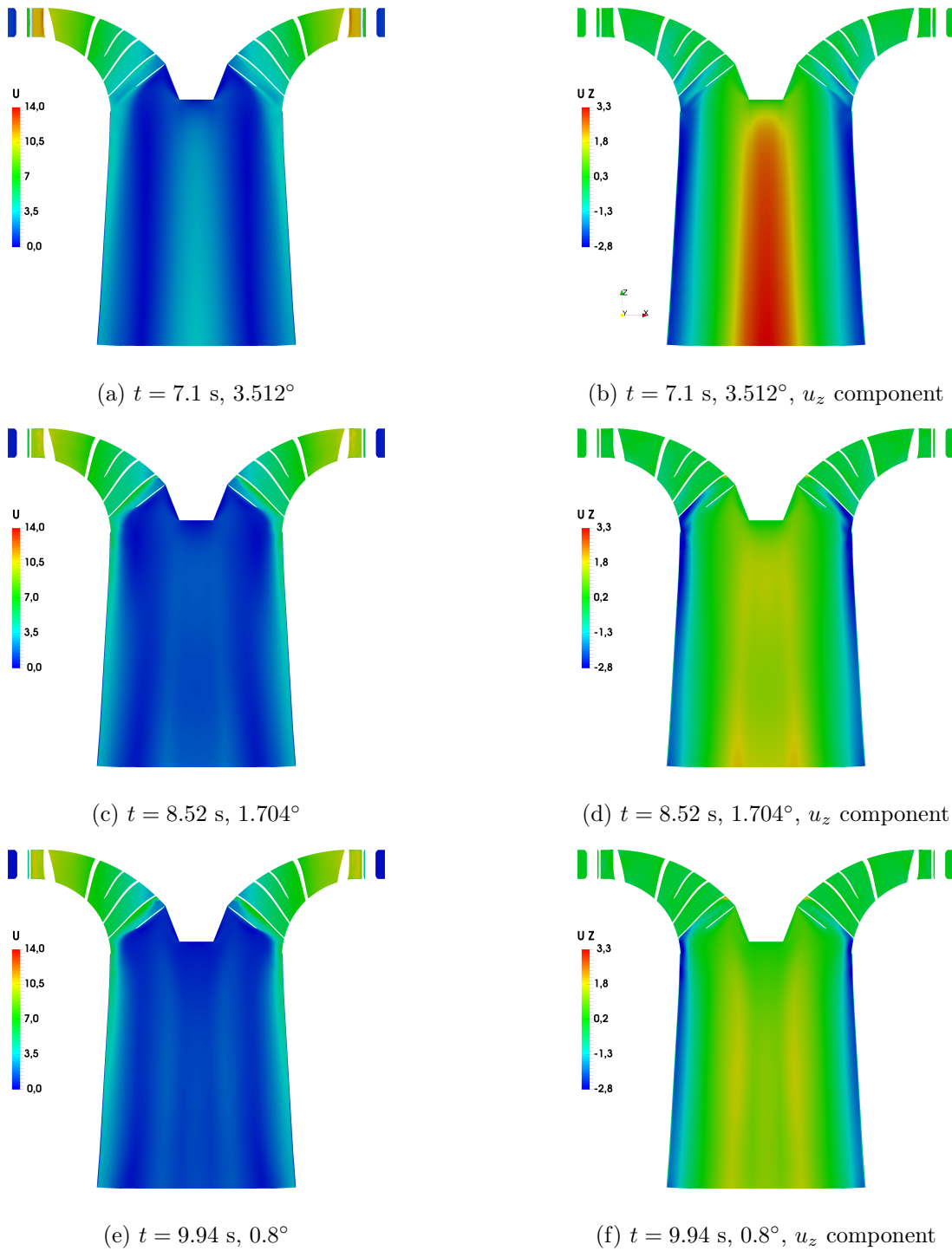
Figure 7.24: Velocity field in the draft tube over time. Magnitude (left) and axial component u_z (right). Positive z-direction is upwards.

7.7   Closure

The main objective of shut-down and start-up comparison of Harmonic Balance simulation with available experimental data was the assessment of the power curve and pressure values at two points in the domain. Good agreement for all three features between Harmonic Balance and experiment was observed, with the error margin of approximately 4%. Based on the relation between power and head, good power agreement with experiment also implies a good head prediction. The Harmonic Balance simulation was run using six harmonics, yielding $2n+1 = 13$ time instants with single-harmonic simulations throughout the complete shut-down and start-up period. The proposed composition of $n = 6$ and $m = 1$ harmonics provided close-to-exact boundary conditions for the variation of the mass flow rate and consequently produced results of notable accuracy compared to experimental data.

Chapter 8

Conclusion

In this study, the nested Harmonic Balance approach for turbomachinery start-stop simulations is presented. The common time-spectral Harmonic Balance method is expanded to apply to change of operating regime in turbomachinery, specifically shut-down and start-up procedures. The implementation of the method is done in `foam-extend`, an open source CFD library, while the final validation was performed against available experimental data for the Francis turbine shut-down and start-up.

The Harmonic Balance method is gaining popularity for a number of periodic problems, mainly in turbomachinery and aeronautical applications related to vibrational analyses, flutter, limit cycle oscillations, resonance investigation, airfoils, wings, counter-rotating propellers, helicopters, etc. Furthermore, recently the method found its application in naval hydrodynamics as well, but also in haemodynamics [108]. However, so far the method has never been used for investigation of start-stop effects in turbomachinery. This is the main focus of this work.

The time-spectral Harmonic Balance has been derived and presented in Chapter 2, in order to demonstrate the general idea behind the method and its relation to spectral space. The method is based on Fourier series expansion up to n harmonics resolving the features of dominant frequency f and its n higher harmonics. This requires that the considered problem should be periodic in time and its base frequency should be known in advance. The requirement of temporal periodicity limits its use, but also allows significant CPU time savings compared to conventional time-accurate approach. In case of time-accurate

simulations, only one equation is solved per variable and marched through time in small increments. The temporal derivation term couples the current time instant with the previous one, thus accounting for inertial effects and influence of flow-history. On the other hand, in the Harmonic Balance simulation solved with n harmonics, $2n + 1$ equations per variable are solved. The $2n + 1$ equations present $2n + 1$ equidistantly placed time instants throughout the period. Moreover, these equations are coupled as well through a coupling source term, accounting for inertial effects, although the equations themself are mathematically steady, as no temporal derivation term exists. A major benefit of the Harmonic Balance method is that regardless of the time instants solved, the solution can be reconstructed in any point in time due to Fourier expansion.

The conventional time-spectral Harmonic Balance method is validated using ERCOFTAC centrifugal pump case and Francis-99 turbine. ERCOFTAC pump is a 2D case with available experimental data. The comparison of steady MRF frozen rotor, time-accurate and Harmonic Balance simulations was performed, as well as comparison of the Harmonic Balance with experiment for BEP. Comparison with time-accurate simulation shows good agreement with room for improvement by incorporating higher harmonics, if needed. Up to two harmonics were used as this was sufficient to obtain accurate predictions for power, head, efficiency, etc. with the error margin of 4% . By comparing the CPU time, Harmonic Balance is 30 times faster than conventional time-accurate simulation, which fully justifies the idea of the method. For the Francis-99 turbine case, similar behavior can be observed. However, it was simulated only using the Harmonic Balance method and compared with experimental data, yielding good agreement with discrepancy below 4%. Based on these two validation cases, two main outcomes should be noted here:

- Harmonic Balance error margin of 4% compared to experimental data for power, head, efficiency and pressure probes suggests good reliability of the method,

- CPU time reduction of 30 times than time-accurate simulation justifies the approach.

Based on this, the expansion of the method was proposed for more demanding

cases.

It is known that turbomachinery shut-down or start-up simulations require excessive amount of CPU core-hours, therefore the adapted version of the Harmonic Balance was proposed to deal with the start-stop procedures. The main goal was to predict variables of interest (power, head, efficiency...) for the whole period in a fragment of time needed by the conventional time-accurate simulation. The proposed approach is presented in Chapter 4, by creating the nested structure with two Harmonic Balance coupling terms. By doing this, one coupling term is accounting for smaller time scale, with dominant frequency of rotor rotation, while the second coupling term accounts for effects on a larger scale, related to regime change. As the Harmonic Balance requires periodic problems, both shut-down and start-up are run simultaneously as a complete period shutting down from BEP and charging back to BEP. The start-up and shut-down procedure can be performed in a number of ways, where mostly the variation of mass flow rate or rotor speed dictate the process.

The validation of the nested Harmonic Balance for start-stop simulations is presented using a 2D simplified model of a turbine, followed by a Francis-99 turbine with available experimental data. A comparison of time-accurate simulation with Harmonic Balance is performed for 2D test case by comparing the pressure fluctuations in four probes and CPU time for the whole simulation. Good agreement of pressure and velocity probes with significant CPU time savings deemed the proposed approach valid for start-stop investigation and accurate flow prediction. The validation is therefore continued on real geometry of a Francis-99 turbine, which was analysed experimentally within the scope of a Francis-99 workshop. Start-stop data obtained numerically are compared with real measurements, yielding good agreement of the same order of accuracy as a regular BEP simulation. Maximum error could again be estimated to approximately 4%. The compared features include power and two pressure probes for the complete start-stop period, where the Harmonic Balance results resemble what could be proclaimed as the mean value of experimental data. The comparable level of accuracy proves the presented approach is valid for the prediction of turbine properties and flow patterns during shut-down or start-up.

Based on the presented workflow and results, it can be concluded that the

research objectives set for this thesis are achieved and the research hypotheses are confirmed. Although it is clear that often changes of working regime in turbomachinery are imminent, such occurrences deteriorate the life span of a machine. Computational fluid dynamics presents an important tool in this design process, with the major problem of being extremely expensive and time consuming. A simplified method for investigation of regime change has been presented and validated, which could be a significant tool in the design stage. Future work on this topic would need to address a broader spectrum of problems and types of turbomachinery, as there are a number of processes and phenomena which were not taken into account in the scope of this work: compressibility, non–axisymmetric phenomena such as vortex rope, turbomachinery with large number of stages, etc. All of these aspects impose serious effects on turbomachinery flow, lifespan and internal phenomena, and should be investigated as a topic on its own.

Bibliography

[1] K. C. Hall, J. P. Thomas, W. S. Clark, Computation of unsteady nonlinear flows in cascades using a harmonic balance technique, Aiaa Journal 40 (5) (2002) 879–886. doi:10.2514/2.1754.

[2] T. Chen, P. Vasanthakumar, L. He, Analysis of unsteady blade row interaction using nonlinear harmonic approach, Journal of Propulsion and Power 17 (3) (2001) 651–658. doi:10.2514/2.5792.

[3] G. Cvijetic, H. Jasak, V. Vukcevic, Finite volume implementation of the harmonic balance method for periodic non–linear flows, in: 54th AIAA Aerospace Sciences Meeting, 2016, p. 0070.

[4] K. C. Hall, E. F. Crawley, Calculation of unsteady flows in turbomachinery using the linearized euler equations, AIAA journal 27 (6) (1989) 777–787.

[5] W. S. Clark, K. C. Hall, A time-linearized navier-stokes analysis of stall flutter, in: ASME 1999 International Gas Turbine and Aeroengine Congress and Exhibition, American Society of Mechanical Engineers, 1999, pp. V004T03A040–V004T03A040.

[6] L. He, Method of simulating unsteady turbomachinery flows with multiple perturbations, AIAA Journal 30. doi:10.2514/3.11291.

[7] L. He, W. Ning, Efficient approach for analysis of unsteady viscous flows in turbomachines, Aiaa Journal 36 (11) (1998) 2005–2012. doi:10.2514/2.328.

[8] G. Dufour, F. Sicot, G. Puigt, C. Liauzun, A. Dugeai, Contrasting the harmonic balance and linearized methods for oscillating-flap simulations, Aiaa Journal 48 (4) (2010) 788–797. doi:10.2514/1.43401.

[9] J. Thomas, E. Dowell, K. Hall, C. Denegri, Further investigation of modeling limit cycle oscillation behavior of the f-16 fighter using a harmonic balance approach, Vol. 1917, 2005, p. 2005.

[10] J. Thomas, C. Custer, E. Dowell, K. Hall, Unsteady flow computation using a harmonic balance approach implemented about the overflow 2 flow solver, in: 19th AIAA Computational Fluid Dynamics Conference, 2009.

[11] K. Ekici, K. C. Hall, Harmonic balance analysis of limit cycle oscillations in turbomachinery, Aiaa Journal 49 (7) (2011) 1478–1487. `doi:10.2514/1.j050858`.

[12] F. Sicot, A. Gomar, G. Dufour, A. Dugeai, Time-domain harmonic balance method for turbomachinery aeroelasticity, Aiaa Journal 52 (1) (2014) 62–71. `doi:10.2514/1.j051848`.

[13] K. Hall, J. Thomas, K. Ekici, D. Voytovyc, Frequency domain techniques for complex and nonlinear flows in turbomachinery, Vol. 3998, 2003, p. 2003.

[14] A. Gopinath, E. Van Der Weide, J. Alonso, A. Jameson, K. Ekici, K. Hall, Three-dimensional unsteady multi-stage turbomachinery simulations using the harmonic balance technique, in: 45th AIAA Aerospace Sciences Meeting and Exhibit, Vol. 892, 2007.

[15] T. Guédeney, A. Gomar, F. Sicot, Multi-frequential harmonic balance approach for the computation of unsteadiness in multi-stage turbomachines, AFM, Maison de la Mécanique, 39/41 rue Louis Blanc, 92400 Courbevoie, France (FR), 2013.

[16] T. Guédeney, A. Gomar, F. Gallard, F. Sicot, G. Dufour, G. Puigt, Non-uniform time sampling for multiple-frequency harmonic balance computations, Journal of Computational Physics 236 (2013) 317–345. `doi:10.1016/j.jcp.2012.11.010`.

[17] K. Ekici, K. Hall, Nonlinear analysis of unsteady flows in multistage turbomachines using the harmonic balance technique, in: 44th AIAA Aerospace Sciences Meeting and Exhibit, 2006, p. 422.

[18] K. Ekici, K. C. Hall, Nonlinear analysis of unsteady flows in multistage turbomachines using harmonic balance, Aiaa Journal 45 (5) (2007) 1047–1057. doi:10.2514/1.22888.
URL <GotoISI>://WOS:000246195000010

[19] K. Ekici, K. C. Hall, E. H. Dowell, Computationally fast harmonic balance methods for unsteady aerodynamic predictions of helicopter rotors, Journal of Computational Physics 227 (12) (2008) 6206–6225. doi:10.1016/j.jcp.2008.02.028.

[20] L. He, Fourier methods for turbomachinery applications, Progress in Aerospace Sciences 46 (8) (2010) 329–341.

[21] H. Huang, K. Ekici, Stabilization of high-dimensional harmonic balance solvers using time spectral viscosity, Aiaa Journal 52 (8) (2014) 1784–1794. doi:10.2514/1.j052698.

[22] J. P. Thomas, C. H. Custer, E. H. Dowell, K. C. Hall, C. Corre, Compact implementation strategy for a harmonic balance method within implicit flow solvers, Aiaa Journal 51 (6) (2013) 1374–1381. doi:10.2514/1.j051823.

[23] F. Sicot, G. Puigt, M. Montagnac, Block-jacobi implicit algorithms for the time spectral method, Aiaa Journal 46 (12) (2008) 3080–3089. doi:10.2514/1.36792.

[24] M. A. Woodgate, K. J. Badcock, Implicit harmonic balance solver for transonic flow with forced motions, Aiaa Journal 47 (4) (2009) 893–901. doi:10.2514/1.36311.

[25] X. R. Su, X. Yuan, Implicit solution of time spectral method for periodic unsteady flows, International Journal for Numerical Methods in Fluids 63 (7) (2010) 860–876. doi:10.1002/fld.2111.

[26] S. Antheaume, C. Corre, Implicit time spectral method for periodic incompressible flows, Aiaa Journal 49 (4) (2011) 791–805. doi:10.2514/1.j050785.

[27] L. He, Computational study of rotating-stall inception in axial compressors, Journal of Propulsion and Power 13 (1) (1997) 31–38.

[28] G. J. Hendricks, J. S. Sabnis, M. R. Feulner, Analysis of instability inception in high-speed multi-stage axial-flow compressors, in: ASME 1996 International Gas Turbine and Aeroengine Congress and Exhibition, American Society of Mechanical Engineers, 1996, pp. V001T01A092–V001T01A092.

[29] M. Choi, N. H. Smith, M. Vahdati, Validation of numerical simulation for rotating stall in a transonic fan, Journal of turbomachinery 135 (2) (2013) 021004.

[30] J. Dodds, M. Vahdati, Rotating stall observations in a high speed compressor—part i: Experimental study, Journal of Turbomachinery 137 (5) (2015) 051002.

[31] J. Dodds, M. Vahdati, Rotating stall observations in a high speed compressor—part ii: Numerical study, Journal of Turbomachinery 137 (5) (2015) 051003.

[32] S. Houde, G. Dumas, Y. Maciel, C. Deschênes, Investigations of rotating stall inception in a propeller turbine runner operating in low-load conditions, in: IOP Conference Series: Earth and Environmental Science, Vol. 240, IOP Publishing, 2019, p. 022021.

[33] I. Day, Stall, surge, and 75 years of research, Journal of Turbomachinery 138 (1) (2016) 011001.

[34] G. Pullan, A. Young, I. Day, E. Greitzer, Z. Spakovszky, Origins and structure of spike-type rotating stall, Journal of Turbomachinery 137 (5) (2015) 051007.

[35] C. Trivedi, M. J. Cervantes, O. G. Dahlhaug, Experimental and numerical studies of a high-head francis turbine: A review of the francis-99 test case, Energies 9 (2) (2016) 74.

[36] J. Journèe, W. Massie, Offshore hydrodynamics, Delft University of Technology 4 (2001) 38.

[37] I. Gatin, G. Cvijetić, V. Vukčević, H. Jasak, Š. Malenica, Harmonic balance method for nonlinear and viscous free surface flows, Ocean Engineering 157 (2018) 164–179.

[38] I. Gatin, G. Cvijetić, V. Vukčević, H. Jasak, Wave diffraction cfd nonlinear time–spectral simulations in foam–extend, in: 19th Numerical Towing Tank Symposium, 2016.

[39] V. Vukčević, G. Cvijetić, I. Gatin, H. Jasak, The harmonic balance method for temporally periodic free surface flows in marine hydrodynamics, in: 11th OpenFOAM Workshop, 2016.

[40] G. Cvijetic, I. Gatin, V. Vukcevic, H. Jasak, Harmonic balance developments in openfoam, Computers & Fluidsdoi:https://doi.org/10.1016/j.compfluid.2018.02.023.
URL http://www.sciencedirect.com/science/article/pii/S0045793018300793

[41] H. G. Weller, G. Tabor, H. Jasak, C. Fureby, A tensorial approach to computational continuum mechanics using object-oriented techniques, Computers in physics 12 (6) (1998) 620–631.

[42] G. Cvijetic, H. Jasak, Analysis and implementation of the harmonic balance method in computational fluid dynamics, Master's thesis, University of Zagreb (2015).

[43] K. C. Hall, K. Ekici, J. P. Thomas, E. H. Dowell, Harmonic balance methods applied to computational fluid dynamics problems, International Journal of Computational Fluid Dynamics 27 (2) (2013) 52–67. doi:10.1080/10618562.2012.742512.

[44] M. McMullen, A. Jameson, J. Alonso, Acceleration of convergence to a periodic steady state in turbomachinery flows, in: 39th Aerospace Sciences Meeting and Exhibit, 2001, p. 152.

[45] A. Jameson, J. Alonso, M. McMullen, Application of a non-linear frequency domain solver to the euler and navier-stokes equations, in: 40th AIAA Aerospace Sciences Meeting & Exhibit, 2002, p. 120.

[46] G. Cvijetić, H. Jasak, Harmonic balance method for turbomachinery applications, in: OpenFOAM®, Springer, 2019, pp. 223–233.

[47] J. H. Ferziger, M. Peric, Computational methods for fluid dynamics, in: Springer, 1996.

[48] C. Rhie, W. L. Chow, Numerical study of the turbulent flow past an airfoil with trailing edge separation, AIAA journal 21 (11) (1983) 1525–1532.

[49] H. Jasak, Error analysis and estimation for the finite volume method with applications to fluid flows, Ph.D. thesis, Imperial College of Science, Technology & Medicine, London (1996).

[50] S. Patankar, Numerical heat transfer and fluid flow, in: Taylor and Francis, 1980.

[51] H. Rusche, Computational fluid dynamics of dispersed two - phase flows at high phase fractions, Ph.D. thesis, Imperial College of Science, Technology & Medicine, London (2002).

[52] H. K. Versteeg, W. Malalasekera, An introduction to computational fluid dynamics: the finite volume method, Pearson education, 2007.

[53] Ž. Tuković, H. Jasak, A moving mesh finite volume interface tracking method for surface tension dominated interfacial fluid flow, Computers & fluids 55 (2012) 70–84.

[54] V. Vukcevic, Numerical modelling of coupled potential and viscous flow for marine applications, Ph.D. thesis, Ph. D. Thesis, University of Zagreb, Zagreb, Croatia (2016).

[55] S. V. Patankar, D. B. Spalding, A calculation procedure for heat, mass and momentum transfer in three-dimensional parabolic flows, Int. J. Heat Mass Transf. 15 (10) (1972) 1787–1806.

[56] Y. Saad, Iterative methods for sparse linear systems, Vol. 82, siam, 2003.

[57] I. Demirdžić, M. Perić, Space conservation law in finite volume calculations of fluid flow, International journal for numerical methods in fluids 8 (9) (1988) 1037–1050.

[58] M. Page, M. Beaudoin, A.-M. Giroux, Steady-state capabilities for hydroturbines with openfoam, International Journal of Fluid Machinery and Systems 4 (1) (2011) 161–171.

[59] D. J. Mavriplis, J. C. Vassberg, E. N. Tinoco, M. Mani, O. P. Brodersen, B. Eisfeld, R. A. Wahls, J. H. Morrison, T. Zickuhr, D. Levy, et al., Grid quality and resolution issues from the drag prediction workshop series, Journal of Aircraft 46 (3) (2009) 935–950.

[60] B. Diskin, J. Thomas, Effects of mesh regularity on accuracy of finite-volume schemes, in: 50th AIAA aerospace sciences meeting including the new horizons forum and aerospace exposition, 2012, p. 609.

[61] A. Jalali, C. Ollivier Gooch, Accuracy assessment of finite volume discretizations of diffusive fluxes on unstructured meshes, in: 50th AIAA Aerospace Sciences Meeting including the New Horizons Forum and Aerospace Exposition, 2012, p. 608.

[62] M. Berzins, C. Unit, An introduction to mesh quality, Lecture Notes for Von Karman Institute.

[63] B. Fabritius, G. Tabor, Improving the quality of finite volume meshes through genetic optimisation, Engineering with Computers 32 (3) (2016) 425–440.

[64] P. M. Knupp, C. Ernst, D. C. Thompson, C. Stimpson, P. P. Pebay, The verdict geometric quality library., Tech. rep., Sandia National Laboratories (2006).

[65] F. Juretic, Error analysis in finite volume cfd, Ph.D. thesis, Imperial College London (University of London) (2005).

[66] I. SADREHAGHIGHI, R. SMITH, S. TIWARI, An analytical approach to grid sensitivity analysis, in: 30th Aerospace Sciences Meeting and Exhibit, 1992, p. 660.

[67] M. Beaudoin, H. Jasak, Development of a generalized grid interface for turbomachinery simulations with openfoam, in: Open source CFD International conference, Vol. 2, 2008.

[68] M. Beaudoin, H. Nilsson, M. Page, R. Magnan, H. Jasak, Evaluation of an improved mixing plane interface for openfoam, in: IOP Conference Series: Earth and Environmental Science, Vol. 22, IOP Publishing, 2014, p. 022004.

[69] H. Jasak, M. Beaudoin, Openfoam turbo tools: From general purpose cfd to turbomachinery simulations, in: Proceedings of ASME-JSME-KSME Joint Fluids Engineering Conference (AJK2011-FED), 2011.

[70] I. De Dominicis, G. Cvijetić, M. Willetts, H. Jasak, Enhanced turbomachinery capabilities for foam-extend: Development and validation, in: OpenFOAM®, Springer, 2019, pp. 145–155.

[71] M. Beaudoin, H. Jasak, Adaptation of the general grid interface (ggi) for turbomachinery simulations with openfoam, in: 3rd OpenFOAM Workshop, Milano, Italy, 2008.

[72] G. Cvijetic, H. Jasak, The compressible harmonic balance method for turbomachinery, in: 2018 AIAA Aerospace Sciences Meeting, 2018, p. 0833.

[73] G. Cvijetic, L. Culic, H. Jasak, Analysis of transients in francis turbine using fourier methods, in: AIAA Scitech 2019 Forum, 2019, p. 0904.

[74] M. Page, domadomb testcases - or various ways to compute and connect periodic flow passages, in: 7th OpenFOAM Workshop, Darmstadt, Germany, 2012.

[75] T. Chirag, M. J. Cervantes, G. Bhupendrakumar, O. G. Dahlhaug, Pressure measurements on a high-head francis turbine during load acceptance and rejection, Journal of Hydraulic Research 52 (2) (2014) 283–297.

[76] O. Nilsson, D. Sjelvgren, Hydro unit start-up costs and their impact on the short term scheduling strategies of swedish power producers, IEEE Transactions on power systems 12 (1) (1997) 38–44.

[77] J. F. Gülich, Centrifugal pumps, Vol. 2, Springer, 2008.

[78] L. Culic, H. Jasak, Validation of the harmonic balance solver for turbomachinery start-up and shut-down simulations, Master's thesis, University of Zagreb (2018).

[79] H. Jasak, D. Rigler, Ž. Tuković, Finite volume immersed boundary method for turbulent flow simulations, in: 9th OpenFOAM Workshop, 2014.

[80] R. Mittal, G. Iaccarino, Immersed boundary methods, Annu. Rev. Fluid Mech. 37 (2005) 239–261.

[81] H. Jasak, D. Rigler, Ž. Tuković, Design and implementation of immersed boundary method with discrete forcing approach for boundary conditions, in: 11th World Congress on Computational Mechanics, WCCM 2014, 5th European Conference on Computational Mechanics, ECCM 2014 and 6th European Conference on Computational Fluid Dynamics, ECFD 2014, International Center for Numerical Methods in Engineering, 2014, pp. 5319–5332.

[82] I. Gatin, V. Vukcevic, H. Jasak, I. Lalovic, Manoeuvring simulations using the overset grid technology in foam-extend, in: 32nd Symposium on Naval Hydrodynamics, 2018.

[83] Y. Li, K.-J. Paik, T. Xing, P. M. Carrica, Dynamic overset cfd simulations of wind turbine aerodynamics, Renewable Energy 37 (1) (2012) 285–298.

[84] J.-F. Combes, P.-F. Bert, J.-L. Kueny, Numerical investigation of the rotor-stator interaction in a centrifugal pump using a finite element method, ASME FEDSM97-3454.

[85] M. Ubaldi, P. Zunino, G. Barigozzi, A. Cattanel, An experimental investigation of stator induced unsteadiness on centrifugal impeller outflow,

in: ASME 1994 International Gas Turbine and Aeroengine Congress and Exposition, American Society of Mechanical Engineers, 1994, pp. V001T01A002–V001T01A002.

[86] P. Bert, J. Combes, J. Kueny, Unsteady flow calculation in a centrifugal pump using a finite element method, in: Hydraulic Machinery and Cavitation, Springer, 1996, pp. 371–380.

[87] K. Sato, L. He, Numerical investigation into the effects of a radial gap on hydraulic turbine performance, Proceedings of the Institution of Mechanical Engineers, Part A: Journal of Power and Energy 215 (1) (2001) 99–107.

[88] L. He, K. Sato, Numerical solution of incompressible unsteady flows in turbomachinery, Journal of fluids engineering 123 (3) (2001) 680–685.

[89] K. Sato, Blade row interaction in radial turbomachines, Ph.D. thesis, Durham University (1999).

[90] M. Page, E. Theroux, J. Trepanier, Unsteady rotor-stator analysis of a francis turbine, in: Proceedings of the 22nd IAHR Symposium on Hydraulic Machinery and Systems, Stockholm, 2004.

[91] M. Page, M. Beaudoin, Adapting openfoam for turbomachinery applications, in: 2nd OpenFOAM Workshop Zagreb, Croatia, 2007.

[92] S. Xie, O. Petit, H. Nilsson, Studies of the ercoftac centrifugal pump.

[93] J. Combès, Test case u3: centrifugal pump with a vaned diffuser, in: ERCOFTAC Seminar and Workshop on Turbomachinery Flow Prediction VII, Aussois, 1999.

[94] M. Ubaldi, P. Zunino, G. Barigozzi, A. Ghiglione, Ldv investigation of the rotor-stator aerodynamic interaction in a centrifugal turbomachine, in: Proceedings of the 8th International Symposium on Applications of Laser Techniques to Fluid Mechanics, 1996.

[95] M. Ubaldi, P. Zunino, A. Cattanei, Etude expérimentale de l'écoulement instationnaire dans le diffuseur aubé d'une turbomachine centrifuge, La Houille Blanche (3-4) (1998) 31–37.

[96] K. Suder, T. Okiishi, M. Hathaway, A. Strazisar, J. Adamczyk, Measurements of the unsteady flow field within the stator row of a transonic axial-flow fan: I—measurement and analysis technique, in: ASME 1987 International Gas Turbine Conference and Exhibition, American Society of Mechanical Engineers, 1987, pp. V001T01A082–V001T01A082.

[97] B. Lakshminarayana, Techniques for aerodynamic and turbulence measurements in turbomachinery rotors, Journal of Engineering for Power 103 (2) (1981) 374–392.

[98] J. Gostelow, A new approach to the experimental study of turbomachinery flow phenomena, Journal of engineering for power 99 (1) (1977) 97–105.

[99] S. Xie, Studies of the ercoftac centrifugal pump with openfoam, Master's thesis, Chalmers University of Technology (2010).

[100] C. Trivedi, M. J. Cervantes, O. Dahlhaug, Francis 99: A test-case on a high head francis turbine, Master's thesis, Waterpower laboratory, Department of Energy and Process Engineering, Faculty of Engineering, NTNU, Trondheim, Norway (2019).

[101] M. Cervantes, C. H. Trivedi, O.-G. Dahlhaug, T. Nielsen, Francis-99 workshop 1: steady operation of francis turbines, Journal of Physics: Conference Series 579 (2015) 011001. doi:10.1088/1742-6596/579/1/011001.
URL https://doi.org/10.1088%2F1742-6596%2F579%2F1%2F011001

[102] Francis-99 workshop 2: transient operation of francis turbines, Journal of Physics: Conference Series 782 (2017) 011001. doi:10.1088/1742-6596/782/1/011001.
URL https://doi.org/10.1088%2F1742-6596%2F782%2F1%2F011001

[103] https://www.ntnu.edu/nvks/francis-99, Norwegian Hydropower Center Research Francis-99 (last access: 2019-06-04).

[104] Technical Report IEC 60193, 3, rue de Varemb, PO Box 131, CH-1211 Geneva 20, Switzerland, 1999. Second Edition., International Electrotechnical

Commission. Hydraulic turbines, storage pumps and pump-turbines: Model acceptance tests.

[105] Minakov, A., Sentyabov, A. and Platonov, D., Numerical investigation of flow structure and pressure pulsation in the Francis-99 turbine during startup (IOP Conf. Series: Journal of Physics: Conf. Series 782 (2017) 012004).

[106] Pointwise V18.0R4 Release Notes, http://www.pointwise.com/support/release-notes.shtml (last access: 2019-06-04).

[107] B. E. Launder, D. B. Spalding, The numerical computation of turbulent flows, Computer methods in applied mechanics and engineering 3 (2) (1974) 269–289.

[108] T. S. Koltukluoglu, Data assimilation in computational hemodynamics, Ph.D. thesis, ETH Zurich (2019).

Curriculum Vitae

Gregor Cvijetić was born in Zagreb, Croatia on 28 March 1991. He finished the Gimnazija Lucijana Vranjanina high school in Zagreb in 2009 and enrolled Faculty of Mechanical Engineering and Naval Architecture, Unversity of Zagreb in the same year. He completed the Engineering Modeling and Computer Simulations undergraduate program in 2013 Magna Cum Laude with the BSc thesis on crack propagation with finite element method. In 2013, he enrolled in the Engineering Modeling and Computer Simulations graduate program of the Faculty of Mechanical Engineering and Naval Architecture, University of Zagreb, finally graduating in 2015 with the MSc thesis in CFD, focused on the development and implementation of the Harmonic Balance method. During the studies he received several awards, such as the special Rector's award in 2012. Upon his graduation he started his PhD study in 2015. He is the author of three peer-reviewed journal articles and a number of conference contributions.

Declaration

Parts of the work presented in this Thesis have been published in some articles presented below.

List of Publications

[1] G.Cvijetić, Analysis and implementation of the harmonic balance method in computational fluid dynamics, in: Masters Thesis, 2015.

[2] G.Cvijetić, H.Jasak, V.Vukčević, Finite volume implementation of the harmonic balance method for periodic non-linear flows, in: 54th AIAA Aerospace Sciences Meeting, 2016.

[3] G.Cvijetić, I.Gatin, H.Jasak, Applications of Harmonic Balance Method in Periodic Flows, in: The 4th Annual OpenFOAM User Conference, 2016.

[4] G.Cvijetić, H.Jasak, Primjena metode harmonijske ravnoteže za simulacije turbostrojeva, in: Sedmi susret Hrvatskoga društva za mehaniku, 2016.

[5] V.Vukčević, G.Cvijetić, I.Gatin, H.Jasak, The harmonic balance method for temporally periodic free surface flows in marine hydrodynamics, in: 11th OpenFOAM Workshop, 2016.

[6] H.Jasak, G.Cvijetić, Implementation and Validation of the Harmonic Balance Method for Temporally Periodic Non–Linear Flows, in: ASME Turbo Expo, 2016

[7] I.Gatin, G.Cvijetić, V.Vukčević, H.Jasak, Wave Diffraction CFD Nonlinear Time-Spectral Simulations in foam-extend, in: 19th Numerical Towing Tank Symposium, 2016.

[8] G.Cvijetić, I.Gatin, V.Vukčević, H.Jasak, Harmonic Balance Developments in OpenFOAM, in: 12th OpenFOAM Workshop, 2017.

[9] I.Gatin, G.Cvijetić, V.Vukčević, H.Jasak, Š.Malenica, Harmonic Balance method for nonlinear and viscous free surface flows, in: Ocean Engineering 157 (2018) 164–179

[10] G.Cvijetić, I.Gatin, V.Vukčević, H.Jasak, Harmonic Balance developments in OpenFOAM, in: Computers and Fluids, 2018 .

[11] G.Cvijetić, H.Jasak, The compressible harmonic balance method for turbomachinery, in: AIAA Aerospace Sciences Meeting, 2018.

[12] I.D.Dominicis, G.Cvijetić, M.Willetts, H.Jasak, Enhanced Turbomachinery Capabilities for foam-extend: Development and Validation, in OpenFOAM, Springer, 2019.

[13] G.Cvijetić, L.Čulić, H.Jasak, Analysis of transients in Francis turbine using Fourier methods, in: AIAA Aerospace Sciences Meeting, 2019.

[14] G.Cvijetić, L.Čulić, H.Jasak, Application of the Harmonic Balance method for regime change prediction using Francis-99 test case, in: Francis-99 Workshop, 2019.